HAYATI
Journal of Biosciences

Vol. 31 No. 1, January 2024 110-125
DOI:10.4308/hjb.31.1.110-125
ISSN: 1978-3019
EISSN: 2086-4094

Development of Few Significant SNP Markers from Transcriptomic Data for Selection of Sengon (*Falcataria falcata* (L.) Greuter & R. Rankin) Resistant to Boktor Stem Borer and Gall Rust Disease

Aditya Nugroho[1], Vilda Puji Dini Anita[1], Deden Derajat Matra[2], Iskandar Zulkarnaen Siregar[3], Ulfah Juniarti Siregar[3]*

[1]*Post Graduate Program in Tropical Silviculture, Faculty of Forestry and Environment, IPB University, Bogor 16680, Indonesia*
[2]*Department Agronomy and Horticulture, Faculty of Agriculture, IPB University, Bogor 16680, Indonesia*
[3]*Departement of Silviculture, Faculty of Forestry and Environment, IPB University, Bogor 16680, Indonesia*

ARTICLE INFO

Article history
Received May 2, 2023
Received in revised form September 24, 2023
Accepted September 29, 2023

KEYWORDS
High-Resolution Melting,
Falcataria falcata,
Single Nucleotide Polymorphisms,
Pest and Disease Resistance,
Transcriptome

ABSTRACT

Sengon (*Falcataria falcata* (L.) Greuter & R. Rankin) plantations in Indonesia are threatened by attacks from Boktor stem borers and gall rust disease. Controlling pests and diseases is difficult; therefore, planting resistant trees obtained from tree selection programs is necessary. Currently, genomic breeding often incorporates GWAS, which uses thousands of SNP markers to identify markers with significant associations with the traits studied. This study aimed to bypass such expensive studies by identifying and developing SNP markers from sequences of putative resistance genes to Boktor stem borer and gall rust disease, identified from sengon transcriptomic data analysis. A total of 496,194 putative SNP sites were identified from transcriptomic sequences using the SAMtools and BFCtools programs, of which 119 SNP sites were associated with resistance genes. Of the 101 non-synonymous SNPs selected, only 12 were located in the conserved domain of each gene and were used for primer design. Of the 13 primers designed, only 10 were successfully amplified. Validation of 10 developed SNP markers on 100 sengon accessions using the HRM method confirmed a significant association between SNP markers and resistance traits, with a -log 10 (P-value) between 10.49 and 16.63. A few SNPs markers developed from putative resistance gene sequences are associated with resistance traits in sengon. Therefore, the SNP markers could be applied in selection programs for sengon trees resistant to Boktor stem borers and gall rust disease.

1. Introduction

Sengon (*Falcataria falcata* (L.) Greuter & R. Rankin) is a fast-growing legume tree that has become an economically important species in Indonesia. Currently, sengon wood production is 2,595,175.82 m^3, representing 54.87% of the total wood production of Java Island (BPS 2019). However, plantations face serious pest and disease issues that affect their productivity. The principal pests and diseases that have been observed to harm sengon plantations are the Boktor stem borer (*Xystrocera festiva*) and gall rust infection by Uromycladium falcatariae fungus. So far, there are no effective control methods, so planting resistant clones would be beneficial both economically and ecologically. A selection program to obtain resistant lines has been initiated; however, progress is slow. A molecular approach is required to accelerate the selection process, such as utilizing molecular markers to obtain more reliable findings.

Several studies have shown that several provenances were more tolerant to gall rust infections and Boktor attacks (Baskorowati *et al.* 2012; Setiadi *et al.* 2014; Darwiati and Anggraeni 2018). However, because of the outcrossing nature of this species, these superior provenances have not yet been genetically or molecularly verified. Lelana *et al.* (2018) studied sengon resistance to gall rust disease using RAPD markers. However, RAPD could not differentiate the resistant from the susceptible accessions. Siregar *et al.* (2019) used microsatellite markers to separate resistant sengon accessions from susceptible ones and implied differences in

* Corresponding Author
E-mail Address: ulfahjs@apps.ipb.ac.id

the two accessions' genetic backgrounds. However, many resistant and susceptible accessions were still clustered within the same group. Both studies reported that the markers used were less specific. Therefore, new and more powerful markers are required for fingerprinting sengon accessions in selection programs.

Single-nucleotide polymorphisms (SNPs) have recently become popular and are frequently used as molecular markers in various laboratories for practical applications (Lai *et al.* 2012). SNPs are particularly suitable for studying complex genetic traits and understanding genome evolution (Wellenreuther *et al.* 2019; Mageiros *et al.* 2021). The wide application of SNP markers is due to rapid advances in high-throughput sequencing technology, which is becoming cheaper to obtain high-throughput data sequences rapidly and, when combined with various bioinformatics tools, enables the analysis of many gene functions. Yuskianti and Shirashi (2017) developed SNP markers to study the genetic diversity and relationships of 8 sengon populations from 3 regions in Indonesia, namely Papua, Maluku, and Java, as well as from Mindanao, the Philippines. However, this study was limited to genetic diversity and relationships between provenances without considering the condition of plant resistance to pests and diseases. Therefore, specific SNP markers associated with resistance to Boktor stem borer pest and gall rust disease are required.

SNP markers associated with certain complex traits are usually derived from genome-wide association studies (GWAS) involving thousands of SNP and samples. However, such GWAS studies are often expensive. This study aimed to bypass such expensive studies by identifying and developing SNP markers using transcriptome data analysis of sengon accessions resistant and susceptible to gall rust disease (Shabrina *et al.* 2019) and sengon accessions resistant and susceptible to Boktor stem borer (Siregar *et al.* 2021). The identified and developed SNP primers were tested on small samples of sengon accessions displaying resistance to the pest and disease. By developing SNP markers from sequences of putative functional genes for resistance, it is expected that the markers will be significantly associated with the phenotypic traits studied without spending much on analyzing many unrelated SNPs.

2. Materials and Methods

2.1. Plant Material

The plant materials for SNP validation were collected from sengon tree plantations in Kediri Regency, East Java, Indonesia, under the management of the National Forest Estate (11 resistant and 13 susceptible accessions) and from private plantations in Bogor Regency, West Java, Indonesia (39 resistant and 37 susceptible accessions). The sample trees used were the same five years old and planted in the same plot. Their health was examined before being identified and classified as either resistant or susceptible to Boktor stem borer and gall rust disease. Resistant and susceptible accessions were selected from trees planted in the same plot to eliminate the possibility of environmental factors affecting resistance. Susceptible individuals are trees attacked by pests and diseases with an attack severity level of more than 50%. In contrast, resistant individuals are trees that do not show any symptoms of the pest or gall rust disease infestation. The number of samples used in this study corresponded to the minimum sample size for population genomic analysis by Li *et al.* (2020). Two upper leaves were collected from these trees in January 2018 and January 2019. The upper leaves were chosen because young leaves have more tender tissues that are easily macerated and have lower levels of polyphenolic, polysaccharides, and lignin compounds, which could potentially interfere with the DNA extraction process.

2.2. DNA Isolation

DNA was isolated from 0.1 g leaf samples using the modified CTAB method (Doyle 1991). The quantity and quality of the DNA were measured using a NanoDrop Spectrophotometer (Thermo Fisher Scientific, Waltham, MA, USA) and visualized on 1% agarose gel (1st BASE, 41 Science Park Rd, Singapore) electrophoresis at 100 volts for 25 min.

2.3. Mapping Transcriptome Sequence

The assembled transcriptomic data of sengon susceptible and resistant to Boktor stem borer and gall rust disease were obtained from the Data Bank of Japan (DDBJ) (https://www.ddbj.nig.ac.jp) with accession numbers DRA008389 and DRA007983 published by Shabrina *et al.* (2019) and Siregar *et al.* (2021). The read data used were from eight individual trees, where reads of rust-resistant, rust-

susceptible, Boktor-resistant, and Boktor-susceptible were the results of sequencing using the BGISEQ-500 platform (Siregar *et al.* 2021). Reads of rust on leaves 1 and 2 and stems 1 and 2 were sequenced using the Illumina HiSeq4000 platform (Shabrina *et al.* 2019). The sequences were realigned using CAP3 software (Huang and Madan 1999) to reduce clusters of nearly identical transcripts and obtain more complete contigs. Then, they were clustered to remove redundant or ambiguous contigs using CD-HIT-EST software (Li and Godzik 2006), applying an identity threshold of 95%. FastQC software was used to check the quality of data reads.

Raw reads were trimmed and filtered using Trimmomatic to remove adapter sequences contamination, low-quality bases (>Q30), and 3'/5' bias positions. Clean reads were then mapped to the assembled transcriptome reference using Bowtie2 software (Langmead and Salzberg 2012). The SAM file was sorted according to the position of the reference sequence and then converted to BAM (Binary Alignment/BST) format using SAMtools software.

2.4. SNPs Calling

SNPs were called using the BCFtools program, which includes mpileup, call, and filter steps (Li *et al.* 2009) to identify nucleotide bases that are highly likely to be putative SNPs. The input file in the BAM format resulted in a VCF output that contains various information in the form of the occurrence position, variation quality, alternative bases, and other information related to the identified variations.

2.5. Designing SNPs Primer

Primers were designed to validate the SNP sites of the selected genes. The selected genes were related to resistance to Boktor stem borers and gall rust disease. The genes were identified based on DEG analysis, showing upregulated activity in the previous studies. The sequences were reannotated using BLAST (Basic Local Alignment Search Tools) to confirm that the sequences were highly related to the resistance genes. The target gene sequences were annotated or compared with the GenBank (NCBI) sequences and the results of the whole-genome sequencing of sengon (DRA012508) to ensure the gene sequences were correct before designing the primers. The conserved area was identified in the target gene sequences using the GenBank website's Conserved Domain Database (CDD) (www.ncbi.nlm.nih.gov/Structure/cdd/wrpsb.cgi). The sites of SNPs selected for primer preparation must be in this conservative region, non-synonymous, and there are no other adjacent SNP sites. A pair of primers were then designed using Primer3Plus (https://primer3plus.com).

A primer selection step was performed to obtain primers that could detect SNPs in the assayed samples. The selection was performed by testing several candidate primers under the same PCR conditions and using the same DNA sample to obtain optimum PCR conditions and the level of variation of the bands produced by each primer. The PCR mixture used GoTaq® PCR Core System I (Promega Corporation, Madison, Wisconsin, USA), and amplification was performed in an Applied Biosystems Veriti 96-Well Thermocycler (Thermo Fisher Scientific, Waltham, MA, USA) for 35 cycles with the following steps: pre-denaturation at 95°C for 2 min, denaturation at 95°C for 30 s, annealing at 56°C to 60°C for 30 s, extension at 72°C for 1 min, followed by a final extension at 72°C for 5 min.

2.6. SNPs Genotyping and Validation

The 10 selected primers were used to validate SNPs in the DNA samples from resistant and susceptible plants using the StepOne™ Real-Time PCR System (Thermo Fisher Scientific, Waltham, MA, USA). High-Resolution Melting (HRM) reaction was performed using the SensiFAST™ HRM Kit (Meridian Bioscience Inc, Cincinnati, Ohio, USA) in a final volume of 20 µl containing 2× SensiFAST HRM Mix, 6.4 µl H_2O, 10 µM of each primer, and 2 µl of DNA template (approx. 100 ng/µl). The qPCR condition followed: initial denaturation at 95°C for 1 min, denaturation at 95°C for 5 s, annealing/extension at 60°C for 25 s, and the PCR process was carried out as many as 40 cycles. This was followed by forming a melt curve process to determine the base variation that occurred with the following steps: denaturation at 95°C for 10 s, annealing at 60°C for 1 min, high-resolution melting at 95°C for 15 s, and annealing at 60°C for 15 s with a ramp rate of 0.3%.

Melt curve analysis was performed using HRM software with normalization and temperature shift of the fluorescence data, followed by fluorescence difference plots. A reference sample was used for observation. The present study used a wild-type sample based on transcriptomic data analysis as a reference. The software grouped data that were

similar and assigned a cluster number. The melt curve corresponding to each cluster was color-coded for ease of visualization. The cluster detection settings included melt curve shape sensitivity (50% cluster default value) and melting temperature difference threshold (Tm) (default: 0.15).

2.7. Chi-Square Test

Chi-square analysis was used to determine the correlation between genotypes based on the results of HRM analysis with phenotypes. The following chi-square test formula was used:

$$x^2 = \sum_{i=1}^{p} \frac{(|O_j - E_j| - 0.5)^2}{E_j}$$

O_j = value of observations in J class = 1, 2; E_j = expected value in J-class = 1, 2. Each primer's "-log10(p)" value was calculated and plotted against each contig to generate Manhattan plots using the ggplot2 package in RStudio. We declared SNPs significant at an FDR-adjusted p-value of less than 0.001 to minimize the risk of false positives, which can lead to spurious associations and waste resources for follow-up studies (Duggal *et al.* 2008).

3. Results

3.1. Reference Sequence Design

This study used reads from the results of transcriptomic data assembly of Boktor- and gall rust-resistant and susceptible sengon samples. Two assembled transcriptome references were reassembled using CAP3 and CH-HIT-EST, resulting in 150,197 contigs (Table 1).

3.2. Quality Control and Filtering of Raw Reads

Raw data may contain low-quality bases and adapters that can cause errors in the alignment process. Filtering and trimming were performed to remove the low-quality bases and adapters (Table S1). Reads of boktor-resistant, boktor-susceptible, rust-resistant, and rust-susceptible had high base quality (>Q30), as seen from the results of quality control before filtering (Figure S1), indicating that the number of reads did not decrease.

Table 1. Number of contigs obtained from each read used in this study

Reads	Number of contigs
Boktor resistant-susceptible	70,089
Gall rust resistant-susceptible	96,164
Reassembly	150,197

3.3. Mapping and Detection of SNPs

Eight samples with clean reads against the transcriptome reference had an overall alignment rate of 90.78%. Quality control and trimming were performed on the eight clean-read samples. The alignment results were then used for the SNP calling stage using SAMtools. There were 496,194 nucleotide site changes or putative SNPs predicted in the resulting sengon transcriptome contigs, with an estimated frequency of one SNP per 608 bp. The identified SNPs were dominated by transition changes of 323,370 (65.21%) bases, whereas transversion changes were only 172,824 (34.79%) bases (Table 2).

3.4. Development and Selection of SNP Primers

The annotated transcriptomic data from previous studies showed that some genes play a role in plant resistance to pests and diseases, such as alpha-amylase inhibitors, trypsin inhibitors, ubiquitin carboxyl-terminal hydrolase 13, NADH-ubiquinone oxidoreductase, Indole-3-acetic acid-amido synthetase, and the WRKY transcription factor. A total of 119 SNPs were identified from the sequences of these resistance genes and categorized as synonymous or non-synonymous; 18 synonymous and 101 non-synonymous SNPs were identified (Table 3).

Twelve non-synonymous SNP sites in the seven target genes were selected for developing SNP markers and designed into 13 primers. List of SNP primers generated for the target genes (Table S2). The selection of primers based on the PCR process showed that only ten primers could be amplified, whereas two were unamplified and discarded. The amplified product sizes ranged from 107 to 216 bp. The amplification results of each primer and the product size predictions are listed in Table S3. Meanwhile, primers NUOR-2, UB13-1, and UB13-2 were not successfully amplified, presumably because of the presence of introns in the DNA region flanked by the primer pairs.

Table 2. The number of identified putative SNPs in the transcriptomes of sengon used in this study

Alternative base	Reference base			
	C	G	A	T
C		18,372	19,216	90,788
G	13,482		72,081	26,583
A	25,472	93,277		29,593
T	67,224	18,630	21,476	
Total	496,194 SNPs			

C-G-A-T refers to cytosine (C), guanine (G), adenine (A), and thymine (T)

Table 3. Summary of SNPs distribution across the sequences of resistance-associated genes

Name of gene	Number of contigs	SNPs	
		Synonymous	Non-synonymous
Alpha-amylase inhibitor (AAI)	1	-	10
Trypsin inhibitor (TI)	3	6	28
Ubiquitin carboxyl-terminal hydrolase 13 (UB13)	5	2	9
NADH-ubiquinone oxidoreductase (NUOR)	16	3	19
Indole-3-acetic acid-amido synthetase (IAA)	3	6	30
Transcription factor WRKY 11	3	1	4
Transcription factor WRKY 40	3	-	1
Total	119		

3.5. SNPs Validation and Genotyping

The selected primers were validated on 100 samples of sengon DNA with the following details: 50 susceptible tree samples versus 50 resistant tree samples. Ten primers were used for amplification. Based on the correlation analysis, we observed that the samples susceptible to Boktor stem borer were also susceptible to gall rust disease and vice versa ($R = 0.69$, p-value = 2.2×10^{-8}). Thus, we combined the susceptibility and resistance of both attackers into one category (Figure S2).

Differential plots from HRM analysis in this study showed curve-shape differences between wild-type and mutant DNA. The proper plot shows a clear melt profile, a single peak, and grouping, as seen in the differential plots of the IAA-2 primer (Figure 1). The wild-type sample was a sample with a reference base from the identification of SNPs, and the mutant sample was a sample with changes in the nucleotide base according to the results of SNPs identification. The list of references and alternative bases for each primer is presented in Table S2.

DNA mutations can cause allele pairs to be either the same (homozygous) or different (heterozygous) (Table S4). For example, in the TI-2 primer, the allele pair could be AA or GA by changing the DNA base G (guanine) to A (adenine) at a position of 850 bp. Only 7 primers, i.e. TI-2, NUOR-1, NUOR-3, WRKY-11, WRKY-40, IAA-1, and IAA-2 primers used in the HRM analysis, successfully differentiated wild-types and mutant samples. However, the wild-types and mutant samples were not categorized according to their resistance level (resistant or susceptible) yet.

Furthermore, a chi-square test was performed using data from the SNP detection of 100 samples to determine the allele segregation pattern at each locus. As shown in Table S4, there were three expected genotypes for each locus, of which the expected Mendelian ratio of the genotypes was 1:2:1 (AA:AB:BB), where AA was the homozygous genotype for the wild-type allele, AB was the heterozygous genotype, and BB was the homozygous genotype for the mutant allele. If the calculated χ^2 value < χ^2 table, then the observed segregation pattern follows Mendelian law, meaning that the allele pair formed results from an independent segregation process.

In addition to the chi-square test, the p-value (-log 10) was calculated to determine the SNP markers association level with resistance properties. A higher p-value indicated that the association between SNP markers and resistance properties was more significant. All SNP markers showed high p-values, with WRKY 40 and NUOR 3 having the highest p-values of 16.63 and 14.65, respectively (Table 4) (Figure 2).

The dendrogram of grouping samples based on genotyping using seven SNP primers in 100 samples of *F. falcata* (Figure 3) showed that most samples

were grouped according to their phenotypes, namely resistant or susceptible. Some samples were still incorrectly clustered into the resistant or susceptible groups, presumably because these samples probably had intermediate resistance or susceptibility and required more precise phenotyping. Thus, the developed SNP marker can distinguish between susceptible and resistant samples.

4. Discussion

The observation of read quality follows that of Zhu *et al.* (2018), who stated that the BGISEQ-500 has a higher base and raw data quality than HiSeq4000. Library construction on the BGISEQ-500 using DNA nanoballs (DNB) technology can minimize replication errors. Quality control and trimming processes aimed to avoid sequence contamination, adapters, low-quality bases (<Q30), and 3'/5 end nucleotide position bias (Indriani *et al.* 2020).

The estimated frequency of SNPs in this study was lower than that in *Pinus pinaster* (1/192 bp) (Modesto *et al.* 2022), *Hevea brasiliensis* (1/308 bp) (Pootakham *et al.* 2015), and *Pisum sativum* (1/475 bp) (Leonforte *et al.* 2013). According to Pootakham *et al.* (2014), the number of samples studied impacts the frequency

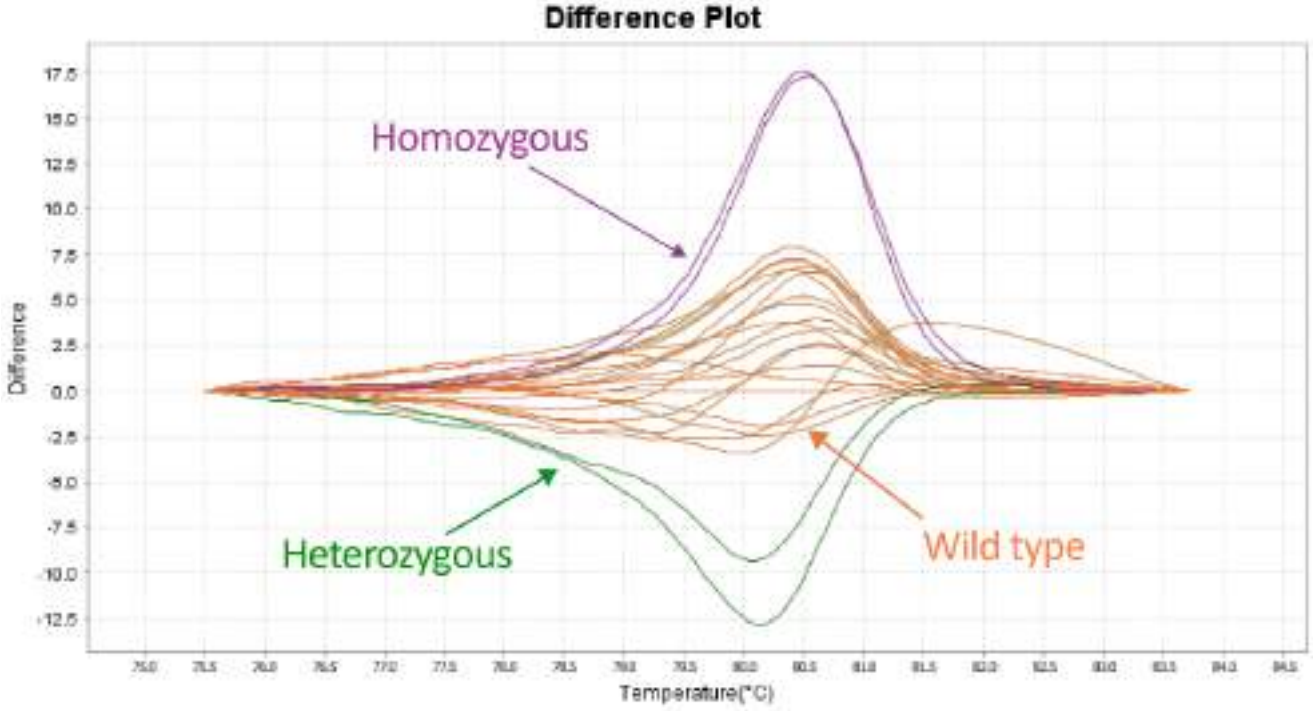

Figure 1. Differential plot of the IAA-2 locus according to the HRM melt curve

Table 4. Chi-square test of sengon trait resistance

Mendel's ratio	Primer	χ^2	-log 10 (P-value)	χ^2 table (0.05)
1:2:1	TI 2	48.32*	10.49	
	NUOR 1	60.12*	13.05	
	NUOR 3	67.48*	14.65	
	WRKY 11	63.48*	13.78	5.99
	WRKY 40	76.60*	16.63	
	IAA 1	61.56*	13.37	
	IAA_2	56.64*	12.29	

Degrees of freedom = 2. * = significant on p<0.05

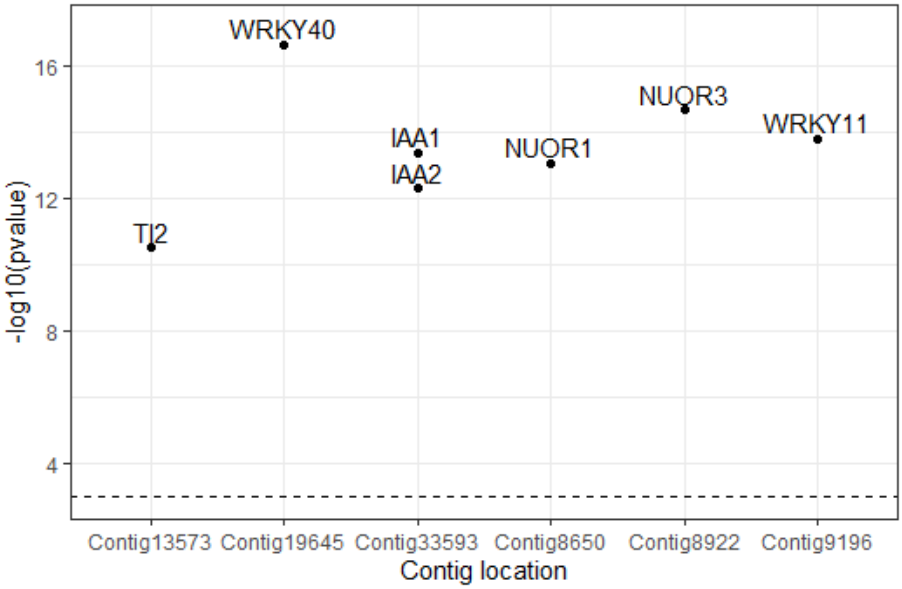

Figure 2. Manhattan plot of seven SNP loci from 100 samples showing either resistant or susceptible against boktor stem borer and gall rust disease in Sengon (*Falcataria falcata*) with threshold significance 0.05

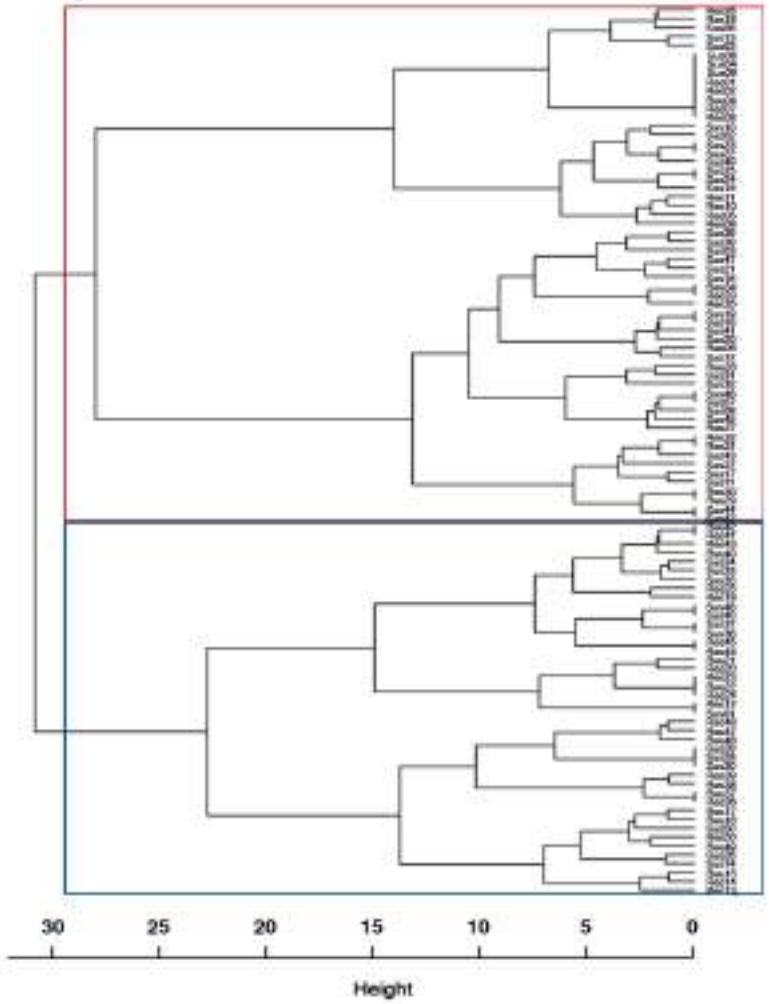

Figure 3. Dendrogram of 100 samples of sengon that are resistant and susceptible to boktor stem borer and gall rust. Res = resistant samples, Sus = susceptible samples. Red box = cluster one, blue box = cluster two

value of SNPs. The more samples used, the greater the chance to find new SNPs and, thus, would likely increase the frequency value of SNPs. Additionally, the frequency of SNPs in the previous transcriptome data, on which this study was based, was lower than that in the whole genome data (Anita *et al.* 2023) because the transcriptome consists of only part of the whole genome, that is, only expressed genes. Also, the coding region (exons) of an expressed gene used in this study to find the SNPs is relatively more conserved than other regions of the gene, i.e. introns (Wu *et al.* 2019).

SNPs can be classified as either transitions or transversions. Transition is a change in the nucleotide base adenine with guanine and cytosine with thymine, or vice versa. At the same time, transversion is a change in guanine and adenine with thymine and cytosine, or vice versa (Luo 2016). Based on these results, the transition-transversion ratio of 1.8 was observed. Similar findings have been reported for *Cryptomeria japonica* (Uchiyama *et al.* 2012), *Elaeis guineensis* (Pootakham *et al.* 2013) and *Hevea brasiliensis* (Pootakham *et al.* 2011, 2014; Shearman *et al.* 2015). Transition substitutions are more frequent than transversion and are thought to be due to the 5-methylcytosine reaction, which occurs frequently at CpG sites (Holliday and Grigg 1993; Zhang and Zhang 2005).

The advantage of detecting SNPs using transcriptome data is that the identified nucleotide base changes may be directly related to the traits to be observed, such as disease resistance and plant growth (Yu *et al.* 2014). Two important genes related to resistance to herbivore insects were AAI (alpha-amylase inhibitor) and TI (trypsin inhibitor) genes. Alpha-amylase inhibitors and trypsin inhibitors are inhibitory compounds that hinder the activity of amylase and proteinase enzymes in the digestive tract of insects; thus, they can inhibit the breakdown of starch into simpler carbohydrate molecules and proteins to be used in the insect metabolic system as an energy source (Siregar *et al.* 2021; Karray *et al.* 2022). In the case of resistance against gall rust disease, Ubiquitin carboxyl-terminal hydrolase 13 plays a role in the jasmonic acid signaling pathway (Jeong *et al.* 2017). Transcription factor genes are a group of genes that regulate the expression of other genes that are involved in resistance mechanisms. WRKY transcription factor 11 and WRKY transcription factor 40 respond positively to plant defense against pathogens (Jiang *et al.* 2016; Lee *et al.* 2018). NADH-ubiquinone oxidoreductase (Kant *et al.* 2019) and Indole-3-acetic acid-amido synthetase have been reported to increase plant susceptibility to pathogens. Indole-3-acetic acid-amido synthetase regulates auxin, stimulating excessive cell division and causing tumor swelling (Li *et al.* 2022). For the sengon tree improvement and breeding program, any genes involved in the resistance mechanisms against pests and disease are desirable. The SNP markers developed in this study are all needed and will be useful in fingerprinting and differentiating the resistant accessions from the susceptible ones; for example, the SNP markers related to AAI and TI genes will likely link to resistant accessions against the Boktor pest, while the SNP markers from IAA might be linked to susceptible accessions.

Synonymous SNPs are changes in one nucleotide base that do not change amino acids and are often called silent mutations. However, non-synonymous SNPs are changes in one nucleotide base that result in amino acid changes (Studer *et al.* 2013). Non-synonymous SNPs are thought to affect protein activity against genes directly (Yu *et al.* 2014), suggesting that these SNPs can be used as markers to help select resistant plants.

SNP markers were created based on changes in one nucleotide base (A, T, G, and C) in the sequences of target genes. SNP sites located in the conserved region were selected to prepare primers. For example, contig16297, detected as a trypsin inhibitor gene (accession number: cl11466), contains a conserved region between 360 and 875. Therefore, the SNP sites chosen for primer preparation for the trypsin inhibitor gene were at positions 771 and 850.

Even though it is already in conservative territory, the SNP site must be checked again using WGS data to ensure that the SNP site is located in the exon. One example is the results of ubiquitin carboxyl-terminal hydrolase 13 (UB13) gene sequence alignment with whole-genome sequencing (WGS) from Anita *et al.* (2023). It was observed that the Sengon WGS sequence had many introns and might cause the UB13 primer to be unsuccessfully amplified. Introns are DNA bases found between exons removed from the mRNA molecule to leave a series of exons that stick together so that the appropriate amino acid can be encoded (Shao *et al.* 2021).

Primer validation was performed using Real-Time Polymerase Chain Reaction (RT-PCR).

According to Kelly *et al.* (2019), the sample concentration greatly influences the amplification efficiency, resulting in a higher variation that is less favorable for forming a standard curve. In this study, the optimal concentration was in the range of 100-500 ng/µl. However, dilution is required if the DNA concentration is too high; higher dilutions are unsuitable for establishing a standard curve. The average DNA concentration used in this study was 100 ng/µl, per the SensiFAST HRM kit protocol (Bioline) for primer validation.

DNA amplicons were analyzed using HRM software to detect variations in the DNA base arrangement or mutations (Gomes *et al.* 2018). HRM can detect fluorescence when double-stranded DNA is denatured into single strands at high temperatures. The difference in one nucleotide base could give a different curve when the DNA fragment is denatured, so the HRM analysis results provide information about the sample with the target SNPs (Gupta *et al.* 2022), called a differential plot. This could explain the differences between wild-type DNA and DNA with mutations. The wild-type standard curve was used as the reference for the differential plot. The standard curve of the mutant was obtained by subtracting the normalized fluorescence values obtained from the normalized fluorescence standard curve of the wild-type DNA. The transformation of the fluorescence value into a differential plot was conducted and integrated into HRM software (Klafke *et al.* 2019).

According to Krypuy *et al.* (2006), the visualization of curves on different plots is strongly influenced by DNA isolation, DNA quality, amplicon length, primer design, and the reagent used. Moreover, unclear clustering and overlap may occur because of intronic SNPs (unexpected variations) located in the created primer sequence (Słomka *et al.* 2017).

The results of the Chi-Square test showed that the calculated χ^2 value for each primer was bigger than the χ^2 table of 5.99 (Table 4), so the distribution patterns of SNP genotypes regarding the resistance properties were deviated from the Mendelian ratio of 1:2:1. These results indicated that the alleles did not segregate freely. It is suspected that there is a linkage disequilibrium between the genes that control resistance traits. Linkage disequilibrium occurs when alleles of one genetic variant are inherited or correlated with a nearby allele of other genetic variants in the progeny population. The dendrogram (Figure 3) shows that 75% of the samples were separated. Cluster one (red box) was dominated by susceptible samples, and cluster two (black box) was dominated by resistant samples. Some samples that were not separated according to their clusters may have been caused by incorrect phenotyping, in which more phenotype groups or intermediates probably exist between the resistant and susceptible traits. These results were in line with the research of Shrestha *et al.* (2019), Liang *et al.* (2015), and Wanda *et al.* (2015), who reported that the genes for plant resistance to fungi, pests, and viruses were polygenic. This indicates that two or more genes can interact with each other during the formation of enzymes or proteins that affect the emergence of resistance traits.

Xu *et al.* (2006) stated that WRKY transcription factor 40 is essential in the signaling pathway of plant defense systems against pathogens. NUOR functions as a mitochondrial component in the ETC pathway, which plays a critical role in energy production and metabolism in plant cells. Compromised mitochondrial function can decrease the production of reactive oxygen species (ROS), important signaling molecules that play a key role in plant defense against pathogens (Cvetkovska *et al.* 2014). ROS production is typically induced in response to pathogen attacks. It helps to activate downstream signaling pathways that trigger various defense responses, such as programmed cell death and the production of antimicrobial compounds. NUOR also regulates programmed cell death, a key component of the plant immune response. When plant cells detect pathogen invasion, they often undergo programmed cell death to limit pathogen spread. Disruptions to the function of the ETC pathway can interfere with this process and impair the plant's ability to limit pathogen infection (Kant *et al.* 2019) effectively.

We discovered 496,194 SNPs in the transcriptomes of sengon-resistant and susceptible to Boktor stem borer and gall rust disease. SNP identification revealed putative 119 SNPs that may be linked to seven disease and pest-resistance genes. A few SNPs markers developed from putative resistance gene sequences are associated with resistance and susceptible traits in sengon. The bypass methodology of developing SNP markers for specific characters using the RNAseq data has proven desirable results. Those SNP markers are important for assisting in

fingerprinting resistant and susceptible accessions. Therefore, SNP markers could be applied in selection programs for sengon trees resistant to boktor stem borers and gall rust disease.

Conflict of Interest

The authors declare no conflicts of interest.

Acknowledgements

This study was supported and funded by the Ministry of Education and Culture, Directorate General of Higher Education of the Republic of Indonesia with the scheme of Penelitian Pendidikan Magister menuju Doktor untuk Sarjana Unggul (PMDSU) based on contract number 200/SP2H/PMDSU/DRPM/2020. The authors are grateful to the National Forest Estate (Perum Perhutani) for giving access to their plantation for sampling and thankful to Ms. Aprilia Damayanti for helping with the collection of the sengon samples and Dr. M. Iqbal Maulana for his advice in the manuscript preparation.

References

Anita, V.P.D., Matra, D.D., Siregar, U.J., 2023. Chloroplast genome draft assembly of *Falcataria moluccana* using hybrid sequencing technology. *BMC Research Notes*. 16, 1-4. https://doi.org/10.1186/s13104-023-06290-6

Baskorowati, L., Susanto, M., Charomaini. M., 2012. Genetic variability in resistance of *Falcataria moluccana* (Miq.) Barneby and JW Grimes to gall rust disease. *Indonesian Journal of Forestry Research.* 9, 1-9. https://doi.org/10.20886/ijfr.2012.9.1.1-9

[BPS] Badan Statistics Indonesia, 2019. *Forest Production Statistics 2019*. Central Agency on Statistics, Jakarta.

Cvetkovska, M., Dahal, K., Alber, N. A., Jin, C., Cheung, M., Vanlerberghe, G.C., 2014. Knockdown of mitochondrial alternative oxidase induces the 'stress state' of signaling molecule pools in *Nicotiana tabacum*, with implications for stomatal function. *New Phytol.* 203:449-461. https://doi.org/10.1111/nph.12773

Darwiati, W., Anggraeni, I., 2018. The boktor and tumor attack at sengon in the plantation of tea ciater. *Jurnal Sains Natura.* 8, 59-69. https://doi.org/10.31938/jsn.v8i2.119

Duggal, P., Gillanders, E.M., Holmes, T.N., Bailey-Wilson, J.E., 2008. Establishing an adjusted p-value threshold to control the family-wide type 1 error in genome wide association studies. *BMC Genomics*. 9, 516. https://doi.org/10.1186/1471-2164-9-516

Doyle, J., 1991. DNA protocols for plants, in: Hewitt, G.M., Johnston, A.W.B., Young, J.P.W. (Eds.), *Molecular Techniques in Taxonomy*. Springer., Berlin, pp. 283-293.

Gomes, S., Castro, C., Barrias, S., Pereira, L., Jorge, P., Fernandes, J.R., Martins-Lopes, P., 2018. Alternative SNPs detection platforms, HRM and biosensors, for varietal identification in *Vitis vinifera* L. using F3H and LDOX genes. *Scientific Reports.* 8, 1-12. https://doi.org/10.1038/s41598-018-24158-9

Gupta, E., Kaushik, S., Srivastava, V.K., Saxena, J., Jyoti, A., 2022. Real-time PCR high-resolution melting analysis, in: Kaushik, S., Singh, N. (Eds.), *Current Developments in the Detection and Control of Multi Drug Resistance.* Bentham Science Publisher, Netherlands, pp. 50-65.

Holliday, R., Grigg, G.W., 1993. DNA methylation and mutation. *Mutation Research.* 285, 61-70. https://doi.org/10.1016/0027-5107(93)90052-h

Huang, X., Madan, A., 1999. CAP3: A DNA sequence assembly program. *Genome Research.* 9, 868-877. https://doi.org/10.1101/gr.9.9.868

Indriani, F., Siregar, U.J., Matra, D.D., Siregar, I.Z., 2020. De novo transcriptome datasets of *Shorea balangeran* leaves and basal stem in waterlogged and dry soil. *Data in Brief.* 28, 1-3. https://doi.org/10.1016/j.dib.2019.104998

Jeong, J.S., Jung, C., Seo, J.S., Kim, J.K., Chua, N.H., 2017. The deubiquitinating enzymes UBP12 and UBP13 positively regulate MYC2 levels in jasmonate responses. *Plant Cell.* 29, 1406–1424. https://doi.org/10.1105/tpc.17.00216

Jiang, C.H., Huang, Z.Y., Xie, P., Gu, C., Li, K., Wang, D.C., Yu, Y.Y., Fan, Z.H., Wang, C.J., Wang, Y.P., Guo, Y.H., Guo, J.H., 2016. Transcription factors WRKY70 and WRKY11 served as regulators in rhizobacterium *Bacillus cereus* AR156-induced systemic resistance to *Pseudomonas syringae* pv. tomato DC3000 in Arabidopsis. *Journal of Experimental Botany.* 67, 157-174. https://doi.org/10.1093/jxb/erv445

Kant, R., Tyagi, K., Ghosh, S., Jha, G., 2019. Host alternative NADH: ubiquinone oxidoreductase serves as a susceptibility factor to promote pathogenesis of Rhizoctonia solani in plants. *Phytopathology.* 109, 1741-1750. https://doi.org/0.1094/PHYTO-02-19-0055-R

Karray, A., Alonazi, M., Jallouli, R., Alanazi, H., Ben, B.A., 2022. A proteinaceous alpha-amylase inhibitor from *Moringa oleifera* leaf extract: purification, characterization, and insecticide effects against *C. maculates* insect larvae. *Molecules.* 27, 1-15. https://doi.org/10.3390/molecules27134222

Kelly, R.P., Shelton, A.O., Gallego, R., 2019. Understanding PCR processes to draw meaningful conclusions from environmental DNA studies. *Scientific Reports.* 9, 1-14. https://doi.org/10.1038/s41598-019-48546-x

Klafke, G.M., Miller, R.J., Tidwell, J.P., Thomas, D.B., Sanchez, D., Feria-Arroyo, T.P., Pérez de León, A.A., 2019. High-resolution melt (HRM) analysis for detection of SNPs associated with pyrethroid resistance in the southern cattle fever tick, *Rhipicephalus* (Boophilus) microplus (Acari: Ixodidae). *International Journal of Parasitology: Drugs and Drug Resistance.* 9, 100-111. https://doi.org/10.1016/j.ijpddr.2019.03.001

Krypuy, M., Newnham, G.M., Thomas, D.M., Conron, M., Dobrovic, A., 2006. High resolution melting analysis for the rapid and sensitive detection of mutations in clinical samples: KRAS codon 12 and 13 mutations in non-small cell lung cancer. *BMC Cancer.* 21, 1-12. https://doi.org/10.1186/1471-2407-6-295

Lai, K., Duran, C., Berkman, P.J., Lorenc, M.T., Stiller, J., Manoli, S., Hayden, M.J., Forrestm, K.L., Fleury, D., Baumann, U., Zander, M., Mason, A.S., Batley, J., Edwards, D., 2012. Single nucleotide polymorphism discovery from wheat next-generation sequence data. *Plant Biotechnology Journal.* 10, 743-749. https://doi.org/10.1111/j.1467 7652.2012.00718.x

Langmead, B., Salzberg, S.L., 2012. Fast gapped-read alignment with Bowtie 2. *Nature Methods.* 9, 357-359. https://doi.org/10.1038/nmeth.1923

Lee, H., Cha, J., Choi, C., Choi, N., Ji, H.S., Park, S.R., Lee, S., Hwang, D.J., 2018. Rice WRKY11 plays a role in pathogen defense and drought tolerance. *Rice.* 11, 1-12. https://doi.org/10.1186/s12284-018-0199-0

Lelana, N.E., Wiyono, S., Giyanto, G., Siregar, I.Z., 2018. Genetic diversity of *Falcataria moluccana* and its relationship to the resistance of gall rust disease. *Biodiversitas.* 19, 12-17. https://doi.org/10.13057/biodiv/d190102

Leonforte, A., Sudheesh, S., Cogan, N.O.I., Salisbury, P.A., Nicolas, M.E., Materne, M., Forster, J.W., Kaur, S., 2013. SNP marker discovery, linkage map construction and identification of QTLs for enhanced salinity tolerance in field pea (*Pisum sativum* L.). *BMC Plant Biol.* 13, 1-14. https://doi.org/10.1186/1471-2229-13-161

Liang, D., Hu, Q., Xa, Q., Qi, X., Zhou, F., Chen, X., 2015. Genetic inheritance analysis of melon aphid (*Aphis gossypii* Glover) resistance in cucumber (*Cucumis sativus* L.). *Euphytica.* 250, 361-367. https://doi.org/10.1007/s10681-015-1391-6

Li, W., Godzik, A., 2006. Cd-hit: a fast program for clustering and comparing large sets of protein or nucleotide sequences. *Bioinformatics.* 22, 1658-1659. https://doi.org/ 10.1093/bioinformatics/btl158

Li, H., Handsaker, B., Wysoker, A., Fennell, T., Ruan, J., Homer, N., Marth, G., Abecasis, G., Durbin, R., 2009. The sequence alignment map format and SAMtools. *Bioinformatics.* 25, 2078-2079. https://doi.org/10.1093/bioinformatics/btp352

Li, H., Qu, W., Obrycki, J.J., Meng, L., Zhou, X., Chu, D., 2020. Optimizing sample size for population genomic study in a global invasive lady beetle, *Harmonia axyridis. Insects.* 11, 1-12. https://doi.org/10.3390/insects11050290

Li, F., Zhang, J., Zhong, H., Chen, J., 2022. Germicide fenaminosulf promots gall formation of *Zizania latifolia* without directly affecting the growth of endophytic fungus *Ustilago esculenta. BMC Plant Biology*. 22, 1-13. https://doi.org/10.1186/s12870-022-03803-6

Luo, G.H., Li, X.H., Han, Z.J., Zhang, Z.C., Yang, Q., Guo, H.F., Fang, J.C., 2016. Transition and transversion mutations are biased towards gc in transposons of *Chilo suppressalis* (Lepidoptera: Pyralidae). *Genes.* 7, 1-12. https://doi.org/10.3390/genes7100072

Mageiros, L., Méric, G., Bayliss, S.C., Pensar, J., Pascoe, B., Mourkas, E., Calland, J.K., Yahara, K., Murray, S., Wilkinson, T.S., Williams, L.K., Hitchings, M.D., Porter, J., Kemmett, K., Feil. E.J., Jolley, K.A., Williams, N.J., Corander, J., Sheppard, S.K., 2021. Genome evolution and the emergence of pathogenicity in avian *Escherichia coli. Nature Communications.* 12, 1-13. https://doi.org/10.1038/s41467-021-22238-5

Modesto, I., Inácio, V., Novikova, P., Carrasquinho, I., Van de Peer, Y., Miguel, C.M., 2022. SNP detection in *Pinus pinaster* transcriptome and association with resistance to pinewood nematode. *Forests.* 13, 1-16. https://doi.org/10.3390/f13060946

Pootakham, W., Chanprasert, J., Jomchai, N., Sangsrakru, D., Yoocha, T., Therawattanasuk, K., Tangphatsornruang, S., 2011. Single nucleotide polymorphism marker development in the rubber tree, *Hevea brasiliensis* (Euphorbiaceae). *American Journal of Botany*. 98, 337–338. https://doi.org/10.3732/ajb.1100228

Pootakham, W., Uthaipaisanwong. P., Sangsrakru. D., Yoocha, T., Tragoonrung, S., Tangphatsornruang, S., 2013. Development and characterization of single-nucleotide polymorphism markers from 454 transcriptome sequences in oil palm (*Elaeis guineensis*). *Plant Breeding.* 132, 711-717. https://doi.org/doi.org/10.1111/pbr.12095

Pootakham, W., Shearman, J.R., Ruang-Areerate, P., Sonthirod, C., Sangsrakru, D., Jomchai, N., Yoocha, T., Triwitayakorn, K., Tragoonrung, S., Tangphatsornruang, S., 2014. Large-scale SNPs discovery through RNA sequencing and SNPs genotyping by targeted enrichment sequencing in cassava (*Manihot esculenta* Crantz). *PLoS ONE.* 9, 1-19. https://doi.org/10.1371/journal.pone.0116028

Pootakham, W., Areerate, P.R., Jomchai, N., Sansraku, D., Yoocha, T., Theerawattanasuk, K., Nirapathpongporn, K., Romruensukharom, P., Tragoonrung, S., Tangphatsornruang, S., 2015. Construction of a high-density integrated genetic linkage map of rubber tree (*Hevea brasiliensis*) using genotyping-by-sequencing (GBS). *Frontiers in Plant Science.* 6, 1-12. https://doi.org/10.3389/fpls.2015.00367

Setiadi, D., Susanto, M., Baskorowati, L., 2014. Gall rust disease defense attacks at progeny test of *Falcataria moluccana* in Bondowoso, East Java. *Jurnal Pemuliaan Tanaman Hutan*. 8, 1-13. https://doi.org/10.20886/jpth.2014.8.1.1-13

Shabrina, H., Siregar, U.J., Matra, D.D., Siregar, I.Z., 2019. The dataset of de novo transcriptome assembly of Falcataria moluccana cambium from gall-rust (*Uromycladium falcatarium*) infected and non-infected tree. *Data in Brief.* 26, 1-4. https://doi.org/10.1016/j.dib.2019.104489

Shao, T., Pan, Y.H., Xiong, X.D., 2021. Circular RNA: an important player with multiple facets to regulate its parental gene expression. *Molecular Therapy-Nucleic Acids.* 23, 369-376. https://doi.org/ 10.1016/j.omtn.2020.11.008

Shearman, J.R., Sangsrakru, D., Jomchai, N., Ruang-Areerate, P., Sonthirod, C., Naktang, C., Theerawattanasuk, K., Tragoonrung, S., Tangphatsornruang, S., 2015. SNPs identification from RNA sequencing and linkage map construction of rubber tree for anchoring the draft genome. *PLoS ONE.* 10, 1-12. https://doi.org/10.1371/journal.pone.0121961

Shrestha V, Awale M, Karn A. 2019. Genome wide association study (GWAS) on disease resistance in maize, in: Wani, S.H. (Eds.), *Disease Resistance in Crop Plants.* Springer, Cham, pp. 113–130. https://doi.org/10.1007/978-3-030-20728-1_6

Siregar, U.J., Rahmawati, D., Damayanti, A., 2019. Fingerprinting sengon (*Falcataria moluccana*) accessions resistant to boktor pest and gall rust disease using microsatellite markers. *Biodiversitas.* 20, 2698-2706. https://doi.org/10.13057/biodiv/d200935

Siregar, U.J., Nugroho, A., Shabrina, H., Indriani, F., Damayanti, A., Matra, D.D., 2021. De novo transcriptome assembly data for sengon (*Falcataria moluccana*) trees displaying resistance and susceptibility to boktor stem borers (*Xystrocera festiva* Pascoe). *BMC Research Notes.* 14, 1-4. https://doi.org/10.1186/s13104-021-05675-9.

Słomka, M., Sobalska, K.M., Wachulec, M., Bartosz, G., Strapagiel, D., 2017. High resolution melting (hrm) for high-throughput genotyping-limitations and caveats in practical case studies. *International Journal of Molecular Sciences.* 18, 1-21. https://doi.org/10.3390/ijms18112316

Studer, R.A., Dessailly, B.H., Orengo, C.A., 2013. Residue mutations and their impact on protein structure and function: detecting beneficial and pathogenic changes. *Biochemical Journal.* 449, 581-594. https://doi.org/10.1042/BJ20121221

Uchiyama, K., Ujino-Ihara, T., Ueno, S., Taguchi, Y., Futamura, N., Shinohara, K., Tsumura, Y., 2012. Single nucleotide polymorphisms in *Cryptomeria japonica*: their discovery and validation for genome mapping and diversity studies. *Tree Genetics and Genomes.* 8, 1213–1222. https://doi.org/10.1007/s11295-012-0508-5

Wanda, N., Barmawi, M., Akin, H.M., Sa'diyah, N., 2015. Segregation of resistance character of soybean (*Glycine max* [L]. Merrill) against soybean mosaic virus infection population F2 descendants of Taichung x Tanggamus. *Jurnal Penelitian Pertanian Terapan.* 15, 54-60. https://doi.org/10.25181/jppt.v15i1.112

Wellenreuther, M., Mérot, C., Berdan, E., Bernatchez, L., 2019. Going beyond SNPs: The role of structural genomic variants in adaptive evolution and species diversification. *Molecular Ecology.* 28, 1203-1209. https://doi.org/10.1111/mec.15066

Wu Y., Zhou Q., Huang S., Wang G., Xu L.A., 2019. SNP development and diversity analysis for Ginkgo biloba based on transcriptome sequencing. *Trees.* 33, 587-597. https://doi.org/10.1007/s00468-018-1803-z

Xu X., Chen C., Fan B., Chen Z., 2006. Physical and functional interactions between pathogen-induced Arabidopsis WRKY18, WRKY40, and WRKY60 transcription factors. *Plant Cell.* 18, 1310-26. https://doi.org/10.1105/tpc.105.037523.

Yu, H., Xie, W., Li, J., Zhou, F., Zhang, Q., 2014. A whole-genome SNPs array (RICE6K) for genomic breeding in rice. *Plant Biotechnology Journal.* 12, 28-37. https://doi.org/10.1111/pbi.12113

Yuskianti, V., Shiraishi, S., 2017. Genetic diversity of sengon (*Falcataria moluccana* Miq. Barneby & J.W. Grimes) revealed using single nucleotide polymorphism (SNPs) markers. *Indonesia Journal of Forestry Research.* 4, 85-94. https://doi.org/10.20886/ijfr.2017.4.2.85-94

Zhang, D., Zhang, Z., 2005. Single nucleotide polymorphisms (SNPs) discovery and linkage disequilibrium (LD) in forest trees. *Forestry studies in China.* 7, 1-14. https://doi.org/10.1007/s11632-005-0024-x

Zhu, F.Y., Chen, M.X., Ye, N.H., Qiao, W.M., Gao, B., Law, W.K., Tian, Y., Zhang, D., Zhang, D., Liu, T.Y., Hu, Q.J., Cao, Y.Y., Su, Z.Z., Zhang, J., Liu, Y.G., 2018. Comparative performance of the BGISEQ-500 and Illumina HiSeq4000 sequencing platforms for transcriptome analysis in plants. *Plant Methods.* 14, 1-14 . https://doi.org/10.1186/s13007-018-0337-0

Supplementary Materials

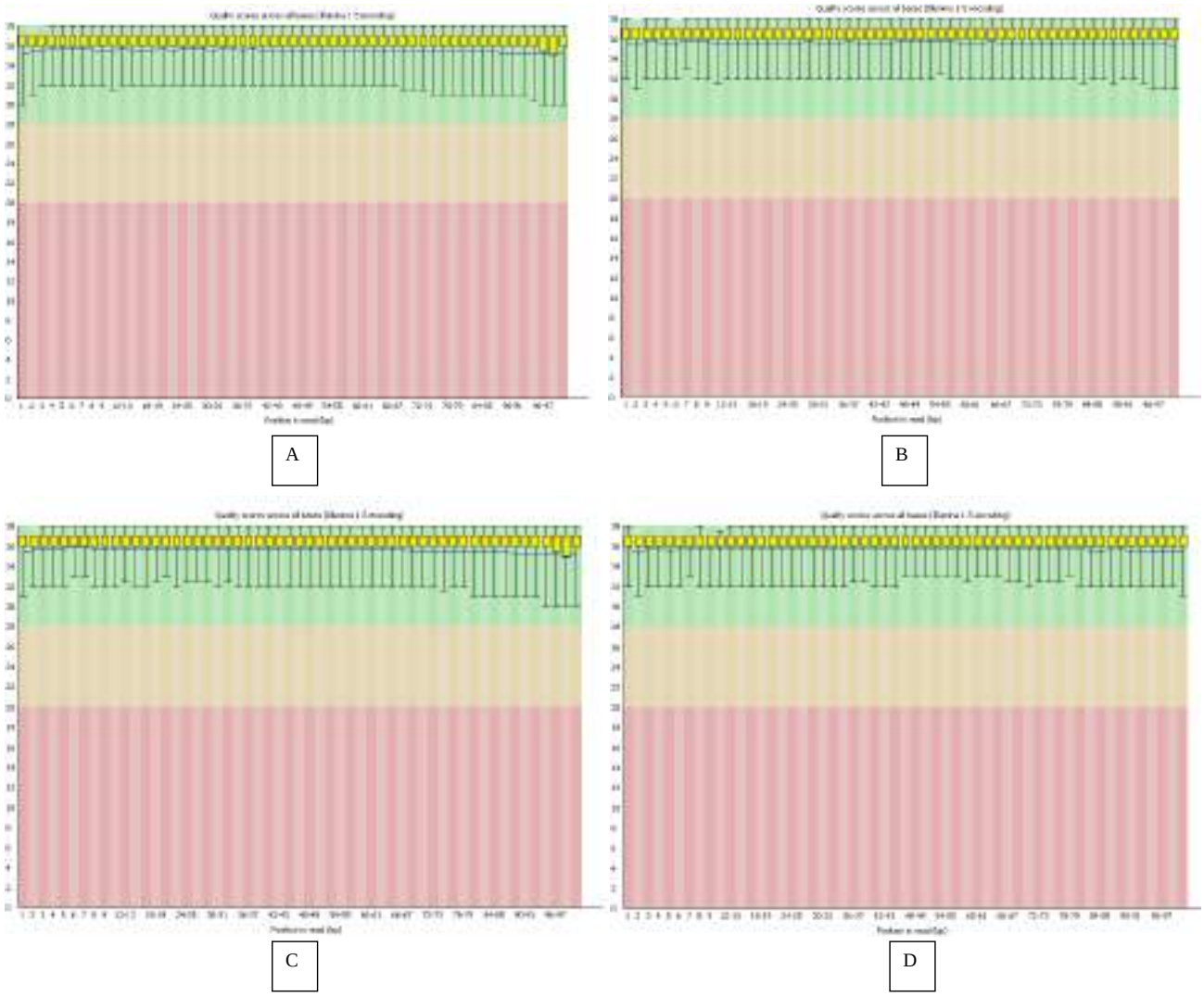

Supplementary Figure 1. Base quality of reads (A) boktor susceptible, (B) boktor resistant, (C) gall rust susceptible, (D) gall rust resistant

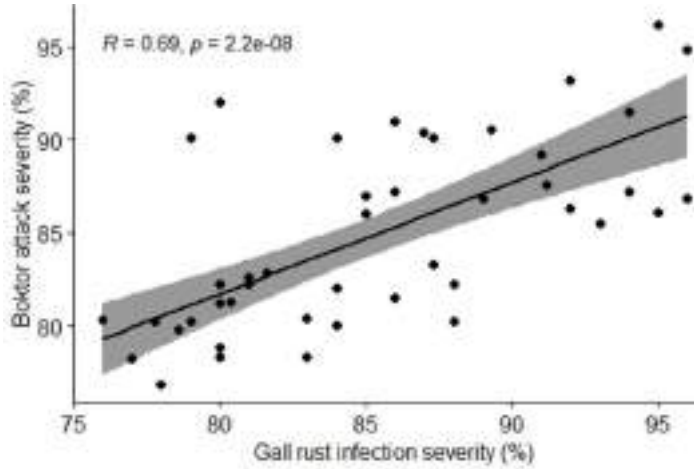

Supplementary Figure 2. Correlation analysis between the percentage of boktor attacks and gall rust infection

Supplementary Table 1. Number of reads before and after filtering

Reads name	Number of reads	
	Before filtering	After filtering
Boktor resistant	Boktor resistant	77,634,868
Boktor susceptible	Boktor susceptible	79,315,980
Rust resistant	Rust resistant	79,037,484
Rust susceptible	Rust susceptible	79,054,112
Rust on leaves 1	Rust on leaves 1	60,259,198
Rust on leaves 2	Rust on leaves 2	64,269,442
Rust on stem 1	Rust on stem 1	64,100,912
Rust on stem 2	Rust on stem 2	58,235,308

Supplementary Table 2. Characteristics of SNP primer developed

Name of gene	Primer code	SNPs position	Nucleotides (5'-3')
Alpha-amylase inhibitor	AAI_1	575 (C>T)	F: TATCCCAATCCGACGACAA R: CGGCTGACGAGAGTGAAG
	AAI_2	944 (G>T)	F: GGTGTCCTACAGAAGTGTGTCC R: CGACAGGAAGAGCATTACCA
Trypsin inhibitor	TI_1	771 (A>G)	F: TTGTGACTTGTGTGTTGATGTG R: CCCATCGGTTCTCTCTCTCT
	TI_2	850 (G>A)	F: AGGTAAGTGTGGACATGTTGGT R: ATGCCCAGGGATGTTTATTC
Indole-3-acetic acid-amido synthetase	IAA_1	568 (C>A)	F: GGAGTTGTCCCATTGAGGTT R: TGCTGTCACCCATTTGTCTC
	IAA_2	568 (C>A)	F: AGTTGTCCCATTGAGGTTGAG R: TGTCACCCATTTGTCTCCTTT
NADH-ubiquinone oxidoreductase	NUOR_1	3392 (C>T)	F: CTTGCTTGCACTGAGAGACC R: GCACGGGACACAGAATAAGA
	NUOR_2	674 (A>G)	F: AGGACACGGATAGAACACAAGA R: TGCGCTTCAAAGGTAATAGG
	NUOR_3	1954 (A>C)	F: GCGATGAGAGGCGAAATAG R: CGACCGACTAAGGGCAAA
Transcription factor WRKY 11	WRKY_11	3272 (C>G)	F: CTTTGACTGTTGACCCTTCCT R: GGCACCCTCACTGTCTTCTT
Transcription factor WRKY 40	WRKY_40	1052 (A>T)	F: AATTGAAACATGGAACAGGAAA R: GATGGGTATCAATGGAGGAAA
Ubiquitin carboxyl-terminal hydrolase 13	UB13_1	4058 (T>C)	F:CCGACATATCTTAGCTCCTCTTTC R: CACCTTGAGGAGACCCAATC
	UB13_2	4114 (A>C)	F: CCGACATATCTTAGCTCCTCTTT R: CACCTTGAGGAGACCCAATC

letters in the SNPs position column are nucleotide thymine (T), cytosine (C), guanine (G), and adenine (A). Symbol > refers to the changes of the reference base to the alternative base. F = forward, R = reverse

Supplementary Table 3. Results of amplification of SNP primers

Primer code	Expected product (bp)	product size (bp)	Result
AAI_1	124	143	Amplified
AAI_2	111	126	Amplified
TI_1	107	107	Amplified
TI_2	189	189	Amplified
IAA_1	123	150	Amplified
IAA_2	118	118	Amplified
NUOR_1	160	160	Amplified
NUOR_2	198	-	Unamplified
NUOR_3	126	146	Amplified
WRKY 11	170	200	Amplified
WRKY 40	216	226	Amplified
UB13_1	197	-	multiple bands
UB13_2	197	-	unamplified

Supplementary Table 4. HRM analysis results on each sample

Sample	TI_2	NUOR_1	NUOR_3	WRKY40	WRKY11	IAA_1	IAA_2
SUS							
1	wt (GG)	wt (CC)	mt (AA)	mt (AA)	mt (CG)	wt (CC)	wt (CC)
2	wt (GG)	mt (TT)	mt (CC)	mt (AA)	wt (CC)	wt (CC)	mt (AA)
3	mt (AA)	wt (CC)	mt (CC)	mt (AA)	wt (CC)	mt (AA)	wt (CC)
4	wt (GG)	wt (CC)	mt (CC)	mt (AA)	wt (CC)	mt (AA)	wt (CC)
5	wt (GG)	wt (CC)	mt (CC)	mt (AA)	mt (GG)	mt (AA)	wt (CC)
6	wt (GG)	wt (CC)	mt (CC)	mt (AA)	wt (CC)	mt (AA)	wt (CC)
7	mt (AA)	wt (CC)	mt (CC)	mt (AA)	wt (CC)	mt (AA)	mt (CA)
8	wt (GG)	wt (CC)	mt (CC)	mt (AA)	wt (CC)	mt (AA)	mt (CA)
9	wt (GG)	wt (CC)	mt (CC)	mt (AA)	wt (CC)	mt (AA)	wt (CC)
10	wt (GG)	wt (CC)	wt (AC)	mt (AA)	wt (CC)	wt (CC)	mt (AA)
11	wt (GG)	wt (CC)	mt (AA)	wt (AT)	wt (CC)	mt (CA)	wt (CC)
12	wt (GG)	wt (CC)	mt (CC)	wt (AT)	wt (CC)	mt (AA)	wt (CC)
13	mt (GA)	wt (CC)	mt (CC)	mt (AA)	wt (CC)	mt (AA)	wt (CC)
14	wt (GG)	wt (CC)	wt (AC)	mt (AA)	mt (CG)	mt (AA)	mt (CA)
15	wt (GG)	wt (CC)	wt (AC)	mt (AA)	wt (CC)	mt (CA)	mt (AA)
16	wt (GG)	wt (CC)	mt (AA)	mt (AA)	wt (CC)	mt (CA)	mt (AA)
17	wt (GG)	wt (CC)	mt (AA)	wt (AT)	wt (CC)	mt (CA)	mt (AA)
18	wt (GG)	wt (CC)	mt (CC)	wt (AT)	wt (CC)	mt (AA)	mt (AA)
19	wt (GG)	wt (CC)	mt (CC)	wt (AT)	wt (CC)	mt (AA)	mt (AA)
20	wt (GG)	mt (TT)	mt (CC)	wt (AT)	wt (CC)	mt (AA)	mt (AA)
21	wt (GG)	mt (TT)	mt (AA)	mt (AA)	wt (CC)	mt (AA)	mt (AA)
22	wt (GG)	mt (TT)	wt (AC)	mt (AA)	wt (CC)	mt (AA)	mt (AA)
23	wt (GG)	mt (TT)	wt (AC)	mt (AA)	wt (CC)	mt (AA)	mt (AA)
24	wt (GG)	mt (TT)	wt (AC)	mt (AA)	wt (CC)	mt (CA)	mt (AA)
25	wt (GG)	mt (TT)	wt (AC)	mt (AA)	wt (CC)	mt (CA)	mt (AA)
26	wt (GG)	wt (CC)	wt (AC)	mt (AA)	mt (CG)	mt (CA)	mt (CA)
27	wt (GG)	wt (CC)	mt (AA)	wt (AT)	mt (CG)	mt (CA)	mt (CA)
28	mt (GA)	wt (CC)	mt (CC)	wt (AT)	mt (CG)	mt (AA)	mt (CA)
29	mt (GA)	wt (CC)	mt (CC)	wt (AT)	mt (CG)	mt (AA)	mt (CA)
30	mt (GA)	wt (CC)	mt (CC)	wt (AT)	mt (CG)	mt (AA)	mt (CA)
31	mt (GA)	wt (CC)	mt (CC)	wt (AT)	wt (CC)	mt (AA)	mt (CA)
32	mt (GA)	mt (CT)	mt (CC)	wt (AT)	wt (CC)	mt (AA)	mt (CA)
33	mt (GA)	mt (CT)	mt (CC)	mt (AA)	mt (CG)	mt (AA)	mt (AA)
34	mt (GA)	mt (CT)	mt (CC)	mt (AA)	mt (GG)	mt (AA)	mt (AA)
35	mt (AA)	mt (CT)	mt (CC)	mt (AA)	mt (GG)	mt (AA)	mt (AA)
36	mt (AA)	mt (TT)	mt (CC)	mt (AA)	mt (GG)	mt (AA)	mt (AA)
37	mt (AA)	mt (TT)	mt (CC)	mt (AA)	mt (GG)	mt (AA)	mt (AA)
38	mt (AA)	mt (TT)	mt (AA)	wt (AT)	mt (GG)	mt (AA)	mt (AA)
39	mt (AA)	mt (TT)	mt (AA)	wt (AT)	wt (CC)	mt (AA)	mt (AA)
40	mt (AA)	mt (TT)	mt (CC)	mt (AA)	wt (CC)	mt (AA)	mt (AA)
41	mt (AA)	wt (CC)	mt (CC)	wt (AT)	wt (CC)	mt (AA)	mt (AA)
42	mt (AA)	wt (CC)	mt (CC)	wt (AT)	wt (CC)	mt (CA)	mt (CA)
43	mt (AA)	wt (CC)	mt (AA)	wt (AT)	wt (CC)	mt (CA)	mt (CA)
44	mt (AA)	wt (CC)	mt (CC)	wt (AT)	wt (CC)	mt (CA)	mt (CA)
45	mt (AA)	wt (CC)	mt (CC)	mt (AA)	wt (CC)	mt (CA)	mt (CA)
46	mt (AA)	wt (CC)	mt (CC)	mt (AA)	wt (CC)	mt (AA)	mt (CA)
47	mt (AA)	mt (TT)	mt (AA)	mt (AA)	wt (CC)	mt (AA)	mt (AA)
48	mt (AA)	mt (TT)	mt (CC)	mt (AA)	wt (CC)	mt (AA)	mt (AA)
49	mt (AA)	mt (TT)	wt (AC)	mt (AA)	wt (CC)	mt (AA)	mt (AA)
50	mt (AA)	mt (TT)	wt (AC)	wt (AT)	mt (GG)	mt (AA)	mt (AA)

SUS = susceptible, RES = resistant, wt = wild type, mt = mutant, C-G-A-T refers to Cytosine (C), Guanine (G), Adenine (A), and Thymine (T)

Supplementary Table 4. Continued

Sample	TI_2	NUOR_1	NUOR_3	WRKY40	WRKY11	IAA_1	IAA_2
RES							
1	wt (GG)	wt (CC)	mt (CC)	mt (AA)	wt (CC)	mt (AA)	wt (CC)
2	wt (GG)	wt (CC)	mt (CC)	mt (AA)	wt (CC)	mt (AA)	wt (CC)
3	wt (GG)	wt (CC)	mt (AA)	wt (AT)	wt (CC)	wt (CC)	wt (CC)
4	wt (GG)	wt (CC)	mt (CC)	mt (AA)	wt (CC)	mt (AA)	wt (CC)
5	wt (GG)	mt (CT)	wt (AC)	mt (AA)	wt (CC)	mt (AA)	wt (CC)
6	wt (GG)	wt (CC)	wt (AC)	wt (AT)	wt (CC)	mt (AA)	wt (CC)
7	wt (GG)	wt (CC)	mt (CC)	mt (AA)	wt (CC)	mt (AA)	wt (CC)
8	wt (GG)	wt (CC)	mt (CC)	mt (AA)	wt (CC)	mt (AA)	wt (CC)
9	wt (GG)	mt (CT)	mt (CC)	wt (AT)	wt (CC)	mt (AA)	wt (CC)
10	wt (GG)	mt (CT)	mt (CC)	mt (AA)	wt (CC)	mt (AA)	wt (CC)
11	wt (GG)	mt (TT)	mt (CC)	mt (AA)	wt (CC)	mt (AA)	wt (CC)
12	wt (GG)	wt (CC)	mt (AA)	mt (AA)	mt (CG)	wt (CC)	wt (CC)
13	wt (GG)	wt (CC)	wt (AC)	mt (AA)	mt (CG)	wt (CC)	wt (CC)
14	wt (GG)	wt (CC)	wt (AC)	wt (AT)	mt (CG)	wt (CC)	wt (CC)
15	wt (GG)	wt (CC)	wt (AC)	wt (AT)	mt (GG)	wt (CC)	wt (CC)
16	wt (GG)	wt (CC)	wt (AC)	wt (AT)	mt (GG)	mt (CA)	wt (CC)
17	mt (AA)	wt (CC)	wt (AC)	wt (AT)	mt (GG)	mt (CA)	wt (CC)
18	mt (AA)	wt (CC)	mt (CC)	mt (AA)	mt (GG)	mt (CA)	wt (CC)
19	mt (AA)	mt (CT)	mt (AA)	mt (AA)	mt (CG)	mt (CA)	wt (CC)
20	mt (AA)	mt (CT)	mt (AA)	mt (AA)	mt (CG)	wt (CC)	wt (CC)
21	wt (GG)	mt (CT)	mt (AA)	mt (AA)	mt (GG)	wt (CC)	wt (CC)
22	wt (GG)	mt (CT)	mt (CC)	mt (AA)	mt (GG)	wt (CC)	wt (CC)
23	wt (GG)	mt (CT)	mt (CC)	mt (AA)	mt (GG)	wt (CC)	wt (CC)
24	wt (GG)	mt (CT)	mt (CC)	mt (AA)	mt (GG)	wt (CC)	wt (CC)
25	wt (GG)	mt (CT)	mt (CC)	mt (AA)	mt (CG)	mt (CA)	wt (CC)
26	wt (GG)	wt (CC)	mt (CC)	mt (AA)	mt (CG)	mt (CA)	wt (CC)
27	mt (AA)	wt (CC)	mt (CC)	mt (AA)	wt (CC)	wt (CC)	mt (CA)
28	mt (AA)	wt (CC)	mt (CC)	wt (AT)	wt (CC)	wt (CC)	mt (CA)
29	wt (GG)	wt (CC)	mt (CC)	wt (AT)	wt (CC)	mt (CA)	mt (CA)
30	wt (GG)	wt (CC)	mt (CC)	wt (AT)	wt (CC)	mt (CA)	mt (CA)
31	wt (GG)	wt (CC)	mt (AA)	wt (AT)	wt (CC)	mt (CA)	mt (CA)
32	wt (GG)	wt (CC)	mt (AA)	wt (AT)	wt (CC)	mt (CA)	mt (CA)
33	mt (GA)	mt (TT)	mt (AA)	wt (AT)	wt (CC)	wt (CC)	wt (CC)
34	mt (GA)	mt (TT)	mt (AA)	wt (AT)	wt (CC)	wt (CC)	wt (CC)
35	mt (GA)	mt (TT)	mt (CC)	wt (AT)	wt (CC)	wt (CC)	wt (CC)
36	mt (GA)	mt (TT)	mt (CC)	wt (AT)	mt (CG)	mt (CA)	wt (CC)
37	mt (GA)	mt (TT)	mt (CC)	wt (AT)	mt (CG)	mt (CA)	wt (CC)
38	mt (GA)	mt (TT)	mt (CC)	wt (AT)	mt (CG)	mt (CA)	mt (AA)
39	mt (GA)	mt (TT)	mt (CC)	wt (AT)	mt (GG)	mt (CA)	mt (AA)
40	mt (GA)	mt (TT)	mt (CC)	mt (AA)	mt (GG)	mt (CA)	mt (AA)
41	mt (GA)	mt (CT)	mt (CC)	mt (AA)	mt (GG)	mt (CA)	mt (AA)
42	mt (GA)	mt (CT)	mt (CC)	mt (AA)	mt (GG)	mt (CA)	mt (AA)
43	mt (GA)	mt (CT)	mt (CC)	mt (AA)	mt (GG)	mt (CA)	mt (CA)
44	mt (AA)	mt (CT)	mt (CC)	mt (AA)	mt (GG)	wt (CC)	mt (CA)
45	mt (AA)	mt (CT)	mt (CC)	mt (AA)	mt (GG)	wt (CC)	mt (CA)
46	mt (GA)	mt (TT)	mt (CC)	mt (AA)	mt (CG)	wt (CC)	mt (CA)
47	mt (GA)	wt (CC)	mt (CC)	mt (AA)	mt (CG)	wt (CC)	mt (CA)
48	mt (GA)	wt (CC)	mt (CC)	mt (AA)	mt (CG)	wt (CC)	mt (AA)
49	mt (AA)	wt (CC)	wt (AC)	mt (AA)	mt (CG)	mt (CA)	mt (AA)
50	mt (AA)	wt (CC)	wt (AC)	wt (AT)	mt (CG)	mt (CA)	mt (AA)

SUS = susceptible, RES = resistant, wt = wild type, mt = mutant, C-G-A-T refers to Cytosine (C), Guanine (G), Adenine (A), and Thymine (T)

HAYATI
Journal of Biosciences

Vol. 31 No. 1, January 2024 133-144
DOI:10.4308/hjb.31.1.133-144
ISSN: 1978-3019
EISSN: 2086-4094

The First Evidence of Potential Antibacterial Activity of Laccase Enzyme from Indonesian White Rot Fungi against Pathogenic Bacteria

Sita Heris Anita[1*], Deni Zulfiana[1], Ananda Digita[2], Nafisah Nuha[2], Vilya Syafriana[2], Amelia Febriani[2], Dede Heri Yuli Yanto[1]

[1]Research Center for Applied Microbiology, National Research and Innovation Agency Republic of Indonesia, Cibinong, Indonesia
[2]Department of Pharmacy, National Institute of Science and Technology, South Jakarta, Jakarta Capital Special Region, Indonesia

ARTICLE INFO

Article history
Received June 13, 2023
Received in revised form September 15, 2023
Accepted October 4, 2023

KEYWORDS
Antibacterial activity,
Laccase enzyme,
Trametes hirsuta,
Leiotrametes menziesii,
Lentinus sajor-caju

ABSTRACT

The antibacterial agent can be extracted from plants, animals, and microorganisms such as fungi. The potential antibacterial activity of laccase derived from fungi remains limited in current reports. This study aimed to investigate the characteristics of laccase from Indonesian white rot fungi (WRF) and explore its potential as an antibacterial agent. The laccases were produced by *Trametes hirsuta* D7, *Trametes hirsuta* EDN 082, *Leiotrametes menziesii* BRB 73, and *Lentinus sajor-caju* BRB 12 using oil palm empty fruit bunch as a substrate. The results showed that the Indonesian WRF tested produced brownish-yellow laccase. FTIR analysis demonstrated similar peak patterns but distinct absorption intensities among the laccases. *Trametes hirsuta* D7 gained 0.044 U/ml of the greatest laccase activity. Laccase, with minimal activity of 0.001 U/ml–0.026 U/ml, suppressed the propagation of *Propionibacterium acnes* and *Staphylococcus aureus. Escherichia coli* and *Pseudomonas aeruginosa* could be inhibited by the laccase with a minimum activity of 0.002 U/ml–0.044 U/ml. However, *S. aureus* and *E. coli* showed the Minimum Bactericidal Concentration in the laccase activity range of 0.018 U/ml–0.308 U/ml. Gram-positive and Gram-negative bacteria grow more slowly when the laccase is present, supposed the laccase as a potential antibacterial agent.

1. Introduction

Infectious disease is still a health issue. Poor hygiene, which promotes the growth of pathogenic bacteria in the environment, is one of the causes of infectious diseases. Pathogenic bacteria are parasitic bacteria that cause disease in their hosts. Diarrhea, digestive tract infections, respiratory tract infections, bladder tract infections, skin lining infections that cause acne, and other diseases are caused by pathogenic bacteria (Hou *et al.* 2022). Pathogenic bacteria commonly found include *Escherichia coli, Salmonella enterica, Propionibacterium acnes, Citrobacter rodentium, Pseudomonas aeruginosa, Listeria monocytogenes*, and *Staphylococcus aureus* (Baumler and Sperandio 2016; McLaughlin *et al.* 2019; Widowati *et al.* 2021). The spread of pathogenic bacteria can be slowed by inhibiting their growth with antibacterial compounds such as antibiotics. However, the current overuse of antibiotics causes issues such as the emergence of multidrug-resistant organisms. Antibacterial compounds are not only used in the medical and pharmaceutical fields but also in other industries such as food, agriculture, and cosmetics. It is typically used as a preservative to inhibit the development of microorganisms in goods that could compromise product quality (Mahmud and Khan 2018).

Antibiotic alternatives include the use of extracts of natural ingredients from plants, animals, or microorganisms that contain active compounds such as alkaloid compounds (AlSheikh *et al.* 2020; Stan *et al.* 2021). Groups of enzymes that include protease, lipase, amylase, cellulase, peroxidase, trypsin, lysozyme, and laccase, in addition to extracts of natural components, exhibit antibacterial activities (Charlotte *et al.* 2006; Aruwa *et al.* 2022). Laccase is a versatile enzyme that can degrade xenobiotic compounds, transform antibiotics and

* Corresponding Author
E-mail Address: sita.heris.anita@brin.go.id

steroids, detoxify water, delignify pulp, and degrade wastewater dyes (Becker *et al.* 2016; Anita *et al.* 2020; Ramadhan *et al.* 2021; Yanto *et al.* 2021). Laccase is extensively present in higher plants (Dana *et al.* 2017), insects (Janusz *et al.* 2020), bacteria, and fungi (Bertrand *et al.* 2013). Laccases generated by microorganisms such as bacteria and fungi are easier to get since the enzyme is released outside the cell. Laccase generated by fungi has a higher redox potential than laccase produced by bacteria. The redox potential value is connected to the ability of these enzymes to digest high-molecular-weight substrates (Janusz *et al.* 2020).

Indonesia is known as a country with mega biodiversity for its flora, fauna, and microorganisms. The diversity of fungi in tropical rainforests ranks second after insects. Fungi are often found in the rainy season on decayed wood, litter, or as parasites in living plants (Khayati and Warsito 2016). Basidiomycota is a fungus with basidiocarps that grows in various shapes, colors, and sizes. White-rot fungi (WRF) are Basidiomycota, which colonize wood in nature and preferentially break down lignin to generate white rotting. Fungi cause three forms of wood decay: white rot, brown rot, and soft rot. These fungi are classified based on the pattern of decay on wood (Godell *et al.* 2008). WRF are the best lignin degraders. Their capacity to digest complex and resistant organic compounds makes them appealing microorganisms for the bioremediation of organically polluted soil as well as the decolorization of wastewater from the textile industry (Koyani *et al.* 2014; Yanto *et al.* 2021; Anita *et al.* 2022).

A previous study has shown that *T. hirsuta* D7 successfully decomposes chrysene, benzo[a]pyrene, and phenanthrene (Hidayat and Yanto 2018). *Trametes hirsuta* EDN 082, *Leiotrametes menziesii* BRB 73, and *Lentinus sajor-caju* BRB 12 proved a good capability to remove the colored textile dyes of anthraquinone, monoazo, and diazo (Anita *et al.* 2022; Nurhayat *et al.* 2022). Charlotte *et al.* (2006) discovered that laccase generated by the fungus *Myceliophtera thermophila* and *Polyporus pinisitus* with activity levels ranging from 0.1 to 5 mg/L could suppress the propagation of Gram-positive bacteria *Staphylococcus epidermidis* and Gram-negative bacteria *Pseudomonas aeruginosa*. Laccase from *M. thermophila* that was immobilized onto bacterial nanocellulose can inhibit the growth of Gram-positive bacteria *Staphylococcus aureus* and Gram-negative bacteria *Escherichia coli* as much as 92% and 26%, respectively (Sampaio *et al.* 2016). Verma *et al.* (2019) also reported that both crude and purified laccase enzymes produced from the bacteria *Pseudomonas putida* LUA15.1 inhibited the growth of fungal plant and bacterial pathogens. However, the antibacterial property of the laccase from white rot fungi has never been examined.

The purpose of this research is to characterize the laccase produced by white rot fungi *Trametes hirsuta* D7, *Trametes hirsuta* EDN 082, *Leiotrametes menziesii* BRB 73, and *Lentinus sajor-caju* BRB 12, and to evaluate its antibacterial activity against various pathogenic bacteria. This research used pathogenic bacteria such as *Staphylococcus aureus, Propionibacterium acnes, Pseudomonas aeruginosa*, and *Escherichia coli.* The antibacterial activity was determined using diffusion and dilution methods to obtain the Minimum Inhibitory Concentration (MIC) and Minimum Bactericidal Concentration (MBC) of laccase against pathogenic bacteria.

2. Materials and Methods

2.1. Substrate, Microbes, and Chemical Components

OPEFB (Oil Palm Empty Fruit Bunch) was collected from an oil palm farm in Cikasungka, West Java, Indonesia., Indonesia. *Trametes hirsuta* D7 (NCBI GenBank, accession No. KX444204) was previously isolated from a peat swamp forest region in Riau, Indonesia. *Trametes hirsuta* EDN 082 (NCBI GenBank, accession No. MT476912) was isolated from Taman Eden 100, Toba Samosir, North Sumatra, Indonesia. *Leiotrametes menziesii* BRB 73 (NCBI GenBank, accession No. MT804553) and *Lentinus sajor-caju* BRB 12 (NCBI GenBank, accession No. OR050821) were isolated from Berbak-Sembilang National Park, Jambi, and South Sumatra, Indonesia. Isolates of *Pseudomonas aeruginosa* ATCC 15442 and *Escherichia coli* ATCC 8739 were obtained from the IPBCC (IPB Culture Collection). *Staphylococcus aureus* ATCC 29213 and *Propionibacterium acnes* ATCC 27853 were purchased from the Indonesian retail market. Malt extract, potato dextrose agar (PDA), peptone, sodium acetate, glucose, ammonium sulfate ($(NH_4)_2SO_4$), and $CuSO_4$ were provided from Merck (Germany). Wako (Japan) supplied the acetic acid. Himedia (India) provided the nutrient agar (NA), nutrient broth (NB), Bradford reagent, and Bovine Serum Albumin (BSA), while Sigma Aldrich provided the 2,2-azino-bis-[3-ethyl benzothiazoline-6-sulphonic acid] (ABTS).

2.2. Fungal Cultivation and Production of Laccase

Fungal culture and laccase synthesis were carried out using the technique described by Ningsih *et al.* (2020), with modifications to the weight of the substrate employed. *Trametes hirsuta* D7, *Trametes hirsuta* EDN 082, *Leiotrametes menziesii* BRB 73, and *Lentinus sajor-caju* BRB 12 were separately cultivated on a PDA medium (39 g/L) and culture for 7 d at room temperature (27±3°C). Laccase was produced via solid-state fermentation using 5 g of OPEFB fiber in 100 ml of Erlenmeyer. The OPEFB substrate was then treated with up to 10 ml of malt extract-glucose-peptone (MGP) medium that consisted of 20 g/L malt extract, 20 g/L glucose, 1 g/L peptone, and 2 mM $CuSO_4$ to increase its moisture content to 60% and induce laccase synthesis, respectively. After sterilizing the mixture for 15 min at 121°C, they were cooled to room temperature. Six plugs (5 mm) of the PDA fungal colony were injected into the sterilized substrate and cultured for 10 d at room temperature.

2.3. Crude Laccase Extraction

Crude laccase extraction was carried out according to Anita *et al.* (2020). After the incubation period, the fermented solid substrates were fully extracted in a homogenizer at a speed of 10,000 rpm for 10 min in a cool environment with 15 ml of 0.1 M acetate buffer, pH 4.5. The mixtures were then filtered through filter fabric. The filtrates were centrifuged at 4°C, 8,000 rpm for 20 min and the supernatant was treated with $(NH_4)_2SO_4$ to produce a 40-60% (w/v) saturated solution. The solution was mixed for 1 h before being centrifuged at 4°C, 8,000 rpm for 20 min. After that, 15 ml of 0.1 M acetate buffer, pH 4.5 was added to the pellet. The crude laccases were then kept at –20°C. For concentrated enzyme, the enzyme solution was placed in an ultrafiltration membrane 10 kDa (YM-10 Amicon, USA) and centrifuged at 4°C, 10,000 rpm for 10 min (Anita *et al.* 2022). The solution retained on the ultrafiltration membrane is the concentrated crude enzyme and is stored at –20°C.

2.4. Laccase Characterization

Laccase color, functional groups, enzyme activity, protein content, and enzyme-specific activity were characterized. The colors of laccase analysis were conducted according to Bahanawan *et al.* (2019). The color of the enzymes produced was compared to commercial enzyme color and the absorbance of both colors was measured using a microplate reader (TECAN Infinite 200 Pro, Switzerland) at 300–500 nm. Color values were also measured using a Konica Minolta CR-10 Plus colorimeter with a D65 lighting source specification, a photodiode array sensor, and a 10° observer standard. Color value (E*) is a quantitative description of color. The color analysis used the CIE-Lab method. The color value was calculated using Eq. 1. (Bahanawan *et al.* 2019).

$$E^* = \sqrt{(L^*)^2 + (a^*)^2 + (b^*)^2} \qquad (1)$$

Where:
E * = color value
L * = brightness
a * = redness, and
b * = yellowness

The functional groups of the crude laccase were analyzed based on the procedure used by Samui and Sahu (2018) and Yanto *et al.* (2021) using Fourier Transform Infrared (FTIR) (Perkin-Elmer) at 400–4,000 nm and 32 scans. The bands were shown in baseline mode. Laccase enzyme activities were determined using the procedure used by Anita *et al.* (2020). The spectrophotometric method was employed to evaluate the activity of laccase. This was achieved by monitoring the oxidation of 1 mM 2,2-azino-bis-[3-ethyl benzothiazoline-6-sulphonic acid] (ABTS) in 0.05 M acetate buffers at a pH of 4.5. The measurements were taken at a wavelength of 420 nm for a duration of 1 minute, while maintaining a room temperature environment. The test combination comprised of 100 µL of the sample, 400 µL of 0.1 M acetate buffer, and 500 µL of 2 mM ABTS. The unit of enzyme activity (U) was established as the quantity of enzyme necessary to catalyze the oxidation of 1 µmol of ABTS per minute. While protein content was determined using the Bradford technique (Bradford 1976). Protein concentrations were measured in milligrams per milliliter (mg/ml). The protein standard in this research was bovine serum albumin (BSA) (1 mg/ml). The specific activity of the enzyme was calculated using Eq. 2. (Ningsih *et al.* 2020).

$$\text{Enzyme specific activity}\left(\frac{U}{mg}\right) = \frac{\text{Enzyme activity}\left(\frac{U}{ml}\right)}{\text{Protein content}\left(\frac{mg}{ml}\right)} \qquad (2)$$

2.5. Antibacterial Activity Test

A bacterial culture with a 10^8 CFU/ml cell count was used for the antibacterial activity assay. The bacterial culture was added to the sterile NA medium that had not yet solidified (medium temperature, 40°C) in amounts up to 1% (v/v) and carefully mixed. Then the media containing the bacterial culture were poured into the sterilized petri dish and allowed to set. Furthermore, on the solid medium, wells were made using a cork borer (Ø5 mm). 20 µl of Laccase enzyme samples (laccase from *T. hirsuta* D7, *T. hirsuta* EDN 082, *Leiotrametes menziesii* BRB 73, and *Lentinus sajor-caju* BRB 12) were added separately to each well, and chloramphenicol (CAP) 30 µg/ml used as a positive control. The plates were placed in an incubator for 24 h at 35±2°C. By measuring the clear area formed surrounding the hole, the inhibition zone in the medium was estimated (Modarresi-Chahardehi *et al.* 2012). Antibacterial inhibition zone activity was classified into categories: weak (less than 5 mm), average (5–10 mm), strong (10–20 mm), and extremely strong (over 20–30 mm) (Rahayu *et al.* 2021).

2.6. Analysis of The Minimum Inhibitory Concentration (MIC)

The MIC was obtained using the liquid dilution technique according to Modarresi-Chahardehi *et al.* (2012) with modification in the dilution series. The enzymes and sterile NB media were diluted in the following ratios: 2:0, 1.6:0.4, 1.2:0.8, 0.8:1.2, 0.4:1.6, 0.2:1.8, and 0.05:1.95 (ml). Each dilution of the enzyme sample was put into a microplate with as much as 500 µL and 25 µL of bacterial suspension (10^8 CFU/ml). As a positive control, 500 µL of NB liquid medium was added to 25 µL of bacterial suspension (10^8 CFU/ml) in a microplate. Cultures were incubated in an incubator for 24 h at 35±2°C. After 24 h, each sample's absorbance was measured by using a microplate reader at 660 nm. The lowest concentration that can inhibit bacteria was indicated by the absence of turbidity after incubation.

2.7. Analysis of The Minimum Bactericidal Concentration (MBC)

As much as 100 µL of bacterial isolates from the results of MIC incubation were spread into Nutrient Agar (NA) medium in sterilized dishes. Cultures were incubated in an incubator at 35±2°C for 24 h. The lowest concentration that can kill bacteria was shown by the absence of microbial growth on the agar media after incubation (Modarresi-Chahardehi *et al.* 2012).

2.8. Statistical Analysis

The assay was performed with three replicates. The data were subjected to analysis of variance (one-way ANOVA) and the means were compared using Tukey's test at the 5% level.

3. Results

3.1. Characterization of Laccase Enzyme

T. hirsuta D7, *T. hirsuta* EDN 082, *Leiotrametes menziesi*i BRB 73, and *Lentinus sajor-caju* BRB 12 produces a brownish-yellow laccase. Meanwhile, the commercial laccase enzyme is white (Figure 1A). The laccase enzymes produced by the four fungi were more intense in color compared to commercial enzymes. The laccase enzyme from *T. hirsuta* D7 showed a higher color spectrum than the other enzymes (Figure 1B). In contrast, the color value of the laccase enzyme from *T. hirsut*a D7 is the lowest at 53.29±0.10 when compared to the color values of other laccase enzymes. The E values of laccase produced by the four fungi ranged between 53.29 to 62.29. While commercial laccase has a value of 91.93±1.15 (Table 1).

The laccase enzyme FTIR spectrum and identified bonds are shown in Figure 2 and summarized in Table 2. Characteristic bands of the commercial laccase were identified at 3298 cm^{-1} (O-H/N-H stretching), which corresponds to carbonyl groups and amide A structure; a peak at 2922 cm^{-1} (C-H/N-H stretching) attributed to CH_2 groups present in laccase protein; a peak at 1642 cm^{-1} (C = O / C - N stretching) from amide I with a β-sheet structure; a peak 1360 cm^{-1} (N-H bending/C-N stretching) from amide III bands, a peak at 1015 cm^{-1} (C-N/C–O–C) characteristic of protein in laccase; and a peak at 572 cm^{-1} (C = O bending) from amide V.

Laccase from *T. hirsuta* D7 and *T. hirsuta* EDN 082 showed the same peak. These laccases contained peaks that were not present in commercial ones, particularly around 3033/3061 to 3179 cm^{-1} (N-H stretching) from amide B and 1553/1555 cm^{-1} (N-H

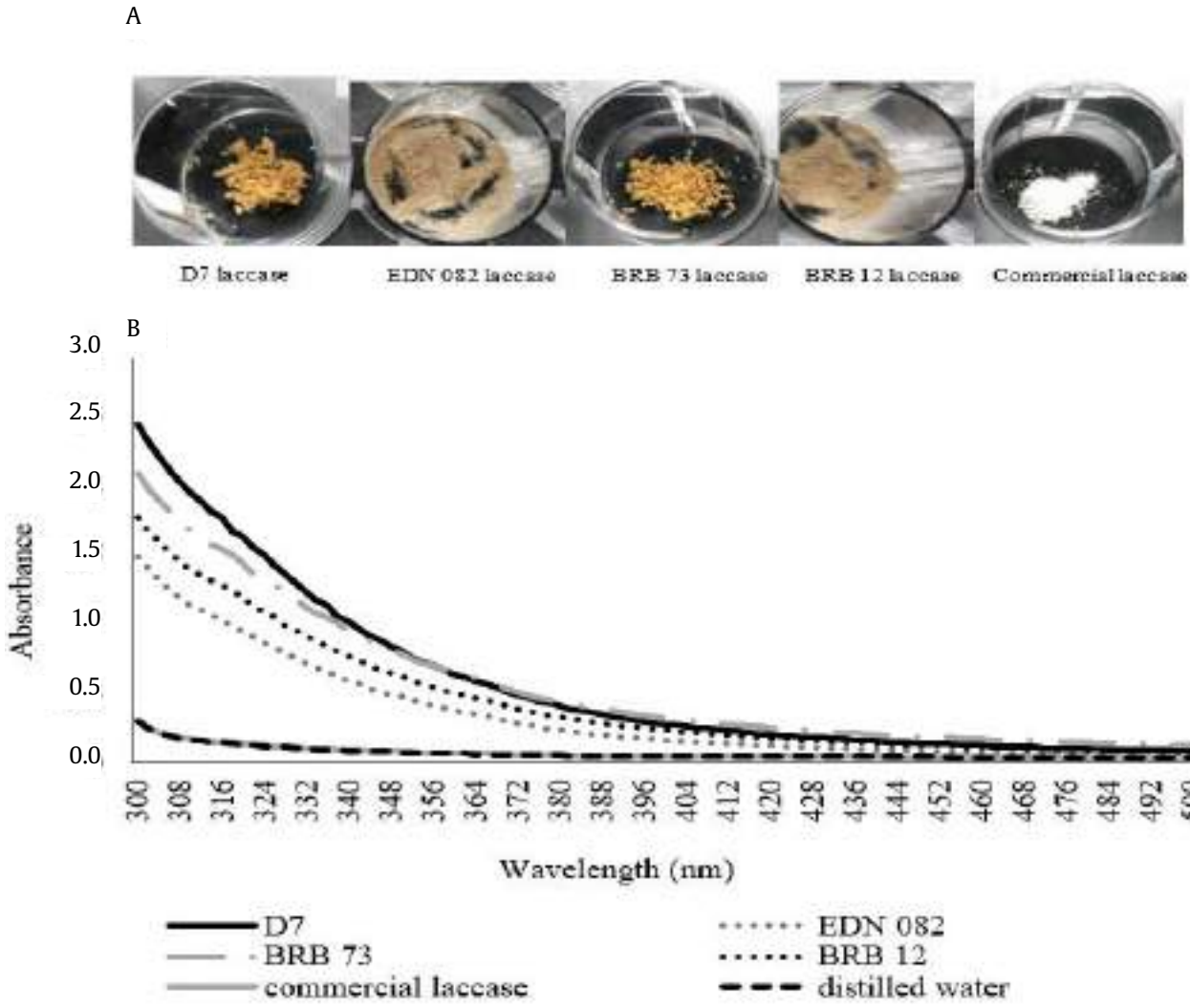

Figure 1. The color (A) and the UV-Vis spectrum (B) of the laccase enzyme

Table 1. Color value of laccase enzyme

Laccase enzyme	L (brightness)	a (redness)	b (yellowness)	E (color value)
D7	52.13±0.45[a]	10.13±0.21[b]	19.60±0.35[b]	53.29±0.47[a]
EDN 082	59.27±1.16[b]	10.00±0.17[b]	24.80±0.56[c]	60.31±1.16[b]
BRB 73	54.13±0.45[a]	10.03±0.15[b]	19.60±0.26[b]	55.23±0.46[a]
BRB 12	61.27±1.16[b]	10.07±0.15[b]	24.67±0.67[c]	62.29±1.15[b]
Commercial	91.90±0.10[c]	-0.43±0.06[a]	5.40±0.00[a]	91.92±0.09[c]

The mean value followed by the same letter is not significantly different according to Tukey (HSD) test at the 0.05 significance level

bending/C-N stretching) from the amide II band. However, some peaks were identical to those of commercial laccases, especially peaks at 1062/1068 cm^{-1} as the characteristic of protein in laccase and 608/609 cm^{-1} from amide V bands.

The peaks of BRB 12 and BRB 73 laccases show a similar pattern. *Leiotrametes menziesii* BRB 73 and *Lentinus sajor-caju* BRB 12 laccases also contained peaks that did not appear in commercial laccases. The peaks are at 3028/3030 cm^{-1} to 3193/3197 cm^{-1} from the amide B and 1553 cm^{-1} from the amide II band. BRB 12 and BRB 73 laccases have peaks at 1276/1280 cm^{-1} to 1403/1404 cm^{-1}, 1069/1094 cm^{-1}, and 609/610 cm^{-1} attributed to the amide III bands,

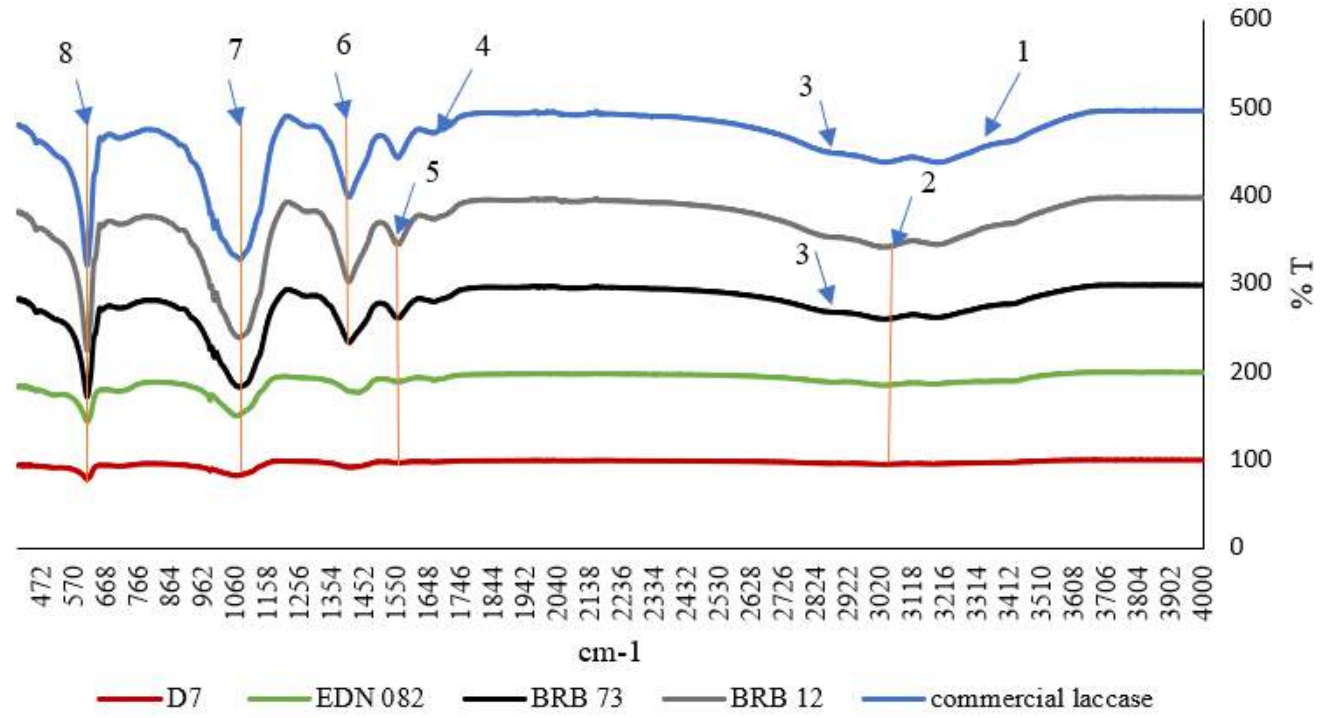

Figure 2. Laccase enzyme FTIR spectrum

Table 2. Functional groups of laccase enzyme FTIR spectrum

D7 laccase	EDN 082 laccase	BRB 12 laccase	BRB 73 laccase	Commercial laccase	Functional group assignment (references)	Class compound
Wave number (cm^{-1})						
-	-	-	-	3298	O-H stretching, N-H stretching	Carbonyl group, Amide A
3061	3179-3033	3193-3028	3197-3030	-	N-H stretching	Amide B
-	-	-	2851	2922	C-H stretching, N-H stretching	CH_2 group
-	-	-	-	1642	C=O stretching vibration, C-N stretching vibration	Amide I with a β-sheet structure
1555	1553	1553	1553	-	N-H bending,C-N stretching vibration	Amide II bands
-	-	1403-1280	1404-1276	1360	N-H bending, C-N stretching	Amide III bands
1062	1068	1069	1094	1015	C-N stretching, C–O–C stretching	Protein in laccase, Aromatic amine
608	609	609	610	572	C=O bending	Amide VI bands

characteristic of protein in laccases, and the amide VI band, respectively. The three peaks are identical to those of commercial laccases.

The maximum laccase enzyme activity was obtained in *Trametes hirsuta* D7, which was 0.044 U/mL. In contrast, the protein content of *T. hirsuta* D7 laccase was lower than that of other fungi. Due to this, the laccase from *T. hirsuta* D7 has the greatest specific enzyme activity compared to the other laccases. The ultrafiltration technique increased the activity of concentrated laccase enzymes up to 12 times. Table 3 describes the laccase enzyme in greater depth.

3.2. Antibacterial Activity

The width of the inhibitory area was used to evaluate the bacteria-static effect of the laccase enzyme (Table 4). The results showed that almost all of the inhibition zones for crude laccase enzyme from fungi were less than 7 mm in diameter. However, once the enzyme was concentrated, the width of the inhibitory zone over *S. aureus, P. acnes, P. aeruginosa*, and *E. coli* increased from 7 to 12 mm.

3.3. Minimum Inhibitory Concentration (MIC)

Table 5 shows the MIC values of the laccase enzyme against various bacterial species, indicating antibacterial activity. Laccase activity isolated from *T. hirsuta* D7 ranged from 0.001U/ml to 0.044 U/ml, whereas that of *T. hirsuta* EDN 082 ranged from 0.001 U/ml to 0.009 U/ml. Laccase activity from *Leiotrametes menziesii* BRB 73 and *Lentinus sajor-caju* BRB 12 was 0.002–0.028 U/ml and 0.001–0.01 U/ml, respectively. In general, minimal laccase enzyme concentrations of 0.001 to 0.015 U/ml suppressed *S. aureus* growth.

The concentration of laccase enzyme necessary to suppress the growth of *P. acnes* was higher, at 0.002–0.026 U/ml. The growth of *P. aeruginosa* could be suppressed with a minimal laccase concentration of 0.004–0.026 U/ml. Meanwhile, the lowest laccase enzyme concentration required to inhibit *E. coli* growth is 0.002–0.044 U/ml.

3.4. Minimum Bactericidal Concentration (MBC)

Table 6 shows the MBC value of the laccase enzymes. The MBC value for *S. aureus* was a laccase enzyme with activity between 0.018 U/ml and 0.112

Table 3. The characterization of laccase enzyme produced by *T. hirsuta* D7, *T. hirsuta* EDN 082, *Leiotrametes menziesii* BRB 73, and *Lentinus sajor-caju* BRB 12

Parameter	D7	EDN 082	BRB 73	BRB 12
Crude enzyme activity (U/ml)	0.044	0.009	0.028	0.010
Crude protein content (mg/ml)	18.36	22.67	22.34	21.10
Crude enzyme-specific activity (U/mg)	0.0020	0.0004	0.0013	0.0005
Concentrated enzyme activity (U/ml)	0.308	0.112	0.076	0.018
Concentrated protein content (mg/ml)	25.10	20.95	24.88	25.40
Concentrated enzyme-specific activity (U/mg)	0.012	0.005	0.003	0.0007

Table 4. Inhibition zone of laccase enzyme against *S. aureus, P. acnes, P. aeruginosa,* and *E. coli*

Laccase enzyme	Crude enzyme				Concentrated enzyme			
	Inhibition zone (mm)				Inhibition zone (mm)			
	S. aureus	*P. acnes*	*P. aeruginosa*	*E. coli*	*S. aureus*	*P. acnes*	*P. aeruginosa*	*E. coli*
D7	0.0±0.0^{a}	4.5±2.5^{b}	0.0±0.0^{a}	5.0±0.0^{a}	8.0±0.0^{ab}	7.0±0.0^{a}	10.0±0.0^{a}	7.7±0.6a
EDN 082	1.0±0.0^{a}	5.0±0.0^{b}	0.0±0.0^{a}	5.0±0.0^{a}	8.0±0.0^{ab}	9.0±0.0^{b}	10.0±0.0^{a}	7.5±0.5a
BRB 73	6.5±0.1^{c}	1.0±0.0^{a}	1.0±0.1^{a}	5.0±0.0^{a}	9.0±1.0^{b}	7.0±0.0^{a}	12.0±1.0^{b}	9.0±1.0^{ab}
BRB 12	4.5±0.2^{b}	0.0±0.0^{a}	0.0±0.0^{a}	5.0±0.0^{a}	7.0±0.0^{a}	7.5±0.5^{a}	10.0±0.0^{a}	7.7±0.6^{a}
Chloramphenicol (CAP)	12.3±1.3^{d}	13.0±0.0^{c}	19.3±1.2^{b}	11.0±1.7^{b}	12.3±1.3^{c}	13.0±0.0^{c}	19.3±1.2^{c}	11.0±1.7^{b}

The mean value followed by the same letter is not significantly different according to Tukey (HSD) test at the 0.05 significance level

Table 5. Minimum Inhibitory Concentration (MIC) of laccase enzyme against bacterial strain

Laccase	Gram type	Test organism	Minimal inhibitory concentration (MIC)		
			Enzyme activity (U/ml)	Protein content (mg/ml)	Specific activity (U/mg)
T. hirsuta D7	Gram (+)	*S. aureus*	0.015	3.67	0.0040
		P. acnes	0.026	7.35	0.0040
	Gram (-)	*P. aeruginosa*	0.015	3.67	0.0040
		E. coli	0.026	7.35	0.0040
T. hirsuta EDN 082	Gram (+)	*S. aureus*	0.001	4.53	0.0002
		P. acnes	0.004	9.07	0.0004
	Gram (-)	*P. aeruginosa*	0.004	9.07	0.0004
		E. coli	0.006	13.60	0.0004

Table 5. Continued

Laccase	Gram type	Test organism	Minimal inhibitory concentration (MIC)		
			Enzyme activity (U/ml)	Protein content (mg/ml)	Specific activity (U/mg)
Leiotrametes menziesii BRB 73	Gram (+)	*S. aureus*	0.003	4.47	0.0006
		P. acnes	0.006	8.94	0.0007
	Gram (-)	*P. aeruginosa*	0.014	13.96	0.0010
		E. coli	0.003	4.47	0.0006
Lentinus sajor-caju BRB 12	Gram (+)	*S. aureus*	0.002	4.22	0.0005
		P. acnes	0.002	8.44	0.0002
	Gram (-)	*P. aeruginosa*	0.008	13.19	0.0006
		E. coli	0.002	4.22	0.0005

Table 6. Minimum bactericidal concentration (MBC) of laccase enzyme against bacterial strain

Laccase	Gram type	Test organism	Minimum bactericidal concentration (MBC)		
			Enzyme activity (U/ml)	Protein content (mg/ml)	Specific activity (U/mg)
T. hirsuta D7	Gram (+)	*S. aureus*	0.044	18.36	0.002
		P. acnes	-	-	-
	Gram (-)	*P. aeruginosa*	-	-	-
		E. coli	0.308	25.10	0.012
T. hirsuta EDN 082	Gram (+)	*S. aureus*	0.112	20.95	0.005
		P. acnes	-	-	-
	Gram (-)	*P. aeruginosa*	-	-	-
		E. coli	0.112	20.95	0.005
Leiotrametes menziesii BRB 73	Gram (+)	*S. aureus*	0.076	24.88	0.003
		P. acnes	-	-	-
	Gram (-)	*P. aeruginosa*	-	-	-
		E. coli	0.076	24.88	0.003
Lentinus sajor-caju BRB 12	Gram (+)	*S. aureus*	0.018	25.40	0.001
		P. acnes	-	-	-
	Gram (-)	*P. aeruginosa*	-	-	-
		E. coli	0.018	25.40	0.001

U/ml. Meanwhile, greater laccase enzyme activities (0.018 to 0.308 U/ml) were required to kill *E. coli* bacteria completely. However, the laccase enzyme in the activity range of 0.018–0.308 U/ml could not kill *P. acnes* and *P. aeruginosa* bacteria.

4. Discussion

Four enzymes produced by four distinct microorganisms were investigated as antibacterial agents. Laccases are produced by *Trametes hirsuta* D7, *Trametes hirsuta* EDN 082, *Leiotrametes menziesii* BRB 73, and *Lentinus sajor-caju* BRB 12. The laccase enzymes produced by these different kinds of fungi have distinct properties. The laccases generated by all the fungi exhibited a brownish-yellow hue. This color contrasts with the commercial laccase enzyme from *Trametes versicolor*, which is white. The brown color appears because the extracted laccase enzyme has not been purified like commercial laccase; therefore, there are still numerous impurities that may be found in the crude laccase. Dhevagi *et al.* (2021) reported that the crude enzyme mixtures are complex, multielement, and consist of nonenzymatic proteins as well as secondary metabolites. The color of crude enzymes can also be caused by the residual fermentation medium used to cultivate enzyme-producing microorganisms. Crude enzymes from culture broth, including the growth media, organisms (whole or fragmented), and enzymes of interest (Robinson 2015). Zaccaria *et al.* (2019) used activated carbon to pre-treat crude enzyme extract to remove colors and inhibiting compounds. The UV-Vis spectra of crude laccase from four fungi were compared to the spectra of commercial enzymes and distilled water to evaluate the color intensity of the crude enzymes. Crude laccase from *T. hirsuta* D7 has the highest color

absorption compared to laccase from other fungi. Even the absorbance of commercial enzymes is comparable to distilled water's color absorption. A high absorbance value implies a higher quantity of substances, making the exhibited color darker (Neldawati *et al.* 2013). The color values (E) of the laccase enzyme generated by four white rot fungi were lower than those of commercial laccase, indicating that the laccase produced is less bright. In this study, the color values of laccase are related to lightness and yellowness values. Other studies have found a correlation between increased lightness (L) and yellowness (b) and higher E values, but not redness (a) levels (Bahanawan *et al.* 2019).

Enzymes are proteins that are composed of amino acids connected by one or more peptide bonds. Protein-peptide bonds are amide groups. Protein-peptide linkages are amide groups. In an IR spectrum between 4000 and 400 cm^{-1}, protein-containing samples show 9 unique vibrational absorption bands caused by various vibrational modes of the amide groups of proteins, notably amides A, B, and I-V (Bart 2007; Ji *et al.* 2020; Sadat and Joye 2020). The amide A, absorbing between 3500 and 3270 cm^{-1}, arises from N-H stretching vibration. While amide B absorbs weakly between 3100 and 3030 cm^{-1} (Bart 2007; Ji *et al.* 2020). Around 1600 and 1700 cm^{-1}, amide I vibrations absorb significantly and are particularly sensitive to the secondary protein structure. The amide II band absorbs at around 1550 cm^{-1} due to a combination of C-N stretching and N-H bending motions (Chatterley *et al.* 2022). The interaction of the N-H bending and the C-N stretching vibrations gives rise to the amide III bands between 1420 and 1200 cm^{-1} (Bart 2007; Samui and Sahu 2018). The amide IV and amide V areas are represented by absorption bands at 625–770 cm^{-1} and 640–800 cm^{-1}, respectively. The band of absorption at 537–606 cm^{-1} is associated with the amide VI regions because of the out-of-plane C = O bending (Darwish and Darwish 2022).

Laccase enzyme, as a protein, mostly exhibits peaks from nine distinct vibrational absorption bands in the IR spectrum. However, laccase's characteristic bands were identified at 1624 and 1690 cm^{-1} (amide I), 1420-1210 cm^{-1} (amide III), 1165–948 cm^{-1} (characteristic of protein in laccase), and at 800–500 cm^{-1} (amide V and VI) (Samui and Sahu 2018; Yanto *et al.* 2021). The peaks that were characterized as laccase were also seen in the laccase generated by the four fungi in this investigation. Laccase from *T. hirsuta* D7 and *T. hirsuta* EDN 082 showed the same peaks in the spectra at 155-153 cm^{-1} (amide II) and 609-608 cm^{-1} (amide VI). Meanwhile, the peaks laccase from *Leiotremetes menziesii* BRB 73 were more comparable to the laccase from *Lentinus sajor-caju* BRB 12. They shared the same peaks at 1404–1276 cm^{-1} (amide III) and 610–609 cm^{-1} (amide VI). Several peaks differed when the laccase IR spectra of the four fungi were compared to commercial *T. versicolor* laccase. The commercial laccase of *T. versicolor* has a peak at 1642 cm^{-1} (amide I), 1360 cm^{-1} (amide III), and 572 cm^{-1} (amide VI).

The differences in the peaks achieved could be because laccase was produced by different species of fungi, so the functional groups of the proteins tend to be slightly different. Nandiyanto *et al.* (2019) explained that the fingerprint area (600–1500 cm^{-1}) tends to be unique and distinct for any compound. However, the laccase produced by the four fungi shows a peak at 1094–1062 cm^{-1}, indicating the protein properties of the laccase enzyme.

Trametes hirsuta D7 produced the highest crude laccase enzyme activity with the lowest protein content compared to laccase from other species of fungi. As a result, *T. hirsuta* D7 laccase showed the greatest specific activity. Specific activity determines the purity of the enzymes in the mixture. It is the quantity of product generated by an enzyme in a specific period under specific circumstances per milligram of total proteins. The value increases when the amount of protein in an enzyme preparation decreases. At the same time, the reaction rate remains constant or may increase due to less interference or the elimination of inhibitors (Robinson 2015).

The crude laccase extract was then concentrated, and the laccase produced by *T. hirsuta* D7 enhanced its enzyme activity by up to 12-fold. *Trametes hirsuta* D7-specific laccase enzyme activity rises in proportion to enzyme activity. The findings of this study can be compared to those of earlier investigations. Laccase activity from *Aspergillus nidulans* increases 5.5-fold after the ultrafiltration process (Vivekanandan *et al.* 2014). Laccase activity after the ultrafiltration process compared to crude enzyme broth extracted from *Pleurotus sajor-caju* PS-2001 also increased 14-fold (Zaccaria *et al.* 2019). A 20-fold concentration of crude laccase by *Trametes*

versicolor was obtained using a UF membrane (10 kDa) (Antecka *et al.* 2019). After ultrafiltration, the crude enzyme laccase generated by *Pleurotus ostreatus* increases enzymatic activity by 6.6-fold. (Nguyen *et al.* 2020). Ultrafiltration membranes were shown to be effective in eliminating bigger particles from the medium and in concentrating certain enzymes (Zaccaria *et al.* 2019).

Laccase enzyme bactericidal activity was tested using *S. aureus, P. acnes, P. aeruginosa*, and *E. coli*. The clear zone generated surrounding the hole was used to determine the antibacterial action. The zone of bacterial growth inhibition was measured in millimeters. Crude laccase enzymes from *T. hirsuta* D7, *T. hirsuta* EDN 082, *Leiotrametes menziesii* BRB 73, and *Lentinus sajor-caju* BRB 12 created an inhibitory zone in the weak to moderate category. After the laccase enzyme was concentrated, it created an inhibitory zone ranging from moderate to strong. Li *et al.* (2019) also reported that the diameter of the inhibition zone of laccase-catalyzed chitosan–gallic acid derivative against *E. coli* and *S. aureus* was 11.36 and 12.65 mm, respectively, indicating the strong antibacterial activity of laccase. Rahayu *et al.* (2021) classified antibacterial inhibition zone activity into categories: weak (less than 5 mm), average (5–10 mm), strong (10–20 mm), and extremely strong (over 20–30 mm).

The diffusion approach was used in this study to detect the antibacterial properties of the laccase enzymes; however, it was unable to quantify the number of enzymes that inhibited or killed bacterial growth. As a result, the MIC of the laccase enzyme was measured to identify the lowest laccase concentration required to inhibit the growth of the bacterial strains, including *Staphylococcus aureus, Propionibacterium acnes* (Gram-positive bacteria) and *Pseudomonas aeruginosa, Escherichia coli* (Gram-negative bacteria). The crude extract laccase enzyme produced by the four fungi suppressed the propagation of pathogenic bacteria, with MIC values that ranged from 0.001 to 0.026 U/ml for Gram-positive bacteria and 0.002 to 0.044 U/ml for Gram-negative bacteria (Table 5). Li *et al.* (2019) also reported that *S. aureus* was slightly more sensitive to laccase-catalyzed chitosan–gallic acid derivative than *E. coli.* The activity of the laccase enzyme to suppress Gram-negative bacteria was greater than that to suppress Gram-positive bacteria. This is probably due to the more complex structure of the cell wall and outer membrane in Gram-negative bacteria which play a role in the mechanism of their resistance to exposure to antibacterial agents. Gram-negative bacteria have a wall and an outer complex membrane while having low levels of peptidoglycan, which contributes to their resilience (Sampaio *et al.* 2016; Besufekad *et al.* 2017).

Crude extract laccase enzyme exhibited poor bactericidal activity against pathogenic bacteria. Therefore, greater laccase enzyme activity from concentrated laccase is required to kill bacteria completely. MBC values ranging from 0.018 to 0.308 U/ml indicated their ability to kill *S. aureus* and *E. coli*. However, higher laccase enzyme activity was needed to kill *P. acnes* and *P. aeruginosa*. Many previous studies have found differences in laccase reactivity of the same or different types of fungi on various substrates. One of the elements influencing the differential in reactivity to the substrate is the laccase enzyme's molecular mass (Mansur *et al.* 2003). In general, the antibacterial process can be triggered for numerous reasons, including destroying or disrupting the molecules that constitute the bacterial wall, removing cell components, and carrying out processes that disturb the function of genetic material. Bioactive substances can disrupt the synthesis of RNA and DNA, causing harm to the resulting genetic material. Inhibition of bacterial growth can also occur due to the inhibition of enzymes by microbes, resulting in the destabilization of the cytoplasmic membrane found in these bacteria (Aruwa *et al.* 2022). The antibacterial activity of laccases is attributed to their method of action, which involves an electrochemical process that enables them to enter the cell walls of microbes. This penetration leads to the leaking of important metabolites and the physical disruption of crucial cell activities (Sampaio *et al.* 2016). Apart from the type of bacteria, the effectiveness of the antibacterial compounds of the enzymes is greatly influenced by the characteristics of the enzymes, such as their molecular mass and subunits (Mansur *et al.* 2003).

In conclusion, the four crude laccase enzymes produced by the Indonesian white rot fungi *Trametes hirsuta* D7, *Trametes hirsuta* EDN 082, *Leiotrametes menziesii* BRB 73, and *Lentinus sajor-caju* BRB 12 exhibited inhibitory effects on both Gram-positive and Gram-negative bacteria. The effectiveness of inhibition was found to be correlated with the

laccase activities employed in the experiment. The activity of the concentrated laccase enzyme increased by up to 12-fold, demonstrating its capability to eradicate *Propionibacterium acnes* and *Pseudomonas aeruginosa*. These significant findings contribute to the exploration of native Indonesian white rot fungi as potential sources of antibacterial enzymes.

Acknowledgements

The project was funded by the National Research and Innovation Agency Republic of Indonesia (BRIN) and used the facility of the Integrated Laboratory for Bioproducts (ILaB) BRIN, through E-Layanan Sains BRIN, Indonesia.

References

AlSheikh, H.M.A., Sultan, I., Kumar, V., Rather, I.A., Al-Sheikh, H., Tasleem Jan, A., Haq, Q.M.R., 2020. Plant-based phytochemicals as possible alternative to antibiotics in combating bacterial drug resistance. *Antibiotics.* 9, 480. https://doi.org/10.3390/antibiotics9080480

Anita, S.H., Ardiati, F.C., Oktaviani, M., Sari, F.P., Nurhayat, O.D., Ramadhan, K.P., Yanto, D.H.Y., 2020. Immobilization of laccase from *Trametes hirsuta* EDN 082 in light-expanded clay aggregate for decolorization of Remazol Brilliant Blue R dye. *Bioresour. Technol. Rep.* 12, 100602. https://doi.org/10.1016/j.biteb.2020.100602

Anita, S.H., Ardiati, F.C., Ramadhan, K.P., Laksana, R.P.B., Sari, F.P., Nurhayat, O.D., Yanto, D.H.Y., 2022. Decolorization of synthetic dyes by tropical fungi isolated from Taman Eden 100, Toba Samosir, North Sumatra, Indonesia. *Hayati J. Biosci.* 29, 417–427. https://doi.org/10.4308/hjb.29.4.417-427

Antecka, A., Blatkiewicz, M., Boruta, T., Górak, A., Ledakowicz, S., 2019. Comparison of downstream processing methods in purification of highly active laccase. *Bioprocess Biosyst. Eng.* 42, 1635–1645. https://doi.org/10.1007/s00449-019-02160-3

Aruwa, C.E., Amoo, S.O, Koorbanally, N., Kudanga, T., 2022. Laccase-mediated modification of isorhamnetin improves antioxidant and antibacterial activities. *Process Biochem.* 112, 53-61. https://doi.org/10.1016/j.procbio.2021.11.019

Barth, A., 2007. Infrared spectroscopy of proteins. *Biochim. Biophys. Acta.* 1767, 1073–1101. https://doi.org/10.1016/j.bbabio.2007.06.004

Bahanawan, A., Kusumah, A.A., Darmawan, T., Ismadi, Masruchin, N., Sudarmanto, Jayadi, Pramasari, D.A., Triwibowo, D., Kusumaningrum, W.B., Wibowo, E.S., Syamani, F.A., Krishanti, N.P.R.A., Lestari, E., Amin, Y., Sufiandi, S., Syahrir, A., Dwianto, W., 2019. Moisture content, color quantification and starch content of oil palm trunk (*Elaeisguineensis* Jacq.). *IOP Conf. Series: Earth Environ. Sci.* 374, 012041. https://doi.org/10.1088/1755-1315/374/1/012041

Baumler, A, Sperandio, V., 2016. Interactions between the microbiota and pathogenic bacteria in the gut. *Nature.* 535, 85–93. https://doi.org/10.1038/nature18849

Becker, D., Giustina, S.V.D., Mozaz, S.R., Schoevaart, R., Baecelo, D., Cazes, M.D., Belleville, M.O., Marcano, J.S., Gunzburg, J.D., Couillerot, O., Volker, J., Oelhmann, J., Wagner, M., 2016. Removal of antibiotics in wastewater by enzymatic treatment with fungal laccase–degradation of compounds does not always eliminate toxicity. *Bioresour. Technol.* 219, 500–509. https://doi.org/10.1016/j.biortech.2016.08.004

Bertrand, B., Martínez-Morales, F., Trejo-Hernández, M.R., 2013. Fungal laccases : induction and production. *Rev. Mex. Ing. Quím.* 12, 473–488.

Besufekad, S.Y., Mekdes, M., Abebech, M., Delesa, D., Tekalign, D., Demitu, K., Birtukan, B., 2017. The antimicrobial activity of leaf extracts of *Myrtus communis. J. Microb. Biochem. Technol.* 9, 290–292. https://doi.org/10.4172/1948-5948.1000380

Bradford, M.M., 1976. A rapid and sensitive method for the quantitation of microgram quantities of protein utilizing the principle of protein-dye binding. *Anal. Biochem.* 72, 248-254.

Chatterley, A., Laity, P., Holland, C., Weidner, T., Woutersen, S. Giubertoni, G., 2022. Broadband multidimensional spectroscopy identifies the amide II vibrations in silkworm films. *Molecules*. 27, 6275. https://doi.org/10.3390/molecules27196275

Charlotte, J., Hjelholt, P., Crone, F., 2006. Antimicrobial activity of laccases. *European Patent.* 561, 1–34.

Dana, M., Khaniki, G. B., Mokhtarieh, A. A., Davarpanah, S. J., 2017. Biotechnological and industrial applications of laccase: a review. *J. Appl. Biotechnol. Rep.* 4, 675–679.

Darwish, S.M., Darwish, I.M., 2022. Spectroscopic investigation of TAU protein conformational changes by static magnetic field exposure. *J. Phys. Commun.* 6, 075004. https://doi.org/10.1088/2399-6528/ac7d3a

Dhevagi, P., Ramya, A., Priyatharshini, S., Geetha Thanuja, K., Ambreetha, S., Nivetha, A., 2021. Industrially important fungal enzymes: productions and applications, in: Yadav, A.N. (Eds.), *Recent Trends in Mycological Research*. Springer, Cham, pp. 263–309. https://doi.org/10.1007/978-3-030-68260-6_11

Goodell, B., Qian, Y., Jellison, J., 2008. Fungal decay of wood: soft rot, brown rot, white rot. *ACS Symposium Series*. 982, 9—31. https://doi.org/10.1021/bk-2008-0982.ch002

Hidayat, A., Yanto, D.H.Y., 2018. Biodegradation and metabolic pathway of phenanthrene by a new tropical fungus, *Trametes hirsuta* D7. *J. Environ. Chem. Eng.* 6, 2454–2460. https://doi.org/10.1016/j.jece.2018.03.051

Hou, K., Wu, Z.X., Chen, X.Y., Wang, J.Q., Zhang, D., Xiao, C., Zhu, D., Koya, J.B., Wei, L., Li, J., Chen, Z.S., 2022. Microbiota in health and diseases. *Signal Transduct. Target Ther.* 7, 135. https://doi.org/10.1038/s41392-022-00974-4

Janusz, G., Pawlik, A., Świderska-Burek, U., Polak, J., Sulej, J., Jarosz-Wilkołazka, A., Paszczyński, A., 2020. Laccase properties, physiological functions, and evolution. *Int. J. Mol. Sci.* 21, 966. https://doi.org/10.3390/ijms21030966

Ji, Y., Yang, X., Ji, Z., Zhu, L., Ma, N., Chen, D., Jia, X., Tang, J., Cao, Y., 2020. DFT-calculated IR spectrum amide I, II, and III band contributions of N-Methylacetamide fine components. *ACS Omega.* 5, 8572–8578. https://doi.org/10.1021/acsomega.9b04421

Khayati, L., H. Warsito, 2016. Keanekaragaman jamur kelas basidiomycetes di Kawasan lindung KPHP Sorong Selatan. *Prosiding Symbion.* 213–222.

Koyani, R.D., Sharma, R.K., Rajput, K.S., 2014. Biodegradation of synthetic textile dyes by Mn-dependent peroxidase produced by *Phanerochaete chrysosporium*. *Int. J. Environ. Sci.* 5, 652–663. https://doi.org10.6088/ijes.2014050100059

Li, K., Guan, G., Zhu, J., Wu, H., Sun, Q. 2019. Antibacterial activity and mechanism of a laccase-catalyzed chitosan–gallic acid derivative against *Escherichia coli* and *Staphylococcus aureus*. *Food Control.* 96, 234-243. https://doi.org/10.1016/j.foodcont.2018.09.021

Mahmud, J., Khan, R.A., 2018. Characterization of natural antimicrobials in food system. *Adv. Microbiol.* 8, 894–916. https://doi.org/10.4236/aim.2018.811060

Mansur, M., Arias, M.E., Copa-Patino, J.L., Flardh, M., Gonzales, A.E., 2003. The white-rot fungus *Pleurotusostreatus secretes* laccase isozymes with different substrate specificities. *Mycol.* 95, 1013–1020. https://www.jstor.org/stable/3761909

McLaughlin, J., Watterson, S., Layton, A.M., Bjourson, A.J., Barnard, E., McDowell, A., 2019. Propionibacterium acnes and Acne vulgaris: new insights from the integration of population genetic, multi-omic, biochemical, and host-microbe studies. *Microorganisms.* 7, 128. https://doi.org10.3390/microorganisms7050128

Modarresi-Chahardehi, A., Ibrahim, D., Sulaiman, S. F., Mousavi, L., 2012. Screening antimicrobial activity of various extracts of *Urtica dioica*. *Rev. Biol. Trop.* 60, 1567–1576. https://doi.org/10.15517/rbt.v60i4.2074

Nandiyanto, A.S.D., Oktiani, R., Ragadhita, R., 2019. How to read and interpret FTIR spectroscope of organic material. *Indones. J. Sci. Technol.* 4, 97–118. http://doi.org/10.17509/ijost.v4i1.15806.

Neldawati, Ratnawulan, Gusnedi, 2013. Analisis nilai absorbansi dalam penentuan kadar flavonoid untuk berbagai jenisdaun tanaman obat. *Pillar of Physics.* 2, 76–83.

Nguyen, L.N., Vu, M.T., Johir, M.A.H., Pathak, N., Zdarta, J., Jesionowski, T., Semblante, G.U., Hai, F.I., Nguyen, H.K.D., Nghiem, L.D., 2020. A Novel approach in crude enzyme laccase production and application in emerging contaminant bioremediation. *Processes.* 8, 648. https://doi.org/10.3390/pr8060648

Ningsih, F., Yanto, D. H. Y., Mangunwardoyo, W., Anita, S. H.,Watanabe, T., 2020. Optimization of laccase production from a newly isolated *Trametes* sp. EDN134. *IOP Conference Series: Earth Environ. Sci.* 572, 012024. https://doi.org/10.1088/1755-1315/572/1/012024

Nurhayat, O.D., Ardiati, F.C., Ramadhan, K.P., Anita, S.H., Okano H., Watanabe, T., Yanto, D.H.Y., 2022. Bioprospecting three newly isolated white rot fungi from Berbak Sembilang National Park, Indonesia for biodecolorization of anthraquinone and azo dyes. *Biodiversitas.* 23, 613–623. https://doi.org/10.13057/biodiv/d230201

Rahayu, E., Lahay, N., Jamilah., 2021. Antibacterial inhibition test against the combination extract of moringa leaf (*Moringa oliefera*) and basil leaf (*Ocimumbasilicum*) as a substitute for feed additive. *HAJAS.* 3, 85¬–94. https://doi.org/10.20956/hajas.V3i2.20074

Ramadhan, K.P., Anita, S.H., Oktaviani, M., Laksana, R.P.B., Sari, F.P., Nurhayat, O.D., Yanto, D.H.Y., 2021. Biodecolorization of anthraquinone and azo dyes by newly isolated Indonesia white-rot fungi. *Biosaintifika.* 13, 16–25.

Robinson, P.K., 2015. Enzymes: principles and biotechnological applications. *Essays Biochem.* 59, 1–41. https://doi.org/10.1042/BSE0590001

Sadat, A., Joye, I.J., 2020. Peak fitting applied to fourier transform infrared and raman spectroscopic analysis of proteins. *Appl. Sci.* 10, 5918. https://doi.org/10.3390/app10175918

Sampaio, L.M.P., Padrao, J., Faria, J., Silva, J.P., Silva C.J., Dourado, F., Zille, A. 2016. Laccase immobilization on bacterial nanocellulose membranes: Antimicrobial, kinetic and stability properties. *Carbohydr. Polym.* 145, 1-12. http://doi.org/10.1016/j.carbpol.2016.03.009

Samui, A., Sahu, S. K., 2018. One-pot synthesis of microporous nanoscale metal-organic frameworks conjugated with laccase as a promising biocatalyst. *New J. Chem.* 42, 4192–4200. https://doi.org/10.1039/c7nj03619a

Stan, D., Enciu, A-M., Mateescu, A.L., Ion, A.C., Brezeanu, A.C., Stan, D., Tanase, A., 2021. Natural compounds with antimicrobial and antiviral effect and nanocarriers used for their transportation. *Front. Pharmacol.* 12, 723233. https://doi.org/10.3389/fphar.2021.723233

Verma, A., Shirkot, P., Dhiman, K., Sharma, R., Chauhan, A. 2019. First evidence of a potential antimicrobial activity of bacterial laccase against various plant pathogens. *Natl. Acad. Sci. Lett.* 42, 5—8. https://doi.org/10.1007/s40009-018-0695-1

Vivekanandan, K.E., Sivaraj, S., Kumaresan, S., 2014. Characterization and purification of laccase enzyme from *Aspergillus nidulans* CASVK3 from vellar estuary southeast coast of India. *Int. J. Curr. Microbiol. Appl. Sci.* 3, 213–227.

Widowati, R., Handayani, S., Al Fikri, A.R., 2021. Phytochemical screening and antibacterial activities of senggani (*Melastomamalabathricum* L.) ethanolic extract leaves. *JIPI*. 26, 562–568. https://doi.org/10.18343/jipi.26.4.562

Yanto, D. H. Y., Guntoro, M. A., Nurhayat, O. D., Anita, S. H., Oktaviani, M., Ramadhan, K. P., Pradipta, M. F., Watanabe, T., 2021. Biodegradation and biodetoxification of batik dye wastewater by laccase from *Trameteshirsuta* EDN 082 immobilised on light expanded clay aggregate. *3 Biotech.* 1–13. https://doi.org/10.1007/s13205-021-02806-8

Zaccaria, S., Boff, N.A., Bettin, F., Dillon, A.J.P., 2019. Use of micro- and ultrafiltration membranes for concentration of laccase-rich enzymatic extract of *Pleurotussajor-caju* PS-2001 and application in dye decolorization. *Chem. Pap.* 73, 3085–3094. https://doi.org/10.1007/s11696-019-00845-3

HAYATI
Journal of Biosciences

Vol. 31 No. 1, January 2024 145-152
DOI:10.4308/hjb.31.1.145-152
ISSN: 1978-3019
EISSN: 2086-4094

Expression of *APP*, *CDK5*, and *AKT1* Gene Related to Alzheimer Disease in Brain of Long-tailed Macaques

Lis Rosmanah[1,2], Uus Saepuloh[1], Sela Septima Mariya[1,3], Irma Herawati Suparto[1,2,4], Wasmen Manalu[5], Adi Winarto[5], Huda Shalahudin Darusman[1,2,4,5*]

[1]*Primate Research Center, IPB University, Bogor, Indonesia*
[2]*Primatology Graduate School of IPB University, Bogor, Indonesia*
[3]*Center for Biomedical Research, National Research and Innovation Agency of Indonesia, CSC-Cibinong, Bogor, Indonesia*
[4]*Department of Chemistry, Faculty of Mathematics and Natural Sciences, IPB University, Bogor, Indonesia*
[5]*School of Veterinary Medicine and Biomedical Sciences, Bogor Agricultural University, Kampus IPB Dramaga, Bogor, Indonesia*

ARTICLE INFO

Article history
Received November 3, 2022
Received in revised form September 20, 2023
Accepted September 25, 2023

KEYWORDS
Alzheimer,
APP,
CDK5,
AKT1,
Long-tailed Macaques,
Amiloid Plaque

ABSTRACT

Amyloid plaques and Neurofibrillary Tangles (NFTs) are known to be key pathological features of Alzheimer disease. To gain a better understanding of this disease, studies were carried out on the Indonesian primates, the long-tailed macaques, using a spontaneous Alzheimer's disease model. Examining and identifying genetic markers involved in plaque formation and NFTs in long-tailed macaques is necessary to reveal their physiological processes. In this study, the expression of genes involved in the development of amyloid plaque (Amyloid Precursor Protein (*APP*)) and those that control the phosphorylation of tau protein (*CDK5* and *AKT1*) was examined in the long-tailed macaque brain. This study showed that *APP, CDK5*, and *AKT1* may potentially be developed as genetic markers of Alzheimer's disease. Long-tailed macaques exhibited the development of amyloid plaque in the aging brain based on the analysis of the gene expression profile of its biomarker. Furthermore, long-tailed macaques can be optimized for neurodegenerative models.

1. Introduction

Alzheimer's is one of the main causes of dementia, which reduces a person's capacity to carry out daily tasks due to cognitive decline and memory loss. WHO and Alzheimer's Disease International (ADI) reported that 35.6 million persons globally had Alzheimer's disease in 2010. This population is estimated to double by 2030 and triple by 2050, reaching an estimated 115 million individuals (World Health Organization 2012). Over one million cases of Alzheimer's were recorded in Indonesia in 2013, and this condition can continue to increase over time as the life expectancy of the Indonesian people increased (Ministry of Health Republic of Indonesia 2019).

Alzheimer's disease has been associated with beta-amyloid plaques, the main proteins in neuritis deposits and neurofibrillary tangles (NFTs). Beta-amyloid plaques resulting from proteolytic cleavage of the precursor protein amyloid glycoprotein (*APP*). The endoplasmic reticulum produces *APP*, which is then transported to the Golgi complex and then transported to the plasma membrane. Beta and gamma secretases cleave mature *APP* on the plasma membrane to make amyloid beta (Chen *et al.* 2017).

The physiological function of *APP* in the hippocampus has been thoroughly investigated in rodents (Del Turco *et al.* 2016), *APP* transgenic mice (Jia *et al.* 2017), and STZ-induced *Macaca fascicularis* (Park *et al.* 2015; Del Turco *et al.* 2016). NFT is a protein that experiences hyperphosphorylation due to changes in kinase or phosphate activity, which causes the formation of NFT (Bhaskar C *et al.* 2018). Amyloid plaques and NFTs can damage nearby healthy cells, resulting in cell death. Meanwhile, *CDK5* and *AKT1* are two genes linked to tau protein and are involved in the control of tau phosphorylation. *CDK5* increases tau phosphorylation, which in turn can lead to neurodegeneration. In addition, the enzyme's activity is controlled by the endogenous activator p35 *CDK5* kinase, which phosphorylates tau protein (Li *et al.* 2020).

* Corresponding Author
E-mail Address: hudada@apps.ipb.ac.id

Non-human primates have similar anatomy, pathology, and genetics to humans (Mariya *et al.* 2019; Darusman *et al.* 2021; Higo 2021). Primates are potential animal models to explore the molecular mechanism of amyloid plaque formation and tau protein (Darusman *et al.* 2014a; Park *et al.* 2015; Latimer *et al.* 2019). Older vervet monkeys naturally develop amyloid plaques in the cortex region, and paired helix filaments are discovered that help to generate NFTs. According to histology, amyloid plaques have also been found in the frontal, temporal, and parietal lobes, as well as the hippocampus, in the aged monkey's cerebral cortex (Nakamura *et al.* 1998; Darusman *et al.* 2014a).

To determine the occurrence of a physiological process of Alzheimer's disease, it is important to analyze the molecular mechanism based on genetic marker expression in an *APP*ropriate animal model. This study is an *APP*roach to discovering and understanding the underlying mechanisms of Alzheimer's disease using adult and aged long-tailed monkeys as translation in the human body. This study will also examine the expression of gene *APP*, *CDK5*, and *AKT1* in the adult and aged monkeys at the cortex and hippocampus brain region.

2. Materials and Methods

2.1. Samples Collection

The samples are brain tissue archives, where the location of Alzheimer's disease is linked with memory impairment and cognition of six female long-tailed macaques (*Macaca fascicularis*). These samples are divided into two groups: the adult group, which is sampled from animals 10–12 years old, and the old group, which is >15 years old. The animals are from the Primate Research Center Bogor Agricultural University (PRC IPB), West Java, Indonesia. Brain tissue areas are the cortical and hippocampus areas, which are used as samples and an archive stored in a freezer at -20°C in the IPB PRC Pathology Laboratory. Dental scaling is used to determine age (Darusman *et al.* 2014b). Age parameters are defined as adults (between 7 and 15 years) and aged (beyond 15 years) (Gartland *et al.* 2020). All examination was conducted in duplicate, and ethical clearance was obtained by Primates Research Center IPB University as PRC -19-A012.

2.2. RNA Extraction and cDNA Preparation

Total RNA was extracted from 2 mm^3 of cortical and hippocampus sections of 6 long-tailed monkeys using RNeasy Mini Kits (Qiagen, Hilden, Germany) following company procedures. Brain tissues were lysis with RLT buffer, and ethanol absolute was added. Purification was carried out by spin column and washed using RW and RPE buffer. RNAse Free Water elutes the RNA in the column and its concentration was measured using a Nanodrop 1,000 spectrophotometer (Thermofisher Scientific, USA). For the reverse transcription process, three ng/µL RNA was used as a template. According to company procedures, the cDNA synthesis process was carried out using the reverse transcriptase enzyme (Sensifast cDNA Synthesis Kit, Bioline, Meridian Bioscience, USA). A total amount of 10 ul RNA (3 ng/µL) was added to 4 ul RT buffer, 1 µL RT enzyme, and 5 µL nuclease-free water. The RT-PCR mix was then incubated in a thermocycler following the program at 25°C for 10 minutes, 42°C for 15 minutes, and 85°C for 5 minutes, while the cDNA was stored at 4°C.

2.3. RT-qPCR Amplification

The CFX Opus 96 instrument was used for the PCR amplification process (Biorad, USA). A total of 18 µL of a reaction containing 6 µL of Nucleotide Free Water (NFW), 10 µL of Sensifast Sybr mix (Bioline, Meridian Bioscience, USA), and 1µL (10 µM) of forward and reverse primers of *APP*, *CDK5*, *AKT1*, and beta-actin (ACTB) were used in each reaction (Table 1) (Park *et al.* 2015). The RT-qPCR process was carried out at 95°C for 2 minutes as predenaturation, 95°C for 10 seconds as denaturation, 55°C for 20 seconds as annealing, and 65°C for 10 seconds as extension and data collecting. This process was repeated for 40 cycles.

2.4. Data Analysis

The data from the analysis include the Relative Quantification (RQ) value, which was calculated with a 2-ΔCt formula using the Cycle Threshold (Ct) information from qPCR. This value was calculated to measure the mRNA expression level in fold-change after re-normalizing the ACTB housekeeping gene.

Data analysis adopted SPSS version 26 and Microsoft Excel. The Shapiro-Wilk test and genethe

Table 1. Gene target and primers used in this study modified from Park *et al.* (2015)

Gene symbol	Gene name	Primer Forward (F)/Reverse (R)
ACTB	Beta-actin	F: ACAGAGCCTCGCCTTTGC R: CACGATGGAGGGGAAGAC
CDK5	Cyclin-Dependent Kinase 5	F: CAGTGGCCCTCTATGACCAA R: CGTTCACCAGGGATGTTGTG
APP	Amyloid Precursor Protein	F: GCAAACTGAAACCTGGGAA R: TTCCTTCCCTTGCACAGTCT
AKT1	V-akt Murine Thymoma Viral Oncogene Homolog1	F: CCACGCTACTTCCTCCTCAA R: CGGATGATGAAGGTGTTGG
GAPDH	Glyceraldehyde-3-Phosphate Dehydrogenase	F: CAACAGCCTCAAGATCGTCAG R: ACTGTGGT/CATGAGTCCTTCC

Levene test were used to determine the normality and homogeneity of data, respectively. An independent t-test was then performed on the data to check for variations across areas and age groups.

3. Results

Analysis of the RT-qPCR-based relative mRNA levels of *APP*, *CDK5*, and *AKT1* gene in the cortex and hippocampus brain region of adult and aged long-tailed monkeys are presented in Figure 1. *APP* gene is implicated in the formation of beta-amyloid, while *CDK5* and *AKT1* contribute to the production of tau protein.

3.1. Expression Analysis of APP mRNA Gene in the Long-tailed Macaques Brain

The cortical region of the brain of aged monkeys compared to the adults in a quantitative test of *APP* gene expression, and the results revealed a 33-fold increase in gene expression, which was statistically significant at $p<0.05$. Although, not statistically different, expression of the *APP* gene in the hippocampal region of the adult monkeys' brain was 2.03 fold change higher than that of the aged monkeys. The result also showed that expression of the *APP* gene was 2.45-fold higher in the cortical region of the aged monkeys' brains than in the hippocampus region, but it is not statistically significant. However, expression of the *APP* gene was 26 times higher in the hippocampus region of the adult monkey brain than in the cortical region, which is significantly different, as indicated by $p<0.05$ (Figure 2).

3.2. Expression Analysis of CDK5 mRNA Gene in the Long-tailed Macaques Brain

CDK5 expression gene in both groups of monkeys was compared, and the result showed that the expression of *CDK5* gene in the adult monkeys' hippocampus area was 2.7 times higher. This result is statistically significantly different, as indicated by $p<0.05$. Meanwhile, expression of the *CDK5* gene in the cortical region of the brain of adult monkeys was 2.4 foldchange higher than the old cortex region, but not statistically significant.

3.3. Expression Analysis of AKT1 mRNA Gene in the Long-tailed Macaques Brain

The examination of *AKT1* gene expression results in the cortex region of adult and aged monkeys showed almost the same gene expression values. Meanwhile, gene expression in the hippocampal region of aged monkeys showed a 1.9 foldchange higher than adult monkeys but not significantly different.

4. Discussion

There were two significant results findings in this study, namely gene expression of the *APP* gene and expression of the *CDK5* gene. *APP* gene is related to the formation of peptide amyloid beta, and the significance found is in the cortex region, showing that gene expression in the cortex region is higher in aged monkeys. The results' significance statistically indicates a link between this gene's expression and the formation of senile plaques. These amyloid plaques form earlier in the cortex region, indicating that these formations occur in age monkeys.

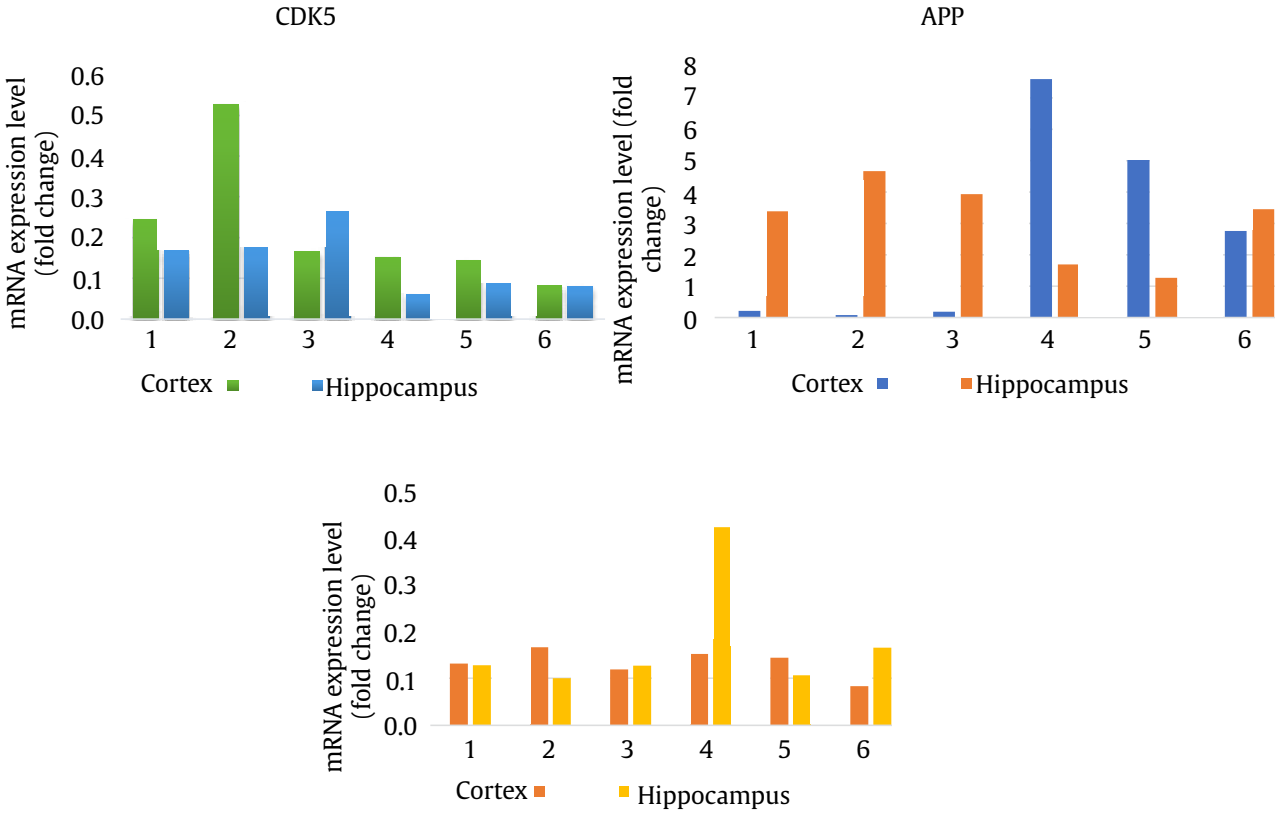

Figure 1. A representation of mRNA level expression of APP, CDK5, and AKT1 of the cortex and hippocampus brain region on adult and aged long-tailed macaques. Quantification data for all genes were normalized using appropriate reference gene ACTB and relative fold changes. Data are expressed as means ± SD

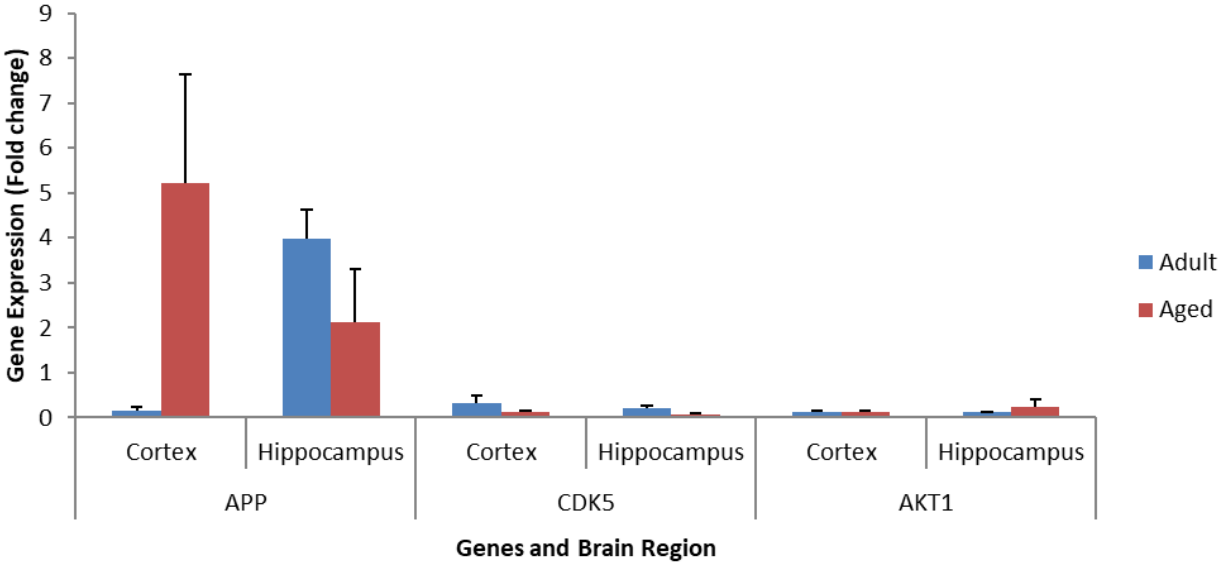

Figure 2. Evaluation of mRNA gene expression related to amyloid plaque and neurofibrillary tangle development of the cortex and hippocampus brain region on adult and aged long-tailed macaques. The histogram displays expression of APP, CDK5, and AKT1, mRNA gene normalize to beta-actin housekeeping gene and measure in foldchange. Data are expressed as means, and error bars = SD. * indicates a significantly different expression

The second finding was statistically significant ($p<0.005$) *CDK5* gene expression in the hippocampal region. *CDK5* gene is related to pTau formation and is statistically significant in adults. Hence, the process of pTau formation has started in adults, or another possibility is that pre- and post-synaptic signaling events in neurons modulate memory formation. *CDK5* neuronal protein kinase phosphorylates various synaptic substrates. It is involved in memory formation (Guan *et al.* 2011), but in old monkeys, the process of memory formation decreases, resulting in lower *CDK5* gene expression or *CDK5* begins to lose its function.

APP is one gene responsible for synthesizing amyloid beta peptide or amyloid plaque. Toxic plaque or amyloid peptide kills neuronal cells, resulting in gradual cognitive impairment. In this study, aged monkeys had a 33-fold higher expression of *APP* gene in the cortical region than adult monkeys. These results are consistent with a study by (Park *et al.* 2015) in long-tailed macaques induced by STZ, in which the frontal cortex showed the highest levels of *APP* gene expression. Additionally, spontaneous *APP*/A-immunoreactive (ir) plaques were discovered in the neocortex and hippocampus areas of 55-year-old female gorillas (Perez *et al.* 2013). In *Macaca fascicularis*, the intracellular amyloid beta was detected by immunohistochemistry in the cortical region at different ages, and the overall level of amyloid beta increased with the aging (Nakamura *et al.* 1996, 1998; Kimura *et al.* 2005). Other studies revealed that the prefrontal brain of aged monkeys exhibits a higher amyloid beta staining (Jester *et al.* 2022). Neuronal synapses are created and repaired in part by *APP*. However, excessive *APP* expression may raise the risk of Alzheimer's disease through decreased long-term potentiation and increasing sensitivity to ischemic brain damage (Zhang *et al.* 1997; Matsuyama *et al.* 2007).

The results of this study are consistent with the report of a previous investigation that the critical region expression of aged monkeys of the *APP* gene was higher than that of adult monkeys. Amyloid beta, which causes the development of senile plaques, can occur due to variations in gene expression levels and noticeably varied outcomes. More functional studies are required to fully comprehend the impact of elevated cortical *APP* expression levels in old monkeys. Furthermore, when *APP* is overexpressed in mouse embryonic neural precursor cells, it speeds up the migration of cells to the cortex, and *APP* contributes quantitatively to the precise location (Young-Pearse *et al.* 2007).

According to the result of this study, *APP* expression in the brain of adult monkeys was 2.03 times higher in the hippocampal region than in the aged monkeys. This can be attributed to one of the roles of *APP*, which is to support neuronal healing and differentiation in the adult monkeys' hippocampal region. (Anand and Dhikav 2012) claim that learning, memory, and spatial navigation occur in the hippocampus in humans at a young age. Still, memory and processing speed skills deteriorate with aging (Reuben *et al.* 2011).

In individuals with Down syndrome, the hippocampus is the primary site of *APP* expression (Del Turco *et al.* 2016) and was markedly expressed in the hippocampus of *APP* transgenic mice (Jia *et al.* 2017). At the early stages of disease progression, the afflicted hippocampus is where memory, learning, and formation take place (Braak and Braak 1991). Expression of *APP* gene in the hippocampal region was higher in adults than in the aged monkeys, which is related to the development and learning of these brain regions. Phosphorylation of *APP* at Thr668 dramatically increased the amount of Ab build-up in the hippocampus of Alzheimer's patients (Lee *et al.* 2003). Another idea is that the development of amyloid plaques via -secretase and -secretase from *APP* is similarly connected to the enhanced gene expression in the hippocampus at a young age.

CDK5 is a serine/threonine kinase protein that plays a role in cell proliferation (Allnutt *et al.* 2020). According to (Cruz *et al.* 2003), *CDK5* is mostly found in postmitotic neurons, which are critical for brain development, neuronal survival, synaptic plasticity, microtubule regulation, and pain signaling (Lopes and Agostinho 2011). The monomeric form of *CDK5* is not enzymatically active, but it functions as an activator and causes an increase in tau phosphorylation and neurodegeneration. In this study, *CDK5* was analyzed using RT-qPCR to examine the potential for tau protein formation in groups of aged and adult long-tailed monkeys in the cortex and hippocampus. While the cortical region did not differ substantially, expression of *CDK5* mRNA in the adult hippocampus

region was 2.7 foldchange higher than that of the old animals. This result is statistically different, as indicated by $p<0.05$. A previous study by Oikawa *et al.* (2010) discovered the production of Paired Helical Filament (PHF), a fibril unit of NFTs, in the hippocampus of the brain of cynomolgus monkeys. According to (Abid *et al.* 2019), examining the p25 gene's expression as a *CDK5* activator implicated in tau hyperphosphorylation in mice revealed that tau pathology worsens with advancing age. This contradicts the result of this study, indicating that the expression of the *CDK5* gene in the hippocampal area of adult monkeys was higher than in the aged monkeys. This is due to the possibility that neurons' pre- and post-synaptic signaling activities influence memory formation. To establish memories, the neuronal protein kinase *CDK5* phosphorylates a variety of synaptic substrates (Guan *et al.* 2011). However, in old monkeys, the memory creation process is slowed, resulting in decreased *CDK5* gene expression or loss of *CDK5* function. Aging affects brain function in the hippocampal region and can result in memory loss. Hence, expression of the *CDK5* gene in the cortex of old monkeys diminishes. Expression of the *CDK5* gene is 2.4 times higher in the cortical region of adults than in old monkeys.

Cruz *et al.* (2003) showed that mice's cortical and hippocampal regions displayed aberrant *CDK5* activity caused by the accumulation of p25 inducing the formation of endogenous tau filaments. The cortical tissue of old primates showed an increase in phosphorylation exposed to Pb, leading to the activation of kinases and activators (Bihaqi and Zawia 2013). According to (Hisanaga and Endo 2010), the *CDK5* gene contains unique activators called p25, p35, and p39 that can create a p35-*CDK5* or a p25-*CDK5* complex and phosphorylate serine/threonine kinase. In humans, the p25-*CDK5* complex has a substantially greater capacity to phosphorylate au than the p35-*CDK5* complex (Hashiguchi *et al.* 2002).

AKT1 gene, often referred to as protein kinase B, is a component of several signaling pathways, and its unique function is believed to be a crucial aspect of various disease processes, such as cancer and diabetes (Curtis and Bandyopadhyay 2021). *AKT1* participates in signaling pathways, resulting in phosphorylated GSK3β, which is essential in controlling the activity of glycogen synthase kinase 3-beta (GSK3-beta) (Sen *et al.* 2020). *AKT1* regulates cell development, proliferation, and metabolism under physiological settings and participates in synaptic plasticity. According to (Levenga *et al.* 2017), it is crucial to the serine/threonine kinase present in nearly all cell types throughout the body. In this study, the hippocampus region of old monkeys had an *AKT1* gene that was 1.9 times higher than that of adult monkeys, but this difference was not statistically significant. *AKT1* gene's expression level in the cortical region was nearly the same in adults and the aged.

This study examined *APP*, *CDK5*, and *AKT1* gene expression in the cortex and hippocampus of two groups of adult and aged monkeys. The results showed that the expression of the *APP* gene was higher in the cortical region of aged monkeys compared to adults, while the *CDK5* gene was higher in the adult hippocampus compared to that of the aged. Furthermore, there was no significant increase in the expression of the *AKT1* gene in either group. According to this study, *APP* gene expression related to amyloid plaques in the cortex brain region of aging cynomolgus monkeys resembles a human phenomenon. Further studies are needed to examine the mechanism of the formation of amyloid beta protein by analyzing other gene expression markers, as well as in older animals (more than 20 years) or longitudinal studies. This is needed to determine the expression of genes at the protein level in monkeys with poor memory and biomarkers of neurogenerative disease of Alzheimer's type.

Acknowledgements

The authors are grateful to the Director of LPPM IPB, Yuliana M.Si, Elis Dwi Ayuningsih, S.Si, drh. Silvia Arin Prabandari, M.Si, drh Dyah Setiawati, Kartika Sari, and Rahmat Supriatna for their technical assistance in the study preparation. The authors are also grateful to the Ministry of Finance of The Republic of Indonesia for The Research and Productive Innovation (RISPRO) LPDP program for funding this study through Contract Id. PRJ/29/LPDP/2019.

References

Abid, N.B, Naseer, M.I., Kim, M.O., 2019. Comparative gene-expression analysis of Alzheimer's disease progression with aging in a transgenic mouse model. *International Journal of Molecular Sciences.* 20, 1219. https://doi.org/10.3390/ijms20051219

Allnutt, A.B., Waters, A. K., Kesari, S., Yenugonda, V.M., 2020. Physiological and pathological roles of Cdk5: potential directions for therapeutic targeting in neurodegenerative disease. *ACS Chemical Neuroscience.* 11, 1218–1230. https://doi.org/10.1021/acschemneuro.0c00096

Anand, K., Dhikav, V., 2012. The hippocampus in health and disease: an overview. *Annals of Indian Academy of Neurology.* 15, 239-246. https://doi.org/10.4103/0972-2327.104323

Bhaskar, CD., Sribidya, P., Devi Prasana, O., Das, A., Hosmana, N., Das, S., 2018. The role of tau protein in diseases. *Annals of Advances in Chemistry.* 2, 1-16. https://doi.org/10.29328/journal.aac.1001010

Bihaqi, S.W., Zawia, N.H., 2013. Enhanced tauopathy and AD-like pathology in aged primate brains decades after infantile exposure to lead (Pb). *NeuroToxicology.* 39, 95-101. https://doi.org/10.1016/j.neuro.2013.07.010

Braak, H., Braak, E., 1991. Neuropathological staging of Alzheimer-related changes. *Acta Neuropathologica.* 82, 239-259. https://doi.org/10.1007/BF00308809

Chen, G.F., Xu, T.H., Yan, Y., Zhou, Y.R., Jiang, Y., Melcher, K., Xu, H.E., 2017. Amyloid beta: structure, biology, and structure-based therapeutic development. *Acta Pharmacologica Sinica.* 38, 1205-1235. https://doi.org/10.1038/aps.2017.28

Cruz, J.C., Tseng, H.C., Goldman, J.A., Shih, H., Tsai, L.H., 2003. Aberrant Cdk5 activation by p25 triggers pathological events leading to neurodegeneration and neurofibrillary tangles. *Neuron.* 40, 471-483. https://doi.org/10.1016/S0896-6273(03)00627-5

Curtis, D., Bandyopadhyay, S., 2021. Mini-review: role of the PI3K/Akt pathway and tyrosine phosphatases in Alzheimer's disease susceptibility. *Annals of Human Genetics.* 85, 1-6. https://doi.org/10.1111/ahg.12410

Darusman, H.S., Sajuthi, D., Schapiro, S.J., Gjedde, A., Kalliokoski, O., Kristianingrum, Y.P., Handharyani, E., Hau, J., 2014a. Amyloid beta 1-42 and phosphorylated tau threonine 231 in brains of aged cynomolgus monkeys (*Macaca fascicularis*). *Frontiers in Aging Neuroscience.* 6, 1-7. https://doi.org/10.3389/fnagi.2014.00313

Darusman, H.S., Call, J., Sajuthi, D., Schapiro, S.J., Gjedde, A., Kalliokoski, O., Hau, J., 2014b. Delayed response task performance as a function of age in cynomolgus monkeys (*Macaca fascicularis*). *Primates.* 55, 259-267. https://doi.org/10.1007/s10329-013-0397-8

Darusman, H.S., Saepuloh, U., Mariya, S.S., Sajuthi, D., Schapiro, S.J., Hau, J., 2021. Increased expression of GAPDH in cynomolgus monkeys with spontaneous cognitive decline and amyloidopathy reminiscent of an Alzheimer's-type disease is reflected in the circulation. *American Journal of Primatology.* 83, 1-12. https://doi.org/10.1002/ajp.23296

Del Turco, D., Paul, M.H., Schlaudraff, J., Hick, M., Endres, K., Müller, U.C., Deller, T., 2016. Region-specific differences in amyloid precursor protein expression in the mouse hippocampus. *Frontiers in Molecular Neuroscience.* 9, 1-12. https://doi.org/10.3389/fnmol.2016.00134

Gartland, K.N., Brand, C.M., Ulibarri, L.R., White, F.J., 2020. Variation in adult male-juvenile affiliative behavior in Japanese Macaques (*Macaca fuscata*). *Folia Primatologica.* 91, 610-621. https://doi.org/10.1159/000508761

Guan, J.S., Su, S.C., Gao, J., Joseph, N., Xie, Z., Zhou, Y., Durak, O., Zhang, L., Zhu, J.J., Clauser, K.R., Carr, S.A., Tsai, L.H., 2011. Cdk5 is required for memory function and hippocampal plasticity via the camp signaling pathway. *PLoS ONE.* 6, 1-16. https://doi.org/10.1371/journal.pone.0025735

Hashiguchi, M., Saito, T., Hisanaga, S.I., Hashiguchi, T., 2002. Truncation of CDK5 activator p35 induces intensive phosphorylation of Ser202/Thr205 of human tau. *Journal of Biological Chemistry.* 277, 44525-44530. https://doi.org/10.1074/jbc.M207426200

Higo, N., 2021. Non-human primate models to explore the adaptive mechanisms after stroke. *Frontiers in Systems Neuroscience.* 15, 1-8. https://doi.org/10.3389/fnsys.2021.760311

Hisanaga, S.I., Endo, R., 2010. Regulation and role of cyclin-dependent kinase activity in neuronal survival and death. *Journal of Neurochemistry.* 115, 1309-1321. https://doi.org/10.1111/j.1471-4159.2010.07050.x

Jester, H., Gosrani, S., H, D., 2022. Characterization of early Alzheimer's-like pathological alterations in non-human primates with aging: a pilot study abbreviated. *Journal of Alzheimer's.* 88, 957-970.

Jia, Y. L., Fu, Z. X., Zhang, B., H., Jia, Y.J., 2017. Hippocampal overexpression of down syndrome cell adhesion molecule in amyloid precursor protein transgenic mice. *Brazilian Journal of Medical and Biological Research.* 50, 1-7. https://doi.org/10.1590/1414-431x20176049

Kimura, N., Yanagisawa, K., Terao, K., Ono, F., Sakakibara, I., Ishii, Y., Kyuwa, S., Yoshikawa, Y., 2005. Age-related changes of intracellular Aβ in cynomolgus monkey brains. *Neuropathology and Applied Neurobiology.* 31, 170-180. https://doi.org/10.1111/j.1365-2990.2004.00624.x

Latimer, C.S., Shively, C.A., Keene, C.D., Jorgensen, M.J., Andrews, R.N., Register, T.C., Montine, T.J., Wilson, A.M., Neth, B.J., Mintz, A., Maldjian, J.A., Whitlow, C.T., Kaplan, J.R., Craft, S., 2019. A nonhuman primate model of early Alzheimer's disease pathologic change: Implications for disease pathogenesis. *Alzheimer's and Dementia.* 15, 93-105. https://doi.org/10.1016/j.jalz.2018.06.3057

Lee, M.S., Kao, S.C., Lemere, C.A., Xia, W., Tseng, H.C., Zhou, Y., Neve, R., Ahlijanian, M.K., Tsai, L.H., 2003. APP processing is regulated by cytoplasmic phosphorylation. *Journal of Cell Biology.* 163, 83-95. https://doi.org/10.1083/jcb.200301115

Levenga, J., Wong, H., Milstead, R.A., Keller, B.N., Laplante, L. E., Hoeffer, C.A., 2017. AKT isoforms have distinct hippocampal expressions and roles in synaptic plasticity. *Elife.* 6, 1-24. https://doi.org/10.7554/eLife.30640

Li, X., Zhou, H., Yang, P., Shi, H., Xiang, Xiong, Y., Nie, Z., Yong, Yu, J., Qiang, Wang, Y., An, Zhou, R., Wang, L., Yun, 2020. Cyclin-dependent kinase 5 regulates cortical neurotransmission and neural circuits associated with motor control in the secondary motor cortex in the mouse. *Neuroscience.* 438, 9-24. https://doi.org/10.1016/j.neuroscience.2020.04.031

Lopes, J. P., Agostinho, P., 2011. *Cdk5*: multitasking between physiological and pathological conditions. *Progress in Neurobiology.* 4, 49–63.

Mariya, S.S., Dewi, F.N., Villiandra, Paramastri, Y.A., Iskandriati, D., Saepuloh, U., Hayes, E., Pamungkas, J., Sajuthi, D., 2019. Isolation and characterization of c-c chemokine ligand 7 (Ccl7) in cynomolgus macaques. *HAYATI J Biosci.* 26, 129-132. https://doi.org/10.4308/hjb.26.3.129

Matsuyama, S., Teraoka, R., Mori, H., Tomiyama, T., 2007. Inverse correlation between amyloid precursor protein and synaptic plasticity in transgenic mice. *Neuroreport.* 18, 3-7. https://doi.org/10.1097/WNR.0b013e3281e72b18

Ministry of Health Republic of Indonesia, 2019. Kementerian Kesehatan Republik Indonesia. Kementerian Kesehatan.

Nakamura, S., Kiatipattanasakul, W., Nakayama, H., Ono, F., Sakakibara, I., Yoshikawa, Y., Goto, N., Doi, K., 1996. Immunohistochemical characteristics of the constituents of senile plaques and amyloid angiopathy in aged cynomolgus monkeys. *Journal of Medical Primatology.* 25, 294-300. https://doi.org/10.1111/j.1600-0684.1996.tb00213.x

Nakamura, S., Nakayama, H., Goto, N., Ono-Ochikubo, F., Sakakibara, I., Yoshikawa, Y., 1998. Histopathological studies on senile plaques and cerebral amyloid angiopathy in aged cynomolgus monkeys. *Experimental Animals. Japanese Association for Laboratory Animal Science.* 43, 711-718. https://doi.org/10.1538/expanim1978.43.5_711

Oikawa , N., Kimura, N., Yanagisawa, K., 2010. Alzheimer-type tau pathology in advanced aged nonhuman primate brains harboring substantial amyloid deposition. *Journal Brain Research.* 1313, 137-149.

Park, S.J., Kim, Y.H., Nam, G.H., Choe, S.H., Lee, S.R., Kim, S.U., Kim, J.S., Sim, B.W., Song, B.S., Jeong, K.J., Lee, Y., Park, Y., Il, Lee, K.M., Huh, J.W., Chang, K.T., 2015. Quantitative expression analysis of APP pathway and tau phosphorylation-related genes in the ICV STZ-induced non-human primate model of sporadic alzheimer's disease. *International Journal of Molecular Sciences.* 16, 2386-2402. https://doi.org/10.3390/ijms16022386

Perez, S.E., Raghanti, M.A., Hof, P.R., Kramer, L., Ikonomovic, M.D., Lacor, P.N., Erwin, J.M., Sherwood, C.C., Mufson, E.J., 2013. Alzheimer's disease pathology in the neocortex and hippocampus of the western lowland gorilla (*Gorilla gorilla gorilla*). *Journal of Comparative Neurology.* 521, 4318-4338. https://doi.org/10.1002/cne.23428

Reuben, A., Brickman, A.M., Muraskin, J., Steffener, J., Stern, Y., 2011. Hippocampal atrophy relates to fluid intelligence decline in the elderly. *Journal of the International Neuropsychological Society.* 17, 56-61. https://doi.org/10.1017/S135561771000127X

Sen, T., Saha, P., Jiang, T., Sen, N., 2020. Sulfhydration of AKT triggers Tau-phosphorylation by activating glycogen synthase kinase 3β in Alzheimer's disease. *Proceedings of the National Academy of Sciences of the United States of America.* 117, 4418-4427. https://doi.org/10.1073/pnas.1916895117

[WHO] World Health Organization, 2012. World Health Organization and Alzheimer's Disease International.

Young-Pearse, T.L., Bai, J., Chang, R., Zheng, J.B., Loturco, J.J., Selkoe, D.J., 2007. A critical function for β-amyloid precursor protein in neuronal migration revealed by in utero RNA interference. *Journal of Neuroscience.* 27, 14459-14469. https://doi.org/10.1523/JNEUROSCI.4701-07.2007

Zhang, F., Eckman, C., Younkin, S., Hsiao, K.K., Iadecola, C. 1997. Increased susceptibility to ischemic brain damage in transgenic mice overexpressing the amyloid precursor protein. *The Journal of Neuroscience.* 17, 7655-7661. https://doi.org/10.1523/JNEUROSCI.17-20-07655.1997

HAYATI
Journal of Biosciences

Vol. 31 No. 1, January 2024 153-160
DOI:10.4308/hjb.31.1.153-160
ISSN: 1978-3019
EISSN: 2086-4094

Diversity of Harvested Gastropods in Guang-Guang, Mati City, Davao Oriental, Philippines

Imee S. Maynawang[1,5*], Edison D. Macusi[2], Nur Fadli[3], Ivy M. Nallos[2,4]

[1]*Fisheries Catch Assessment Project, Davao Oriental State University, Mati City, Davao Oriental, Philippines*
[2]*Faculty of Agriculture and Life Sciences, Davao Oriental State University, Mati City, Davao Oriental, Philippines*
[3]*Faculty of Marine and Fisheries, Universitas Syiah Kuala, Banda Aceh, Indonesia*
[4]*Tuna Traceability Project, University of the Philippines Mindanao, Davao City, Philippines*
[5]*College of Marine and Allied Sciences (CMAS), Mindanao State University-Naawan, Naawan, Misamis Oriental, Philippines*

ARTICLE INFO

Article history
Received July 13, 2023
Received in revised form October 2, 2023
Accepted October 24, 2023

KEYWORDS
abundance,
low diversity,
gastropods,
gleaners,
harvesting

ABSTRACT

Gastropods are a highly abundant group of mollusks in the marine environment. Marine gastropods primarily function as prey for other animals, grazers which help recycle nutrients and increase bioturbation activities in the marine ecosystem. Edible gastropods are significant to the economy of coastal communities. However, overexploitation leads to harming the population of marine gastropods. The study aimed to determine the diversity of gastropods harvested at Guang-guang, Mati City, Davao Oriental. It also assessed the abundance of the identified gastropods in the area. This study used purposive sampling to enroll gleaners (N = 30) who collected shells and monitored their gastropod harvest. The harvested gastropods were segregated, counted, and identified with the help of gleaners. A total of ten gastropod species were identified from the family of Strombidae, Conidae, Neritidae, Cypraeidae, and Turbinidae. The most abundant group after harvest was *Canarium urceus*, with a relative abundance of 67%, followed by *Ilyanassa obsoleta*, with 22%. However, the least harvested species was Nerita, with a relative abundance of 0.18%. The findings revealed that the harvested gastropods in Guang-guang have a diversity index of 0.99, indicating a low diversity of gastropods in the area. This low diversity could mean the area experienced overexploitation through time as gleaners have heavily harvested gastropods. With that, it is highly recommended that conservation should be prioritized to preserve the seashells.

1. Introduction

Gastropods are a highly diverse group of mollusks having single-valve, soft bodies protected by shells (Brown and Lydeard 2010). The gastropods are highly abundant in marine, terrestrial, and freshwater habitats. This group of mollusks has approximately 85,000-100,000 described species of mollusks, including snails, slugs, and limpets (Strong *et al.* 2008). The most abundant and diverse marine species are molluscs, with approximately 32,000 to 40,000 species. This total number of gastropods represents about 23 to 32 percent of the total population of marine gastropods (Smith *et al.* 2011; Appeltans *et al.* 2012; Zapata *et al.* 2014). The biotic and abiotic factors and the gastropods' tolerance to environmental influences determine how gastropods are distributed in the marine environment (Fadliyah *et al.* 2021). The mangrove ecosystem provides suitable habitat characteristics with nutrients or organic matter for marine gastropods and other molluscan shells where it dominates (Kabir *et al.* 2014; Baderan *et al.* 2019).

Moreover, gastropods also act as predators and filter feeders that provide organic materials in the marine ecosystem (Sharma *et al.* 2013; Bhosale *et al.* 2016). A previous study of the diversity of gastropods revealed a high abundance of gastropods such as *Pomacea canaliculata* (Golden Apple Snail) in rivers and lakes in Bukidnon, Philippines (Galan *et al.* 2015). Another study of gastropods from Malaysia concluded that the study area has high species diversity due to the high number of various species present (Hamli *et al.* 2012). The abundance and

* Corresponding Author
E-mail Address: imee.maynawang@msunaawan.edu.ph

diversity of gastropods depend on different factors such as rates of exploitation level, protection of habitat, and other anthropogenic pressures in the area like tourism, collection, and waste management (Cardoso *et al.* 2012; Seddon *et al.* 2014; Gümüş *et al.* 2022).

Gastropods can also serve as an indicator in the marine environment. Their abundance indicates good environmental quality (Bondarev 2014; Wu *et al.* 2017; Ezraneti 2021). The distribution of gastropods is influenced by environmental factors that affect the behavior and diversity of the organisms (Koperski 2010; Scrosati *et al.* 2011; Marques *et al.* 2013). There are environmental factors that influence the distribution and diversity of gastropods, such as temperature, pH, salinity, and CO_2, and these changes in the environment cause stress and significantly affect the intertidal organisms, including gastropods (Parker *et al.* 2013; Wittmann and Pörtner 2013; Llovel and Terray 2016). Additionally, the presence of biological disturbances, such as invasive species, will also influence the distribution of the gastropods (Raffo *et al.* 2014). Moreover, because of their nearshore habitat and accessibility to human settlements, several gastropod species have been used as a source of protein and livelihood through gleaning, particularly in many coastal communities (Flores-Garza *et al.* 2012; Salim *et al.* 2017; de Guzman 2019; Furkon and Ambo-Rappe 2019; Balisco *et al.* 2022; Maynawang and Macusi 2023). This human access resulted in trampling, marine pollution, and threats of overcollection and gastropod population (Nieves *et al.* 2010; Akele *et al.* 2015; Ibarra 2018).

Guang-guang is a marine protected area known for its muddy-sandy substrate, coverage of mangroves, and diverse marine organisms (Macusi and Tipudan 2020; Nallos and Macusi 2023). However, the area is also open to the public for harvesting seashells and other marine species, threatening their population. The study aimed to determine the species composition, relative abundance, and diversity of the identified gastropods from the gleaners in Guang-guang, Davao Oriental, to measure the balance of the ecosystem or if there was a need for the conservation of the species. Given this assessment, the status of gastropods in Guang-guang would result in a corresponding local government policy action.

2. Materials and Methods

2.1. Description of the Study Area

The study area was located at Guang-guang, Barangay Dahican, Mati City, Davao Oriental (Figure 1). The area is characterized by sandy, sandy-coralline, and sandy-muddy substrate and is part of the mangrove area. The area is part of the protected area in Mati City, Davao Oriental.

2.2. Data Collection

A total of 30 gleaners participated in the recording of their harvested marine gastropods in the shoreline of Guang-guang, Dahican, and Davao Oriental. The gleaners randomly collected the gastropods regardless of the species available. On the other hand, gleaners used modified forks and knives to dig any marine seashell. The collected gastropods were segregated, identified through their local names with the help of the gleaners, counted, recorded, and how many hours they were gleaned. The harvesting and recording of data were repeated for three months. After recording the data, the gastropods were returned to the participating gleaner for consumption or marketing. After recording the marine gastropods, the researchers kept a few samples of gastropods from the gleaners to identify every species.

2.3. Data Analysis

Gastropods were identified to the lowest taxonomic level based on morphological characteristics such as shape, color, and shell using journal publication (Dharma 1988; Poppe 2008a, 2008b). The species were also identified and double-checked in the World Register of Marine Species (WoRMS) database. Moreover, the relative abundance of the gastropods was calculated using the equation adopted from the study of Laheng *et al.* (2023):

$$\text{Pi} = \frac{n_i}{N} \times 100$$

Where n_i is the number of species (individuals), and N is the total number of all species. The diversity index was also calculated using the formula of the Shannon-Wiener diversity index (H'):

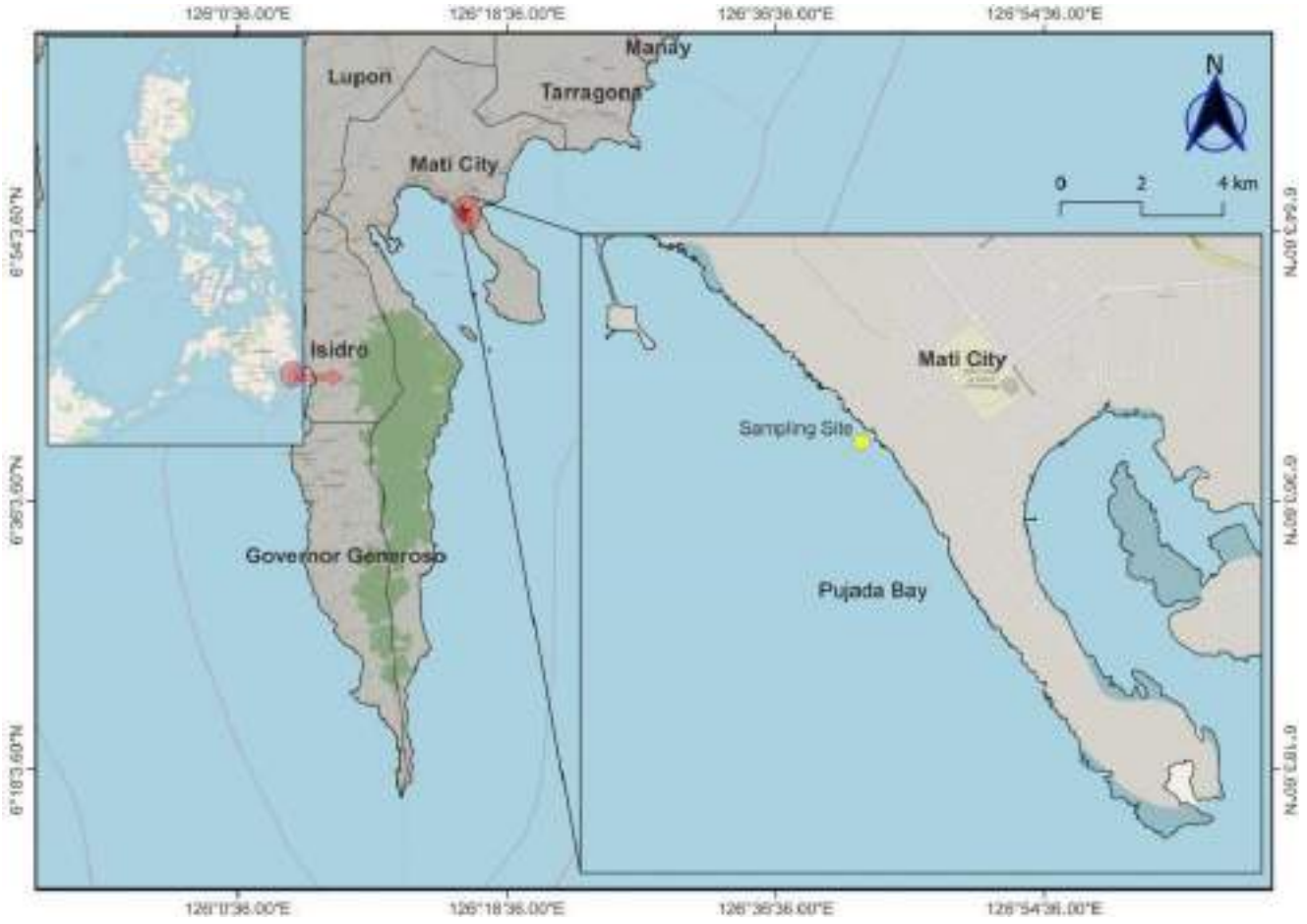

Figure 1. Map of the study site in Guang-guang, Mati City, Davao Oriental

$$H' = - \sum P_i (ln\ P_i)$$

Where *ln* represents the logarithm of P_i. There are three classifications of the Shannon-Wiener diversity index: H' < 1 (low species diversity), 1 < H' < 3 (medium species diversity), H' > 3 (high species diversity) (Brower and Zar 1990).

3. Results

3.1. Species Composition

A total of 10 different species of gastropods were gleaned in Guang-guang, Dahican, Mati City, Davao Oriental (Table 1, Figure 2). The gastropods were identified under eight families: Nassariidae (1 species), Trochidae (1 species), Conidae (1 species), Strombidae (2 species), Turbinidae (1 species), Cypraeidae (2 species), and Neritidae (1 species). The Strombidae are more common gastropods in the gleaning area. Species of *Canarium urceus* and *Ilyanassa obsoletea* are primarily harvested in Guang-guang to be sold in the public markets.

3.2. Abundance of Gastropods

The highest relative abundance value was dominated by *C. urceus*, with 67.15% (n = 115,341) among other harvested gastropods. In addition, the relative abundance of *T. sulcata* from the family of Potamididae is valued at 22.21% with n = 38,143 collected, followed by I. obsoleta at 6.33% (n = 10,880), *M. annulus annulus* at 1.25% (n = 2,144), *C. viridis* at 0.91% (1,560 individuals), *S. limacina limacine* at 0.61% (n = 1,048), *C. capitaneus* at 0.57% (n = 981), *T. sparverius* at 0.54% (n = 925), *E. chrysostomus* at 0.25% (n = 433), and *N. undata* having the lowest value of relative abundance at 0.18% with n = 313 (Figure 3). With these, it signifies that only a few gastropod species were caught but were highly abundant in the area (Figure 4). Most of the identified gastropods, include *C. urceus, M. annulus annulus, C. viridis, C. capitaneus, T. sparverius, N. undata*, were commonly harvested in muddy-sandy and sandy-coralline substrates in the coastal area. However, the *T. sulcata* and I. obsolete were commonly harvested in the

Table 1. The composition of the taxa of harvested gastropods in Guang-Guang, Mati City

Family	Genus	Species
Strombidae	*Euprotomus*	*Euprotomus chrysostomus* (Kuroda, 1942)
Strombidae	*Canarium*	*Canarium urceus* (Linnaeus, 1758)
Potamididae	*Terebralia*	*Terebralia sulcata* (Born, 1778)
Nassariidae	*Ilyanassa*	*Ilyanassa obsoleta* (Say, 1822)
Conidae	*Conus*	*Conus capitaneus* (Linnaeus, 1758)
Trochidae	*Coelotrochus*	*Coelotrochus viridis* (Gmelin, 1791)
Neritidae	*Nerita*	*Nerita undata* (Linnaeus, 1758)
Turbinidae	*Turbo*	*Turbo sparverius* (Gmelin, 1791)
Cypraeidae	*Monetaria*	*Monetaria annulus annulus* (Linnaeus, 1758)
Cypraeidae	*Staphylaea*	*Staphylaea limacina limacina* (Lamarck, 1810)

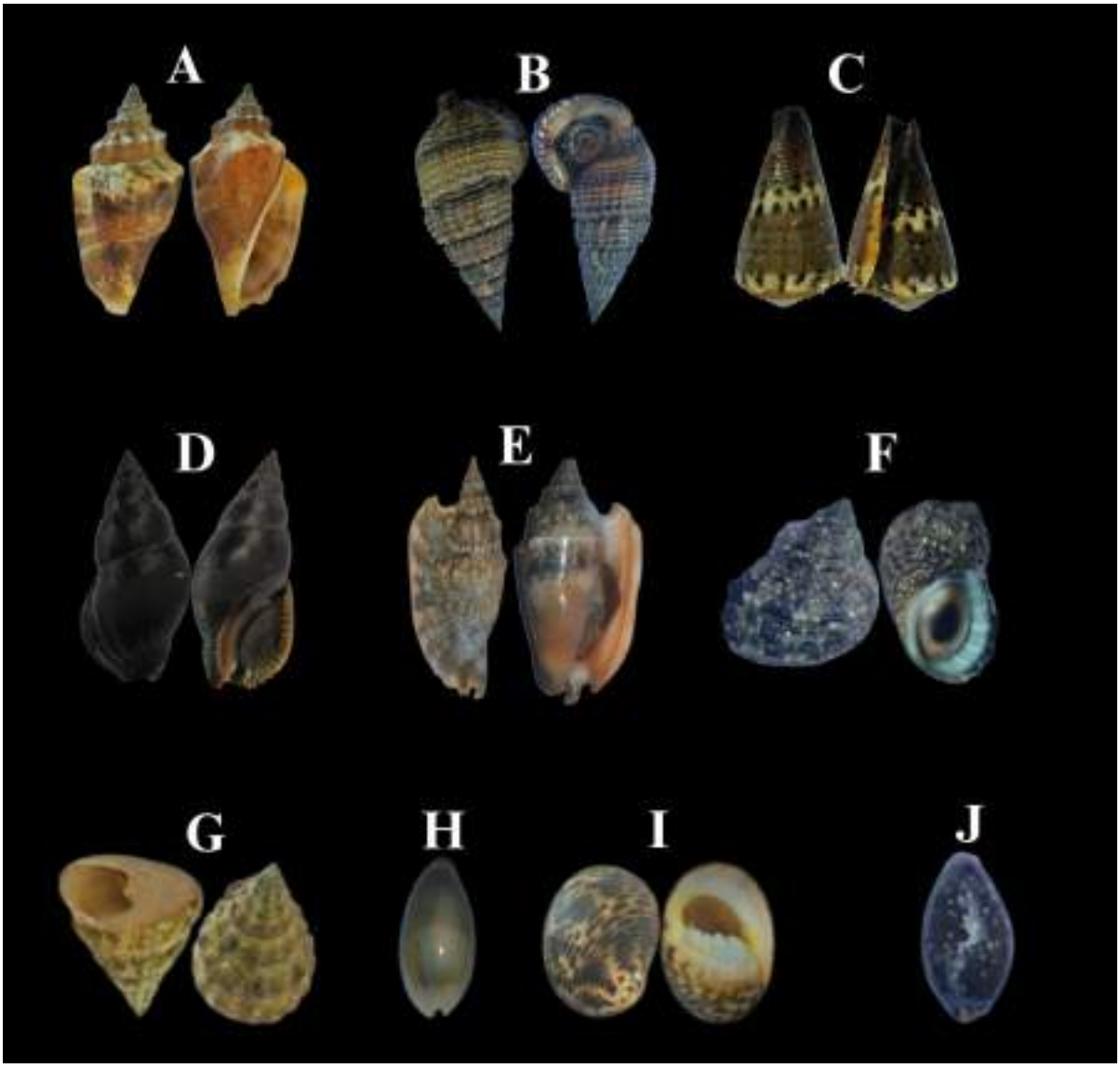

Figure 2. Species composition of gastropods: (A) *Canarium urceus* (Linnaeus, 1758), (B) *I. Terebralia sulcata* (Born, 1778), (C) *Conus capitaneus* (Linnaeus, 1758), (D) *Ilyanassa obsoleta* (Say, 1822), (E) *Euprotomus chrysostomus* (Kuroda, 1942), (F) *Turbo sparverius* (Gmelin, 1791) *Monetaria annulus annulus* (Linnaeus, 1758), (G) *Coelotrochus viridis* (Gmelin, 1791), (H) *Staphylaea limacina limacina* (Lamarck, 1810), (I) *Nerita undata* (Linnaeus, 1758), (J) *Monetaria annulus annulus* (Linnaeus, 1758)

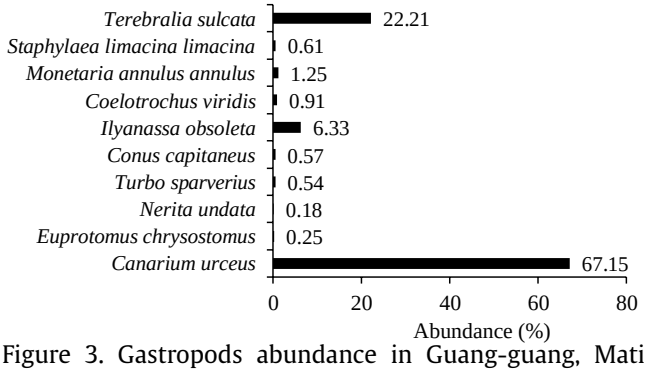

Figure 3. Gastropods abundance in Guang-guang, Mati City, Davao Oriental

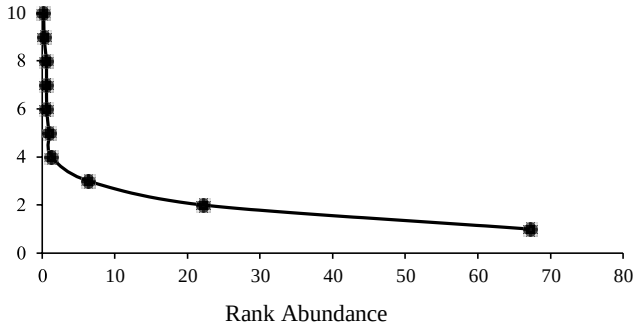

Figure 4. Dominance rank diversity of gastropods species in Guang-guang, Mati City

Table 2. Diversity of harvested gastropods in Guang-guang, Mati City, Davao Oriental (ni = number of species, P_i = relative abundance of species, *ln* = logarithm of Pi)

Species	Count (n_i)	P_i = (ni / *N*)	*ln* (P_i)	(P_i) (*ln* P_i)
Canarium urceus	115,341	0.6715	0.3983	0.2674
Euprotomus chrysostomus	433	0.0025	5.9832	0.0151
Nerita undata	313	0.0018	6.3077	0.0115
Turbo sparverius	925	0.0054	5.2241	0.0281
Conus capitaneus	981	0.0057	5.1653	0.0295
Ilyanassa obsoleta	10,880	0.0633	2.7592	0.1748
Coelotrochus viridis	1,560	0.0091	4.7015	0.0427
Monetaria annulus annulus	2,144	0.0125	4.3835	0.0547
Staphylaea limacina limacina	1,048	0.0061	5.0993	0.0311
Terebralia sulcata	38,143	0.2221	1.5048	0.3342
Total individual	171,768			H = 0.99

mangrove area of Guang-guang. These gastropods were collected by handpicking or using a small knife.

3.3. Diversity of Gastropods

The numbers of gastropod individuals were analyzed to determine the overall diversity of gastropods in the area. The result showed a diversity of 0.99 or a low diversity index (H'<1) of 0.99 (Table 2). Moreover, the rarefaction curve showed that at about ten species, this curve was already reached in the area, showing just a few dominating species that were collected (Figure 5).

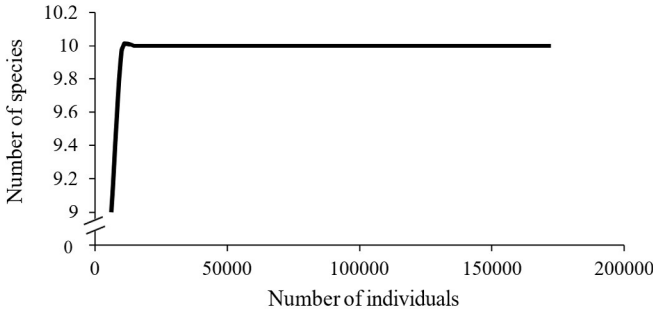

Figure 5. Rarefaction curve of the species

4. Discussion

Strombidae is one of the most familiar molluscan groups composed of about 100 species that mostly live in sand, seagrass, and mud flats area, and they are considered the source of food in many tropical and subtropical regions all over the world (Oo 2018; Ardila *et al.* 2020). However, Strombidae is affected by overexploitation caused by both natural and anthropogenic stressors, which leads to a large decrease in the population of marine species (Stoner *et al.* 2018; Ardila *et al.* 2020). There are about 13 genera of Strombidae, with more than 50 different species reported that are found in the Philippines (Poppe 2008a, 2008b), and these include the *C. urceus* (Pangarungan *et al.* 2022) and *C. urceus* (67.15%) is also the most abundant in the muddy-sandy substrate area in Guang-guang, Dahican, Davao Oriental. The substrate has a presence of seagrasses that serves as nutrient source of Strombidae (Cappenberg *et al.* 2023; Latuconsina

and Buano 2021; Natsir and Dillenia 2023). On the other hand, the other study in Zamboanga del Norte and Misamis Occidental, Philippines, showed that the most abundant species found in the selected area is the *Canarium esculentum* with 33.25% species, followed by the *Canarium urceus* with 17.49%, and the majority of the Strombidae species are found in the sandy-muddy substrate (Pangarungan *et al.* 2022).

The collected gastropods in Guang-guang, Dahican, Davao Oriental consisted of 10 genera and 10 species. The diversity of gastropods in Guang-guang was low (H' = 0.99), which means that certain area need to be protected because the diversity of the gastropods is declining according to the result of the study. Other study in Baganga, Davao Oriental, Philippines shows that the mollusks diversity in Ban- ao is low (H' = 0.81) followed by Kinablangan (H' = 0.46) (Bantayan *et al.* 2023). However, the study in Kapas Island, Indonesia revealed that the diversity of gastropods in the area was medium (H' = 2.09) which means that the gastropod is in the area is in balance condition (Laheng *et al.* 2023). The poor diversity index of gastropods in Guang-guang might be affected by different factors which affect the distribution and composition of gastropods in the area (Setiawan *et al.* 2021). This includes environmental factors, such as pollution from nearby human activities e.g. proximity to residential areas and existing shrimp farms and from overharvesting (Bula *et al.* 2017). Similar findings were found in Surigao del Sur, Philippines, where overharvesting in the area resulted in low diversity of the gastropods (Abarquez *et al.* 2019). The increasing human settlement along coastlines have increased the stress on the coastal ecosystem (Yadav *et al.* 2019). This means that the abundance of invertebrate species depends on their environment for habitat and available food for survival.

In conclusion, the findings of the study revealed that the species with the highest relative abundance value was *Canarium urceus* from the Strombidae with 67.15%, and the least was Nerita undata from the Neritidae with 0.18%. It also revealed that the diversity index of harvested gastropods in Guang-guang, Mati City, Davao Oriental has a value of 0.99, indicating the category of low species diversity. This indicates that Guang-guang area is unstable due to various factors that need to be examined and investigated for management plans to conserve the diversity of the species in the area.

Acknowledgements

The authors are thankful to the gleaners who participated while monitoring their gleaned seashells, especially the patience that was given while sorting seashells. The study was successfully conducted with the gleaners' cooperation. The authors would also thank Mr. Michael Bersaldo for making map used in the study. Lastly, the authors want to express their gratitude to the Department of Science and Technology region 11 (DOST-XI) for providing financial assistance for the publication of this paper.

References

Abarquez, V.R., Mendez, N.P., Galan, GL., 2019. Preliminary study on diversity of intertidal gastropods in Barangay Day-asan, Surigao City, Philippines. *Ruhuna Journal of Science.* 10, 18-31. https://doi.org/10.4038/rjs.v10i1.54

Akele, G.D., Montcho, S.A., Chikou, A., Mensah, G.A., Laleye, P.A., 2015. Traditional exploitation of edible freshwater oyster *Etheria elliptica* (Lamarck, 1807) in Pendjari River (Benin-West Africa): assessment of income, human pressure and options for management. *International Journal of Biological and Chemical Sciences.* 9, 246-258. https://doi.org/10.4314/ijbcs.v9i1.22

Appeltans, W., Ahyong, S.T., Anderson, G., Angel, M.V., Artois, T., Bailly, N., Costello, M.J., 2012. The magnitude of global marine species diversity. *Current Biology.* 22, 2189-2202.

Ardila, N.E., Hernández, H., Muñoz-Ortiz, A., Ramos, Ó.J., Castro, E., Bolaños, N., Sánchez, J.A., 2020. Multi-year density variation of queen conch (*Aliger gigas*) on serrana bank, seaflower biosphere reserve, Colombia: implications for fisheries management. *Frontiers in Marine Science*. 7, 646. https://doi.org/10.3389/fmars.2020.00646

Baderan, D.W.K., Hamidun, M.S., Utina, R., Rahim, S., 2019. The abundance and diversity of Mollusks in mangrove ecosystem at coastal area of North Sulawesi, Indonesia. *Biodiversitas Journal of Biological Diversity*. 20, 987-993. https://doi.org/10.13057/biodiv/d200408

Balisco, R.A.T., Gonzales, B.J., Dolorosa, R.G., 2022. Economically Important Benthic Macroinvertebrates in the Reefs of West Sulu Sea, Palawan, Philippines. *Philippine Journal of Science.* 151, 1119-1133. https://doi.org/10.56899/151.03.27

Bantayan, J.M.D., Bantayan, N.A.L., Villegas, J.P., 2023. Community structure of macroinvertebrates in protected and exploited areas of Baganga, Davao Oriental, Philippines. *Davao Research Journal.* 14, 17-31. https://doi.org/10.59120/drj.v14i1.7

Bhosale, M.M., Mugale, R.R., Honnananda, B.R., Vardia, H.K., Kumar, N., Barik, P., 2016. Biodiversity distribution of bivalves and gastropods along ratnagiri coast, Maharashtra India. *Natural Resources Management: Ecological Perspectives.* 2, 569.

Bondarev, I.P., 2014. Dynamics of *Rapana venosa* (Valenciennes, 1846) (Gastropoda: Muricidae) population in the Black Sea. *International Journal of Marine Science.* 4, 46-60.

Brown, K.M., Lydeard, C., 2010. Mollusca: gastropoda. In: Thorp JH, Covich AP. (Eds.). *Ecology and Classification of North American Freshwater Invertebrates, 3rd edition.* San Diego, Academic Press. 277-306. https://doi.org/10.1016/B978-0-12-374855-3.00010-8

Bula, W., Leiwakabessy, F., Rumahlatu, D., 2017. The influence of environmental factors on the diversity of gastropods in Marsegu Island, Maluku. *Biosaintifika: Journal of Biology & Biology Education*. 9, 483-491.

Brower, J.E., Zar, J.H., 1990. *Field and Laboratory Methods for General Ecology*, third ed. C. Brown Publisher, Dubuque.

Cappenberg, H.A.W., Supriyadi, H.I., Hafitz, H., Salatalohi, A., Sidabutar, T., Wouthuyzen, S., 2023. Macrobenthos in the seagrass meadow of Taka Bonerate National Park South Sulawesi. *In IOP Conference Series: Earth and Environmental Science*. 1207, 1-11. https://doi.org/10.1088/1755-1315/1207/1/012018

Cardoso, R.S., Mattos, G., Caetano, C.H., Cabrini, T.M., Galhardo, L.B., Meireis, F., 2012. Effects of environmental gradients on sandy beach macrofauna of a semi-enclosed bay. *Marine Ecology*. 33, 106-116. https://doi.org/10.1111/j.1439-0485.2011.00457.x

De Guzman, A.B., 2019. Women in subsistence fisheries in the Philippines: the undervalued contribution of reef gleaning to food and nutrition security of coastal households. *SPC Women Fisheries Bull.* 29, 34-40.

Dharma, SP., 1988. *Gastropods and Bivalves of Indonesia.* PT. Sarana Graha, Jakarta.

Ezraneti, R., 2021. *Littoraria* spp. Snail (Mollusca: Gastropoda) as a bioindicator in the mangrove ecosystem. *IOP Conference Series: Earth and Environmental Science.* 695, 1-14. https://doi.org/10.1088/1755-1315/695/1/012008

Fadliyah, S., Sari, L.A., Pursetyo, K.T., Zein, A., Idris, M.H., Cahyoko, Y., 2021. The variability in population structure of gastropods in sedati waters, Sidoarjo Regency, East Java. *IOP Conference Series: Earth and Environmental Science.* 679, 012074. https://doi.org/10.1088/1755-1315/679/1/012074

Flores-Garza, R., Flores-Rodríguez, P., Torreblanca-Ramírez, C., Galeana-Rebolledo, L., Valdés- González, A., Suástegui-Zárate, A., Violante-González, J., 2012. Commercially important marine mollusks for human consumption in Acapulco, México. *Natural Resources.* 3, 11- 17.

Furkon, N.M.N., Ambo-Rappe, R., 2019. Invertebrate gleaning: forgotten fisheries. *IOP Conference Series: Earth and Environmental Science.* 253, 1-7. https://doi.org/10.1088/1755-1315/253/1/012029

Galan, G.L., Ediza, M.M., Servasques, M.S., Porquis, H.C., 2015. Diversity of gastropods in the selected rivers and lakes in Bukidnon. *International Journal of Environmental Science and Development.* 6, 615-619. https://doi.org/10.7763/IJESD.2015.V6.668

Gümüş, B.A., Gürbüzer, P., Altındağ, A., 2022. Towards a sustainable world: diversity of freshwater gastropods in relation to environmental factors-a case in the Konya Closed Basin, Türkiye. *Diversity*. 14, 934. https://doi.org/10.3390/d14110934

Hamli, H., Idris, M.H., Hena, M.A., Wong, S.K., 2012. Taxonomic study of edible bivalve from selected division of Sarawak, Malaysia. *International Journal of Zoological Research.* 8, 52. https://doi.org/10.3923/ijzr.2012.52.58

Ibarra, E.M.F., 2018. Overexploitation of coastal resources at Bajamar-Jatay? size composition of the mollusks consumed prehistorically in Baja California. *Pacific Coast Archaeological Society Quarterly.* 54, 57-82.

Kabir, M., Abolfathi, M., Hajimoradloo, A., Zahedi, S., Kathiresan, K., Goli, S., 2014. Effect of mangroves on distribution, diversity and abundance of molluscs in mangrove ecosystem: a review. *Aquaculture, Aquarium, Conservation and Legislation*. 7, 286-300.

Koperski, P., 2010. Diversity of macrobenthos in lowland streams: ecological determinant and taxonomic specificity. *Department of Hydrobiology*. 69, 88-101. https://doi.org/10.4081/jlimnol.2010.88

Laheng, S., Putri, D.U., Putri, I.W., 2023. Diversity of gastropods in Kapas Island, Indonesia. *Marine and Fishery Sciences.* 36, 101-108. https://doi.org/10.47193/mafis.3612023010106

Latuconsina, H., Buano, T., 2021. Biodiversity and density of marine intertidal gastropods in tropical seagrass meadows on Gorom Island, East Seram, Maluku, Indonesia. *Animal Biology and Animal Husbandry*. 13, 74-83.

Llovel, W., Terray, L., 2016. Observed southern upper-ocean warming over 2005-2014 and associated mechanisms. *Environmental Research Letters*. 11, 124023. https://doi.org/10.1088/1748-9326/11/12/124023

Macusi, E.D., Tipudan, C.D., 2020. Effects of bioturbation of fiddler crabs in relation to the growth of mangrove saplings (*Rhizophora apiculata*) in a mangrove reforested area. *Journal of Marine and Island Cultures.* 9, 1-10. https://doi.org/10.21463/jmic.2020.09.2.06

Marques, L., Carric, A., Bessa, F., Gaspar, R., Neto, J.M., Patrício, J., 2013. Response of intertidal macrobenthic communities and primary producers to mitigation measures in a temperate estuary. *Ecol Indic.* 25, 10-22. https://doi.org/10.1016/j.ecolind.2012.08.022

Maynawang, I.S., Macusi, E.D., 2023. Catch assessment of commercially important gastropods in Guang-Guang, Mati City, Davao Oriental, Philippines. *Academia Biology*. 1, 1-10. https://doi.org/10.20935/AcadBiol6029

Nallos, I., Macusi, E.D., 2023. Behavior and diet composition of fiddler crabs in Guang-guang, Dahica, Mati, Davao Oriental. *Marine and Fisheries Sciences.* 36, 1-11. https://doi.org/10.47193/mafis.3622023010506

Natsir, S.M., Dillenia, I., 2023. The benthic foraminiferal assemblages in the seagrass bed of Tanjung Berakit Waters, Bintan Island. *HAYATI J Biosci.* 30, 1149-1154. https://doi.org/10.4308/hjb.30.6.1149-1154

Nieves, P.M., de Jesus, S.C., Macale, A.M.B., Pelea, J.M.D., 2010. An assessment of macro- invertebrate gleaning in fisheries on the Albay Side of Lagonoy Gulf. *Kuroshio Science.* 4, 27-35.

Oo, N.N., 2018. Distribution of the genus *Strombus linnaeus* 1758 (Gastropoda: Strombidae) in some coastal areas of Myanmar. *J. Aquac. Mar. Biol.* 7, 258-263. https://doi.org/10.15406/jamb.2018.07.00217

Pangarungan, J.N.P., Makasiar, E.A.K., Trillo, J.P., Moneva, C.S.O., 2022. Microhabitat preference of strombidae in selected intertidal areas of Zamboanga del Norte and Misamis Occidental, Philippines. *Mindanao Journal of Science and Technology*. 20, 87-100. https://doi.org/10.61310/mndjstecbe.1043.22

Parker, L.M., Ross, P.M., O'Connor, W.A., Pörtner, H.O., Scanes, E., Wright, J.M., 2013. Predicting the response of molluscs to the impact of ocean acidification. *Biology*. 2, 651-692. https://doi.org/10.3390/biology2020651

Poppe, G.T., 2008a. *Philippine marine mollusks: I. (Gastrpoda-Part 1).* ConchBooks, Hackenheim.

Poppe, G.T., 2008b. *Philippine Marine Mollusks: I. (Gastrpoda-Part 2).* ConchBooks, Hackenheim.

Raffo, M.P., Russo, L., Schwindt, E., 2014. Introduces and native species on rocky shore macroalgal assemblages: zonation patterns, composition and diversity. *Aquatic Botany*. 112, 57-65. https://doi.org/10.1016/j.aquabot.2013.07.011

Salim, S.S., Jagadis, I., Venkatesan, V., Rahman, M.R., Nashad, M., 2017. Gastropod landing, utilisation and trade in India: a case study from Kollam, India. *Journal of the Marine Biological Association of India.* 59, 93-97. https://doi.org/10.6024/jmbai.2017.59.1.1879-14

Scrosati, R.A., Knox, A.S., Valdivia, N., Molis, M., 2011. Species richness and diversity across rocky intertidal elevation gradients in Helgoland: testing predictions from an environmental stress model. *Helgoland Marine Research.* 65, 91-102. https://doi.org/10.1007/s10152-010-0205-4

Seddon, M.B., Kebapçı, Ü., Lopes-Lima, M., Damme, D.V., Smith, K.G., 2014. Freshwater mollusks, in: Smith, K.G., Barrios, V., Darwall, W.R.T., Numa, C. (Eds.), *The Status and Distribution of Freshwater Biodiversity in the Eastern Mediterranean*. IUCN, Cambridge, pp. 43-56.

Setiawan, R., Siddiq, A.M., Wimbaningrum, R., Sulistiyowati, H., Aditiya, M.Y., 2021. Diversity of gastropods at jatipapak mangrove forest, Kucur Resort, Alas Purwo National Park. *Bioeduscience.* 5, 257-262. https://doi.org/10.22236/j.bes/536235

Sharma, K.K., Bangotra, K., Saini, M., 2013. Diversity and distribution of Mollusca in relation to the physico-chemical profile of Gho-Manhasan stream, Jammu (J and K). *International Journal of Biodiversity and Conservation.* 5, 240-249.

Smith, S.A., Wilson, N.G., Goetz, F.E., Feehery, C., Andrade, S.C., Rouse, G.W., Dunn, C.W., 2011. Resolving the evolutionary relationships of molluscs with phylogenomic tools. *Nature.* 480, 364-367. https://doi.org/10.1038/nature10526

Stoner, A.W., Davis, M.H., Kough, A.S., 2018. Relationships between fishing pressure and stock structure in queen conch (*Lobatus gigas*) populations: synthesis of long-term surveys and evidence for overfishing in The Bahamas. *Reviews in Fisheries Science and Aquaculture.* 27, 51-71. https://doi.org/10.1080/23308249.2018.1480008

Strong, E.E., Gargominy, O., Ponder, W.F., Bouchet, P., 2008. Global diversity of gastropods (Gastropoda; Mollusca) in freshwater. In: Balian EV, Lévêque C, Segers H, Martens K (Eds.). *Freshwater Animal Diversity Assessment. Developments in Hydrobiology, Vol 198.* Dordrecht, Springer. pp. 149–166. https://doi.org/10.1007/978-1-4020-8259-7_17

Wittmann, A.C., Pörtner, H.O., 2013. Sensitivities of extant animal taxa to ocean acidification. *Nature Climate Change*. 3, 995-1001. https://doi.org/10.1038/nclimate1982

Wu, H., Guan, Q., Lu, X., Batzer, D.P., 2017. Snail (Mollusca: Gastropoda) assemblages as indicators of ecological condition in freshwater wetlands of Northeastern China. *Ecological Indicators.* 75, 203-209. https://doi.org/10.1016/j.ecolind.2016.12.042

Yadav, R., Malla, P. K., Dash, D., Bhoi, G., Patro, S., Mohapatra, A., 2019. Diversity of gastropods and bivalves in the mangrove ecosystem of Paradeep, east coast of India: a comparative study with other Indian mangrove ecosystems. *Molluscan Research*. 39, 325-332. https://doi.org/10.1080/13235818.2019.1644701

Zapata, F., Wilson, N.G., Howison, M., Andrade, S.C.S., Jorger, K.M., Schrodl, M., Goetz, F.E., Giribet, G., Dunn, C.W., 2014. Phylogenomic analyses of deep gastropod relationships reject Orthogastropoda. *Proceedings of the Royal Society B: Biological Sciences*. 281, 20141739-20141739. https://doi.org/10.1098/rspb.2014.1739

HAYATI
Journal of Biosciences

Vol. 31 No. 1, January 2024 161-170
DOI:10.4308/hjb.31.1.161-170
ISSN: 1978-3019
EISSN: 2086-4094

Antimicrobial Potential of an Actinomycete *Gordonia terrae* JSN1.9-Derived Orange Pigment Extract

Siti Sholekha[1], Sri Budiarti[1], Akhmad Endang Zainal Hasan[2], Ni Putu Ratna Ayu Krishanti[3], Aris Tri Wahyudi[1]*

[1]*Department of Biology, Faculty of Mathematics and Natural Sciences, IPB University, Bogor 16680, Indonesia*
[2]*Department of Biochemistry, Faculty of Mathematics and Natural Sciences, IPB University, Bogor 16680, Indonesia*
[3]*Research Center for Applied Zoology, National Research and Innovation Agency of Indonesia (Badan Riset dan Inovasi Nasional/ BRIN), Bogor, Indonesia*

ARTICLE INFO

Article history
Received July 27, 2023
Received in revised form September 8, 2023
Accepted October 4, 2023

KEYWORDS
actinomycetes,
Candida,
Gram-positive,
natural products,
pigment

ABSTRACT

Actinomycetes are known to be a source of natural products and drugs. *Gordonia terrae*, an actinomycete pigment producer, shows potential in producing pigment with antimicrobial activity. This study aims to determine the antimicrobial activity of the active pigment fraction produced by the actinomycete *G. terrae*, assess the effects of the active pigment fraction on microbial cells, and identify the types of compounds present in the fraction. The pigment extract exhibited antimicrobial activity against Gram-positive bacteria and fungi. Specifically, it showed activity against *Bacillus subtilis* ATCC 6633, *Staphylococcus aureus* ATCC 25293, and *Candida albicans* ATCC 10231. Furthermore, the study evaluated the antimicrobial activities of the active fractions, revealed the active fraction had better antimicrobial activity than the crude extract. Scanning electron microscopy (SEM) confirmed that the active fraction of the pigment causes damage to *B. subtilis* ATCC 6633 cells, inhibits the formation of filaments in *C. albicans* ATCC 10231, and alters the normal shape of the cells. LC-MS/MS results showed that the active fraction contained several compounds known for their antimicrobial activity. Among the dominant compounds identified were cholestyramine, aminopregnane, and sphinganine. Thus, this study demonstrated that the orange pigment extract derived from *G. terrae* JSN1.9 exhibits promising antimicrobial activity.

1. Introduction

Natural products became the main source for hundreds of years of treatment. Application of natural products for medicine and searching for new drugs are still active (Prateeksha *et al.* 2019). Microbes are one of the leading producers of valuable natural products. Various excellent drug was discovered from the natural products produced by microbes; microbes may produce valuable natural products like pigment (Demain 2014).

Pigments are bioactive compounds with wide applications; pigments have been discovered, showing antioxidant, anti-inflammatory, and antimicrobial properties (Ramesh *et al.* 2019). Pigment derived from microbes can be an alternative source of natural products for pharmaceutical purposes. A previous study reported a blue-green pigment from *P. aeruginosa* P1.S9 has a wide range of biological activities, including antibacterial, antioxidant, and cytotoxic (Wahyudi *et al.* 2022). Natural pigments from microbial are abundantly produced from bacteria including actinomycetes, and fungi. Among microbial pigments, actinomycete produced pigments with the potential for antimicrobial production. Actinomycetes are one of the important microbes that account for 70–80% of secondary metabolites available commercially (Parmar and Singh 2018) and can produce bioactive compounds and natural pigments (Ibrahim *et al.* 2023).

Actinomycetes produce various metabolites as pigments that are different in colors, such as blue, brown, green, orange, red, violet, yellow, black, etc. (Hemeda *et al.* 2022). Researchers have done many studies to isolate pigment-producing actinomycetes and screen for antimicrobial activity. It has been

* Corresponding Author
E-mail Address: ariswa@apps.ipb.ac.id

found that novel antimicrobial substances have been produced by actinomycetes (Baniya *et al.* 2019). Rare actinomycetes have attracted more attention with the hope of discovering new antibiotics, some antibiotics such as rifamycins, erythromycin, and teicoplanin discovered from rare actinomycetes (Ding *et al.* 2019). Orange pigment extracts derived from the rare actinomycete *Micromonospora tulbaghiae* SCA54.P2 have been reported to have antibacterial activity, especially against *Escherichia coli* ATCC 8739 (Mesrian *et al.* 2021).

Previous studies have successfully isolated a rare actinomycete named *G. terrae* JSN1.9 from rice leaves from Jasinga, Bogor, and reported antifungal activity against rice blast fungus (Harsonowati *et al.* 2017). The strain *G. terrae* JSN1.9 produce an orange intracellular pigment, and the antimicrobial potential has yet to be studied. Research on pigments from the rare actinomycetes genus in Indonesia still needs to be explored and reported, especially for its antimicrobial activity. Therefore, research on the potential of pigments as a source of compounds with antimicrobial activity must be carried out. This study aimed to determine the antimicrobial activity of the active pigment fraction derived from the actinomycete *G. terrae* JSN1.9, the effect of the active pigment fraction on microbial cells, and identify compounds that might contribute to its antimicrobial activity.

2. Materials and Methods

2.1. Materials

The materials used were pigmented actinomycetes *G. terrae* JSN1.9, this actinomycete was routinely cultured in International Streptomyces Project 2 (ISP2) medium (malt extract 10 g/L, yeast extract 4 g/L, and glucose 4 g/L). Microbes test *B. subtilis* ATCC 6633, *E. coli* ATCC 8739, *P. aeruginosa* ATCC 27853, *S. aureus* ATCC 25293 were routinely cultured in Tryptic Soy Agar (TSA) (OXOID, United Kingdom) medium, and *C. albicans* ATCC 10231 was routinely cultured in Potato Dextrose Agar (PDA) (HIMEDIA, India) medium.

2.2. Pigment Production Media, Extraction, and UV-Vis Analysis

Pigment production was carried out on ISP2 medium. One liter of *G. terrae* JSN1.9 culture was incubated under shaking conditions (120 rpm) at 28°C for 10 days. The culture was centrifuged at 6,000 rpm for 15 minutes, and then the pellet was added with chloroform solvent and centrifuged again for 15 minutes. The supernatant was recovered, filtered, and evaporated using a vacuum evaporator at 40°C. Pigment characterization was carried out by recording the maximum adsorption. As much as 0.03 g of pigment was dissolved in 1 ml of chloroform, and its absorbance was measured at a wavelength range of 200-800 nm using UV/Visible Spectrophotometer (UV-Vis Hitachi U-2800) (Abubakar *et al.* 2022).

2.3. Antimicrobial Activity Test

The microbes test (*B. subtilis, E. coli, P. aeruginosa, S. aureus*, and *C. albicans*) were inoculated by adding 1% (v/v) inoculum into MHA/PDA medium. On the top of paper discs (6 mm) were added with 20 µL of pigment extract in various concentrations (250, 500, 750, and 1,000 µg/ml). The plates were incubated at 37°C (bacteria) and 28°C (*C. albicans*) for 18-24 hours. The inhibition zone around the paper disc indicated antimicrobial activity. The positive controls used were 100 µg/ml tetracycline (bacteria) and nystatin (*C. albicans*), while the negative control was DMSO 10% (v/v) (Mesrian *et al.* 2021).

2.4. Mobile Phase Optimization by Thin Layer Chromatography (TLC) and Bioautography Test

Pigment fractionation was carried out by the TLC method using eight single eluents (*n*-hexane, dichloromethane, chloroform, ethyl acetate, acetone, ethanol, methanol, and propanol) and silica gel as the stationary phase. A total of 10 µL (5% (w/v)) crude pigment extract was applied to silica gel G60F-254 TLC plates (2 cm × 10 cm) using CAMAG Linomat 5 (Switzerland) and eluted in a chromatographic vessel containing 10 ml eluent. The bands were observed under UV light at 254 nm and 366 nm. The best eluent was determined by observing the highest number of bands and good separation. The two best single eluents were mixed in various ratios from 1:9 (v/v) to 9:1 (v/v) as the mobile follow-up phase. The best mixed mobile phase was determined from the highest number of bands and band separation. For the bioautography test, a total of 10 µL of pigment extract (5% (w/v)) was applied to a TLC plate (2 cm × 10 cm). Next, the plate was eluted using the selected mobile phase. The plate was then placed in a Petri dish and added 15 ml of MHA/PDA medium containing 1% (v/v) of the microbe test. Plates were incubated at 37°C (bacteria) and 28°C (*C. albicans*) for 24 hours. The inhibition zone on the TLC plate indicated the active fraction of bands (Dewanjee

et al. 2015 with modifications). These bands were isolated using preparative TLC, a total (10% (w/v)) extract applied on TLC plates. The active fraction of the bioautographic results were marked, scraped, and collected from the plate.

2.5. Observation of Microbes Cell Damage

Cell damage was observed using scanning electron microscopy (SEM). Cultures of *B. subtilis* and *C. albicans* were treated with the active fraction of pigment (1,000 µg/ml) and incubated for 24 hours. The cultures were then centrifuged, and the cell pellet was washed with cacodylate buffer. The cells were treated with 2.5% glutaraldehyde for fixation. The fixation process was carried out by mixing the cells with 2% tannic acid and then washing them four times with cacodylate buffer. Subsequently, the dehydration process was carried out in five steps using alcohol. The dehydrated cells were dried using tert butanol and then attached to the SEM specimen stub. The cells were further coated with gold using an Ion Coater. The JSM-IT200 SEM was used to observe cell damage and leakage. Microbes cultures were used as negative controls, and cultures with the addition of tetracycline/nystatin were used as positive controls.

2.6. Liquid Chromatography Mass Spectrometer (LC-MS/MS) Analysis

The chemical composition of the active fractions was analyzed by Ultra Performance Liquid Chromatography (UPLC) coupled to a Xevo G2-S QTOF-MS (Waters, USA) using electrospray ionization. A mixture of distilled water + 5 mM ammonium formate (A) and acetonitrile + 0.05% formic acid (B) was used for the mobile phase. A total of 5 µL of the active fraction was injected into the High Strength Silica (HSS) LC column with the ACQUITY UPLC® HSS C18 type (1.8 µm 2.1 × 100 mm). The LC-MS/MS analysis results in chromatograms and mass spectra were then interpreted using the MassLynx V.4.1 program.

3. Results

3.1. Actinomycete Morphology

Actinomycete *G. terrae* JSN1.9 produced orange colored pigment with the best pigment color obtained during an incubation period of 10-days (Figure 1). This actinomycete has a rounded colony, convex elevation, entire margin, grows on the surface of the media, looks shiny or slick on ISP2 solid medium, bacilli cell shape, and produces an intracellular pigment.

3.2. Pigment Production Media

The actinomycete *G. terrae* JSN1.9 showed orange colonies on the ISP2 broth medium after 10 days of incubation at room temperature. After extraction using chloroform and evaporation, the crude pigment extract appeared brownish and dry, yielding 9.27±0.34% (w/v) (Figure 2).

The pigment was characterized using spectrum analysis by measuring the maximum adsorption of the pigment. The result showed a single peak, 400-500 nm, was obtained. Based on this maximum adsorption measurement, it is suggested that the pigment *G. terrae* JSN1.9 has maximum adsorption at a wavelength of 410 nm (Figure 3).

3.3. Pigment Chromatogram and Bioautography Test

Eight single eluents were used as the mobile phase in the TLC test. Dichloromethane and chloroform were the best eluents that produced the most bands and were separated from each other. Two eluents with the most bands were mixed in various ratios of 1:9 to 9:1 (v/v); 8:2 is the best mixture ratio because it can produce as many as 13 bands. The bioautography test results showed the fraction with antimicrobial activity (Figure 4).

3.4. Antimicrobial Activity

The crude pigment extract and the active fraction showed antimicrobial activity against *B. subtilis, S. aureus*, and *C. albicans albicans* (Figure 5). The active fraction showed stronger antimicrobial activity than the crude pigment. The active fraction has the best activity against *B. subtilis* and *C. albicans* at a concentration of 1,000 µg/ml with inhibition zone diameters of 4.00±0.41 and 3.00±0.00, respectively (Table 1). Both crude pigment extract and active fraction have no activity against Gram-negative bacteria (*E. coli* and *P. aeruginosa*).

3.5. Observation the Effect of Active Fraction on Microbes Cell

SEM results demonstrated distinct differences in the morphology of both microbe cells (Figure 6). The SEM analysis showed that the untreated *B. subtilis*

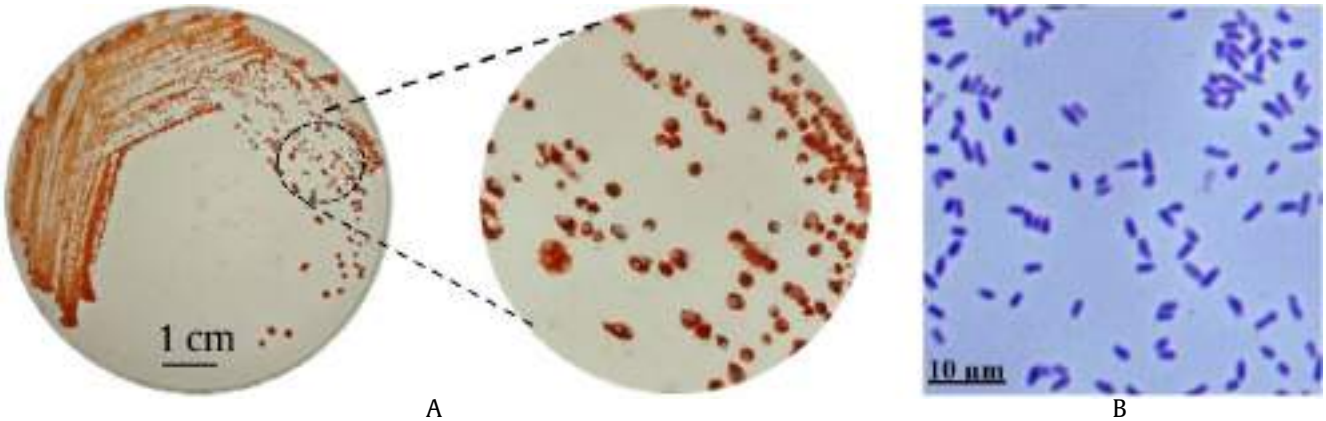

A B

Figure 1. Colonies of *G. terrae* JSN1.9 on ISP2 solid medium (A) and Gram staining (B) (magnification 1.000×)

A B C

Figure 2. (A) Pigment production of *G. terrae* JSN1.9 on ISP2 medium, (B) pigment extraction result using chloroform, (C) and crude pigment extract

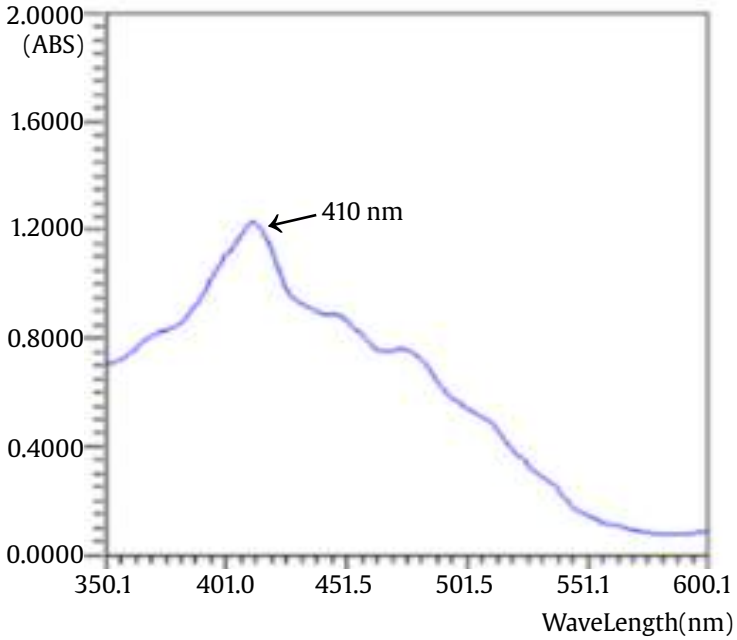

Figure 3. Maximum adsorption of *G. terrae* JSN1.9 crude pigment extract on UV-Vis spectrophotometer

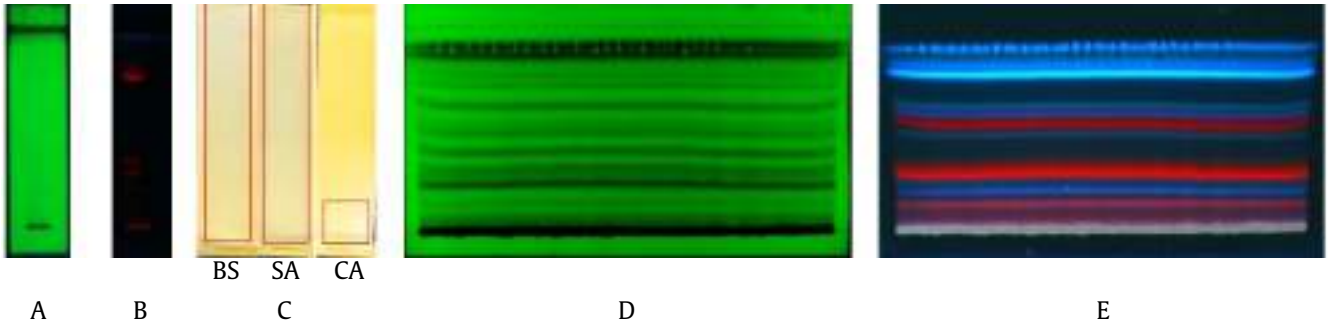

Figure 4. Chromatogram of *G. terrae* JSN1.9 pigment extract on a TLC plate. The active fraction is marked with a red box. TLC plate visualization at 254 nm (A) and 366 nm (B) at UV light, the results of the bioautographic test (C) (BS: *B. subtilis*, SA: *S. aureus*, and CA: *C. albicans*). Preparative TLC visualization at 254 nm (D) and 366 nm (E) at UV light

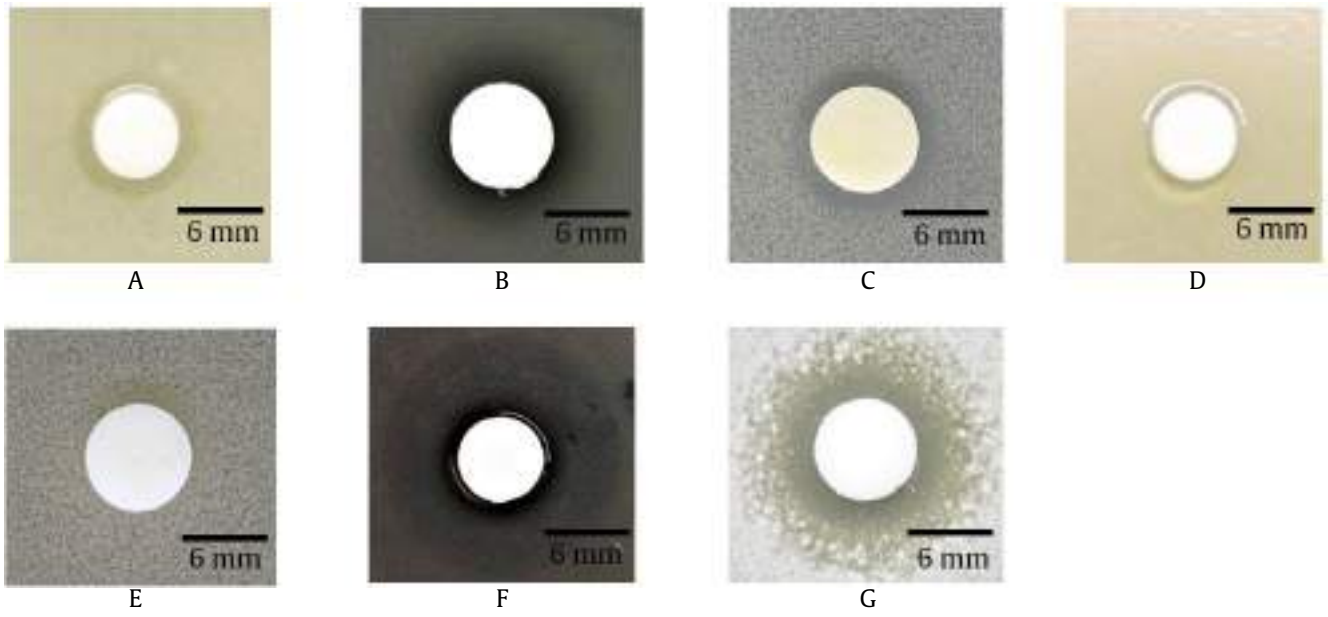

Figure 5. Antimicrobial activity test of the active fraction of *G. terrae* pigment JSN1.9 on *B. subtilis* (A), *S. aureus* (B), and *C. albicans* (C) at concentrations of 1,000 µg/ml, DMSO 10% on *B. subtilis* (D), and *C. albicans* (E), tetrasiklin 100 µg/ml on *S. aureus* (F), and nystatin 100 µg/ml on *C. albicans* (G)

Table 1. Antimicrobial activity of the active fraction of *G. terrae* pigment extract JSN1.9

Active fraction	Concentration (µg/ml)	Inhibition zone (mm)*				
		BS	EC	PA	SA	CA
G. terrae JSN1.9	250	2.00±0.00	2.00±0.00	0.00±0.00	1.50±0.58	1.00±0.00
	500	3.00±0.81	3.00±0.81	0.00±0.00	1.50±0.58	2.00±0.82
	750	3.50±0.00	3.50±0.00	0.00±0.00	2.00±0.00	2.50±0.58
	1,000	4.00±0.41	4.00±0.41	0.00±0.00	2.25±0.58	3.00±0.00
Tetracycline	100	11.00±1.41	17.00±0.82	12,75±0.29	4.00±0.81	nd
Nystatin	100	nd	nd	nd	nd	nd
DMSO 10%	100	0.00±0.00	0.00±0.00	0.00±0.00	0.00±0.00	0.00±0.00

nd: not determined
*BS: *B. subtilis*, EC *E. coli*, PA: *P. aeruginosa*, SA: *S. aureus*, CA: *C. albicans*
*Weak: 0.1-5.0 mm, Moderate: 6.0-10.0 mm, Strong: 11.0-15.0 mm

and *C. albicans* cells displayed smooth surfaces with a plump appearance and uniform sizes (Figure 6A1 and 6B1). However, cells treated with tetracycline and the active fraction treatment showed noticeable damage in the cells (Figure 6A2 and 6A3). The SEM results for tetracycline and active fraction treatments showed cell with wrinkled surfaces. SEM analysis for *C. albicans* cells displayed diverse cells shapes and filaments structures (Figure 6B). Untreated cells exhibited smooth surfaces and a plump appearance (Figure 6B1). On the other hand, cells treated with nystatin display cell leakage on the surfaces (Figure 6B2). When treated with the active fraction, the cells showed uneven shapes and lesser cells. Furthermore, the growth of filaments was inhibited (Figure 6B3).

3.6. Compound Identification by LC-MS/MS Analysis

The LC-MS/MS analysis of the active fraction of *G. terrae* JSN1.9 pigment showed the presence of various compounds in the active fraction of pigments (Figure 7). Dominant peaks marked various compounds. The most dominant compound based on the ten highest chromatogram peaks is cholestyramine, aminopregnane, sphinganine, dioctadecylamine, lauryldiethanolamine, and eudesmin (Table 2).

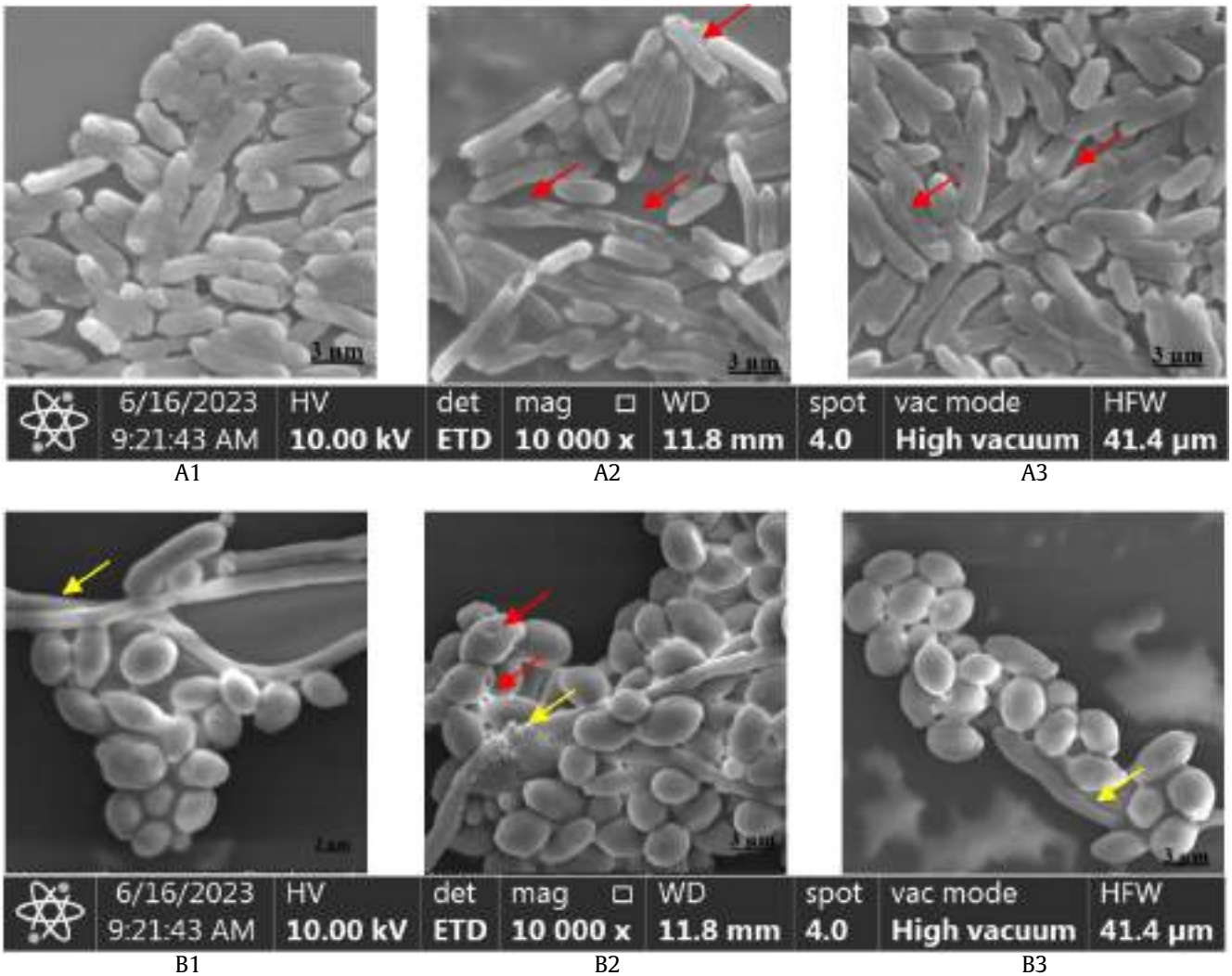

Figure 6. SEM images of *B. subtilis* (A) and *C. albicans* (B) at 10.000 magnification. (1) no treatment (negative control), (2) treatment with tetracycline/nystatin (positive control), and (3) treatment with the *G. terrae* JSN1.9 active fraction. Red arrows indicate cell damage and yellow arrows indicate filaments

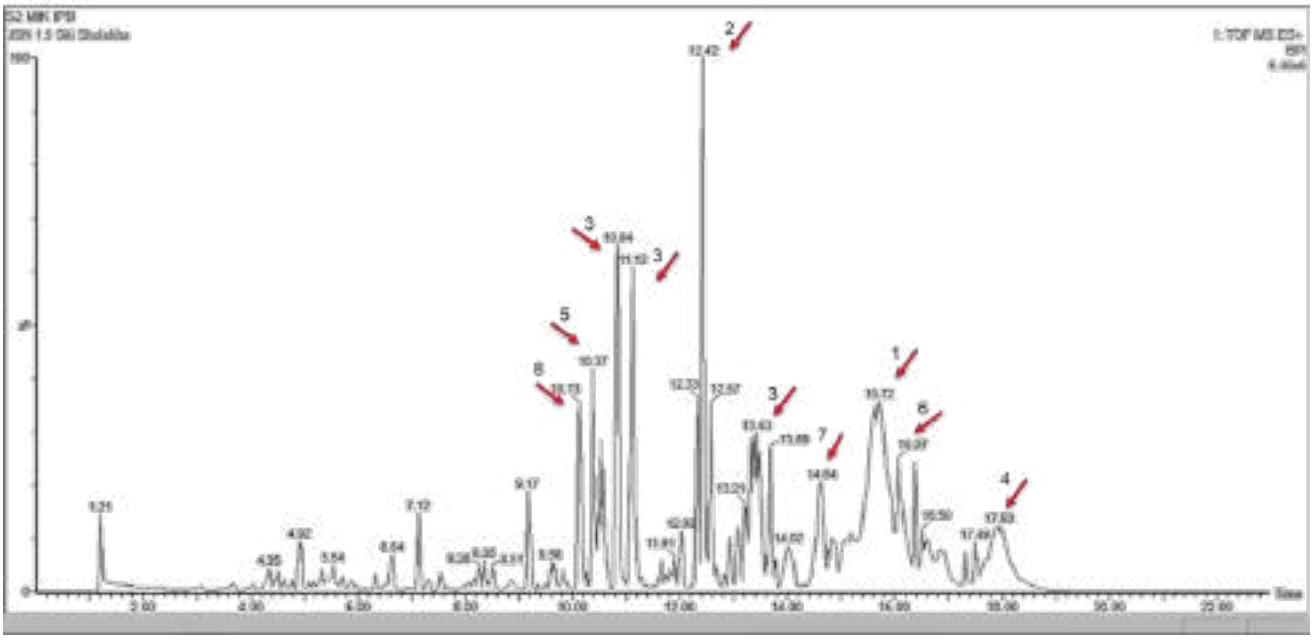

Figure 7. LC-MS/MS chromatogram of the active fraction of *G. terrae* JSN1.9. Red arrows indicate the abundance of most compounds

Table 2. Compound content in the active fraction of *G. terrae* pigment JSN1.9 as a result of LC-MS/MS analysis

Compound names	Peak area (%)	Formula	Retention time	Biological activities	References
Cholestyramine	25.64	$C_{27}H_{49}N$	15.72	Lowering high cholesterol	Morley *et al.* 2020
Aminopregnane	10.50	$C_{21}H_{37}N$	12.42	Antimicrobial	Kull *et al.* 1953
	9.85		13.39		
Sphinganine	6.17	$C_{17}H_{37}NO_2$	11.12	Antibacterial	Kunz and Kozjak-Pavlovic 2019
	5.64		10.84		
Dioctadecylamine	7.07	$C_{36}H_{75}N$	17.93	Antimicrobial	Seitz *et al.* 2021
Lauryldiethanolamine	6.02	$C_{16}H_{35}NO_2$	10.46	Antimicrobial	Chaouat et al. 2013
Unknown	5.37	$C_{39}H_{62}O_5$	16.38	-	-
Unknown	5.26	$C_{22}H_{46}O_5$	14.62	-	-
Eudesmin	3.06	$C_{22}H_{26}O_6$	10.13	Antimicrobial Anticancer	Patel and Patel 2022

4. Discussion

Microbes play a crucial role in developing natural products and medical therapies. As a rich source of natural products, microbes are considered a rich source of diverse and unique bioactive compounds (Abdel-Razek *et al.* 2020). Among these microbes, a rare genus of actinomycetes shows particular promise as a valuable source of bioactive compounds (Ma *et al.* 2021). Notably, Gordonia has been recognized for its capability of pigment biosynthesis (Loh *et al.* 2020). In this study, Actinomycete *G. terrae* JSN1.9 demonstrated the high production of an orange pigment on the ISP2 solid medium. The pigment was intracellular pigment because it did not diffuse to the ISP2 medium. The orange color was shown in the ISP2 liquid medium because the cell biomass was still mixed with the medium. Previous reports said that ISP2 is a medium that can be used for pigment production in actinomycetes (Ratte *et al.* 2022) and is the best media for higher pigment production (Ayoubi *et al.* 2018).

Pigment characterization is used to classify pigments into different groups. Based on the maximum adsorption results (Figure 3), it is assumed that the pigment produced by *G. terrae* JSN1.9 belongs to the carotenoid group, which typically exhibits colors ranging from yellow to orange. Carotenoids absorb light in the visible region of 400–500 nm (Udensi *et al.* 2022). Supporting this finding, Loh *et*

al. (2020) also reported that actinomycete *G. terrae* produced carotenoid pigment under fermentation conditions.

This study investigated the antimicrobial activity of the pigment extract from *G. terrae* JSN1.9 against various microbes, showing stronger effects on *B. subtilis, S. aureus*, and *C. albicans* (Table 1). The inhibition zone expands as the pigment concentration increases from 250 µg/ml to 1,000 µg/ml. Notably, the pigment extract exhibited selective activity, primarily inhibiting Gram-positive bacteria, which aligns with Yolmeh *et al.*'s findings (2016), where pigments from *Rhodotorula glutinis* were more effective against Gram-positive bacteria than Gram-negative bacteria. Moreover, Kazi *et al.* (2022) reported that the bioactive pigments derived from the strain BJZ10 also showed potential as antimicrobial agents against Gram-positive bacteria. Bioautography assay results demonstrated that the pigment extract of *G. terrae* JSN1.9 had a single active fraction with inhibition activity against the tested microbes, evident from the formation of an inhibition zone around the first band. The bioautography technique offers rapid screening for bioactivity, particularly for antibacterial, antifungal, antioxidant, enzyme inhibition, and other activities, facilitating targeted isolation of active compounds/fractions (Dewanjee *et al.* 2015).

The best activity of the active fraction was obtained at a concentration of 1,000 µg/ml with an inhibition zone diameter of 4.00±0.41 mm; 2.25±0.58 mm; and 3.00±0.00 mm for each test microbe *B. subtilis, S. aureus*, and *C. albicans,* respectively. The active pigment fraction of *G. terrae* JSN1.9 has higher antimicrobial activity against *B. subtilis* than previous studies by Keceli *et al.* (2013), which reported no activity from the tested orange pigment. These results proved that the pigment *G. terrae* JSN1.9 has the potential as an antimicrobial agent.

SEM results showed that administration of the active pigment fraction at a concentration of 1,000 µg/ml induced cell damage in *B. subtilis* and inhibited the formation of filaments and cell growth in *C. albicans* (Figure 6). This damage was evident through the observed shrinkage of cell-cultures, non-uniform cell shapes, and cracks in the cell walls, which can lead to cell lysis. This finding is similar to Feng *et al.* study (2019), where bacteria cells treated with an orange pigment displayed irregular and wrinkled surfaces compared to untreated cells with regular and smooth surfaces. On the other hand, the transition from yeast to filament plays a critical role in virulence and pathogenesis in *Candida* (Kadosh 2019). This transition is influenced by various inducing signals present in the environment. However, the active fraction in the tested *Candida* cells inhibited the formation of filaments, suggesting a potential reduction in pathogenicity. This result is consistent with Romo *et al.* findings (2017), where a small molecule compound named N-[3-(allyloxy)-phenyl]-4-methoxybenzamide (9029936) had potent inhibitory activity against filamentation and biofilm formation by *C. albicans* SC5314 strain.

Through LC-MS/MS analysis (Figure 7 and Table 2), several compounds were identified in the active fraction extract. Compounds detected in the LC-MS analysis were based on the literature reported to have antimicrobial activity with very diverse modes of action. Based on SEM and LC-MS analyses, the compounds belonging to the fraction actively have bactericidal activity against *B. subtilis* ATCC 6633 and fungistatic activity against *C. albicans* ATCC 10231.

The most abundant compound found in the LC-MS analysis was cholestyramine. Cholestyramine is a drug that can be used with antibiotics for therapeutic purposes (Morley *et al.* 2020). Aminopregnane was a member of the steroid class with antimicrobial activity (Kull *et al.* 1953). Sphinganine has antibacterial activity against Gram-positive and negative bacteria (Kunz and Kozjak-Pavlovic 2019), and dioctadecylamine was a compound reported antimicrobial activity (Seitz *et al.* 2021). Lauryldiethanolamine is a metabolite compound with antimicrobial activity (Chaouat *et al.* 2013). Additionally, eudesmin, present in the pigment extract, has diverse biological activities, including antibacterial, anti-inflammatory, anticancer, and anticonvulsant activities (Patel and Patel 2022). These identified compounds in the pigment extract suggest its potential as a source of various bioactive agents with promising antimicrobial properties.

In conclusion, the orange pigment produced by actinomycete *G. terrae* JSN1.9 demonstrated significant antimicrobial activity against Gram-positive bacteria (*B. subtilis* and *S. aureus*) and *C. albicans*. UV-Vis analysis confirmed that the pigment belongs to the carotenoid group. Furthermore, the active fraction exhibited stronger antimicrobial activity than the crude extract. SEM analysis clearly

revealed the noticeable differences between the treated and untreated microbe cells, displaying evident damage to the cells and inhibition of filament formation. LC-MS/MS analysis also provided insights into certain compounds that potentially contribute to the observed antimicrobial activity. Overall, this study highlights the potency of the orange pigment produced by *G. terrae* JSN1.9 as a promising antimicrobial agent. The findings underline the potential of this pigment and its active fraction for further exploration and development as a novel antimicrobial therapy.

Acknowledgements

This research was partly funded by the Basic Research from the Ministry of Education, Culture, Research and Technology of the Republic of Indonesia grants in 2022 to ATW (Contract no. 001/E5/PG.02.00PT/2022). The authors thank for all the support to carry out this research.

References

Abdel-Razek, A.S., El-Naggar, M.E., Allam, A., Morsy, O.M., Othman, S.I., 2020. Microbial natural products in drug discovery. *Processes*. 8, 1–19. https://doi.org/10.3390/PR8040470

Abubakar, H., Astuti, R.I., Listyowati, S., Batubara, I., Wahyudi, A.T., 2022. An orange pigment from the marine bacterium *Paracoccus haeundaensis* SAB E11 as a prospective source of natural antioxidants. *Biodiversitas.* 23, 4730–4737. https://doi.org/10.13057/biodiv/d230940

Ayoubi, H., Mouslim, A., Moujabbir, S., Amine, S., Azougar, I., Mouslim, J., Menggad, M., 2018. Isolation and phenotypic characterization of actinomycetes from Rabat neighborhood soil and their potential to produce bioactive compounds. *Afr. J. Microbiol. Res.* 12, 186–191. https://doi.org/10.5897/ajmr2017.8761

Baniya, A., Singh, S., Singh, M., Nepal, P., Adhikari, M., Aryal, S., Adhikari, A., 2019. Isolation and screening of antibiotics producing Streptomyces spp from the soil collected around the root of *Alnus nepalensis* from Godawari. *NepJOL.* 6, 46–56. https://doi.org/10.3126/njb.v6i1.22337

Chaouat, C., Balor, S., Roques, C., Franceschi-Messant, S., Perez, E., Rico-Lattes, I., 2013. Antimicrobial catanionic vesicular self-assembly with improved spectrum of action. *J. Surfactants Deterg.* 16, 717–722. https://doi.org/10.1007/s11743-013-1451-7

Demain, A.L. 2014. Importance of microbial natural products and the need to revitalize their discovery. J. Ind. Microbiol. Biotechnol. 41 185–201. https://doi.org/10.1007/s10295-013-1325-z

Dewanjee, S., Gangopadhyay, M., Bhattacharya, N., Khanra, R., Dua, T.K., 2015. Bioautography and its scope in the field of natural product chemistry. *J. Pharm. Anal.* 5, 75–84. https://doi.org/10.1016/j.jpha.2014.06.002

Ding, T., Yang, L.J., Zhang, W.D., Shen, Y.H., 2019. The secondary metabolites of rare actinomycetes: chemistry and bioactivity. *RSC Adv.* 9, 21964–21988. https://doi.org/10.1039/c9ra03579f

Feng, L.H., Li, Y.Q., Sun, G.J., Zhao, X.Z., 2019. Antibacterial effect of orange *Monascus* pigment against *Staphylococcus aureus. Acta Aliment.* 48, 169–176. https://doi.org/10.1556/066.2019.48.2.4

Harsonowati, W., Astuti, R.I., Wahyudi, A.T., 2017. Leaf blast disease reduction by rice-phyllosphere actinomycetes producing bioactive compounds. *J. Gen. Plant Pathol.* 83,98–108. https://doi.org/10.1007/s10327-017-0700-4

Hemeda, N.A., Hegazy, G.E., Abdelgalil, S.A., Soliman, N.A., Abdel-Meguid, D.I., El-Assar, S.A., 2022. Maximization of red pigment production from *Streptomyces* sp. LS1 structure elucidation and application as antimicrobial/antifouling against human pathogens and marine microbes. *J. Genet. Eng. Biotechnol.* 20, 168. https://doi.org/10.1186/s43141-022-00452-y

Ibrahim, W.M., Olama, Z.A., Abou-elela, G.M., Ramadan, H.S., Hegazy, G.E., El Badan, D.E.S., 2023.Exploring the antimicrobial, antiviral, antioxidant, and antitumor potentials of marine *Streptomyces tunisiensis* W4MT573222 pigment isolated from Abu-Qir sediments, *Egypt. Microb. Cell Factories.* 22, 1–17. https://doi.org/10.1186/s12934-023-02106-1

Kadosh, D., 2019. Regulatory mechanisms controlling morphology and pathogenesis in *Candida albicans. Curr. Opin. Microbiol.* 52, 27–34. https://doi.org/10.1016/j.mib.2019.04.005

Kazi, Z., Hungund, B.S., Yaradoddi, J.S., Banapurmath, N.R., Yusuf, A.A., Kishore, K.L., Soudagar, M.E.M., Khan, T.M.Y., Elfasakhany, A., Buyondo, K.A., 2022. Production, characterization, and antimicrobial activity of pigment from *Streptomyces* species. *J. Nanomater.* 2022, 1-8. https://doi.org/10.1155/2022/3962301

Keceli, T.M., Erginkaya, Z., Turkkan, E., Kaya, U., 2013. Antioxidant and antibacterial effects of carotenoids extracted from *Rhodotorula glutinis* strains. *Asian J. Chem.* 25, 42–46. https://doi.org/10.14233/ajchem.2013.12377

Kull, F.C., Castellano, G.A., Mayer, R.L., 1953. The *in vitro* antimicrobial activities of certain amino ateroids. *J. invest. Dermatol.* 21, 227-228. https://doi.org/10.1038/jid.1953.94

Kunz, T.C., Kozjak-Pavlovic, V., 2019. Diverse facets of sphingolipid involvement in bacterial infections. *Front. Cell Dev. Biol.* 7, 1–10. https://doi.org/10.3389/fcell.2019.00203

Loh, W.L.C., Huang, K.C., Ng, H.S., Lan, J.C.W., 2020. Exploring the fermentation characteristics of a newly isolated marine bacteria strain, *Gordonia terrae* TWRH01 for carotenoids production. *J. Biosci. Bioeng.* 130, 187–194. https://doi.org/10.1016/j.jbiosc.2020.03.007

Ma, Y., Xu, M., Liu, H., Yu, T., Guo, P., Liu, W., Jin, X., 2021. Antimicrobial compounds were isolated from the secondary metabolites of Gordonia, a resident of intestinal tract of *Periplaneta americana. AMB Express*. 11, 111. https://doi.org/10.1186/s13568-021-01272-y

Mesrian, D.K., Purwaningtyas, W.E., Astuti, R.I., Hasan, A.E.Z., Wahyudi, A.T., 2021. Methanol pigment extracts derived from two marine actinomycetes exhibit antibacterial and antioxidant activities. *Biodiversitas*. 22, 4440–4447. https://doi.org/10.13057/BIODIV/D221037

Morley, V.J., Kinnear, C.L., Sim, D.G., Olson, S.N., Jackson, L.M., Hansen, E., Usher, G.A., Showalter, S.A., Pai, M.P., Woods, R.J., Read, A.F., 2020. An adjunctive therapy administered with an antibiotic prevents enrichment of antibiotic-resistant clones of a colonizing opportunistic pathogen. *ELife*. 9, 1–17. https://doi.org/10.7554/ELIFE.58147

Parmar, R.S., Singh, C., 2018. A comprehensive study of eco-friendly natural pigment and its applications. *Biochem. Biophys. Rep.* 13, 22–26. https://doi.org/10.1016/j.bbrep.2017.11.002

Patel, D.K., Patel, K., 2022. Potential therapeutic applications of eudesmin in medicine: An overview on medicinal importance, pharmacological activities and analytical prospects. *Pharmacol. Res. - Mod. Chin*. 5, 100175. https://doi.org/10.1016/j.prmcm.2022.100175

Prateeksha, Yusuf, M.A., Singh, B.N., Sudheer, S., Kharwar, R.N., Siddiqui, S., Abdel-Azeem, A.M., Fernandes Fraceto, L., Dashora, K., Gupta, V.K., 2019. Chrysophanol: a natural anthraquinone with multifaceted biotherapeutic potential. *Biomolecules.* 9, 68. https://doi.org/10.3390/biom9020068

Ramesh, C., Vinithkumar N.V., Kirubagaran, R., 2019. Marine pigmented bacteria: a prospective source of antibacterial compounds. *J. Nat. Sci. Biol. Med.* 10, 104–113. https://doi.org/10.4103/jnsbm.JNSBM_201_18

Ratte, M., Batubara, I., Lestari, Y., 2022. Morphological characterization and antioxidant activity of actinobacteria from *Xylocarpus granatum* growing in mangrove habitat. *Biotropika.* 10, 1–10. https://doi.org/10.21776/ub.biotropika.2022.010.01.01

Romo, J.A., Pierce, C.G., Chaturvedi, A.K., Lazzell, A.L., Mchardy, S.F., Saville, S.P., Lopez-Ribot, J.L., 2017. Development of anti-virulence approaches for candidiasis via a novel series of small-molecule inhibitors of *Candida albicans* filamentation. *MBio*. 8, e01991-17. https://doi.org/10.1128/mBio.01991-17

Seitz, A., Baker, JE., Levinsky, N.C., Morris, M.C., Edwards, M.J., Gulbins, E., Blakeman, T.C., Rodriquez, D., Branson, R.D., Goodman, M., 2021. Antimicrobial coating prevents ventilator-associated pneumonia in a 72 hour large animal model. *J. Surg. Res.* 267, 424–431. https://doi.org/10.1016/j.jss.2021.05.046

Udensi, J., Loskutova, E., Loughman, J., Byrne, H.J., 2022. Quantitative raman analysis of carotenoid protein complexes in aqueous solution. *Molecules.* 27, 4724. https://doi.org/10.3390/molecules27154724

Wahyudi, A.T., Nursari, R., Purwaningtyas, W.E., Cahlia, U., Priyanto, J.A., 2022. Crude extract of blue-green pigment derived from the marine bacterium *Pseudomonas aeruginosa* P1.S9 has antibacterial, antioxidant and cytotoxic activities. *Online J. Biol. Sci.* 22, 118–125. https://doi.org/10.3844/ojbsci.2022.118.125

Yolmeh, M., Hamedi, H., Khomeiri, M., 2016. Antimicrobial activity of pigments extracted from *Rhodotorula glutinis* against some bacteria and fungi. *Zahedan J. Res. Med. Sci.* 18, e4954. https://doi.org/10.17795/zjrms-4954